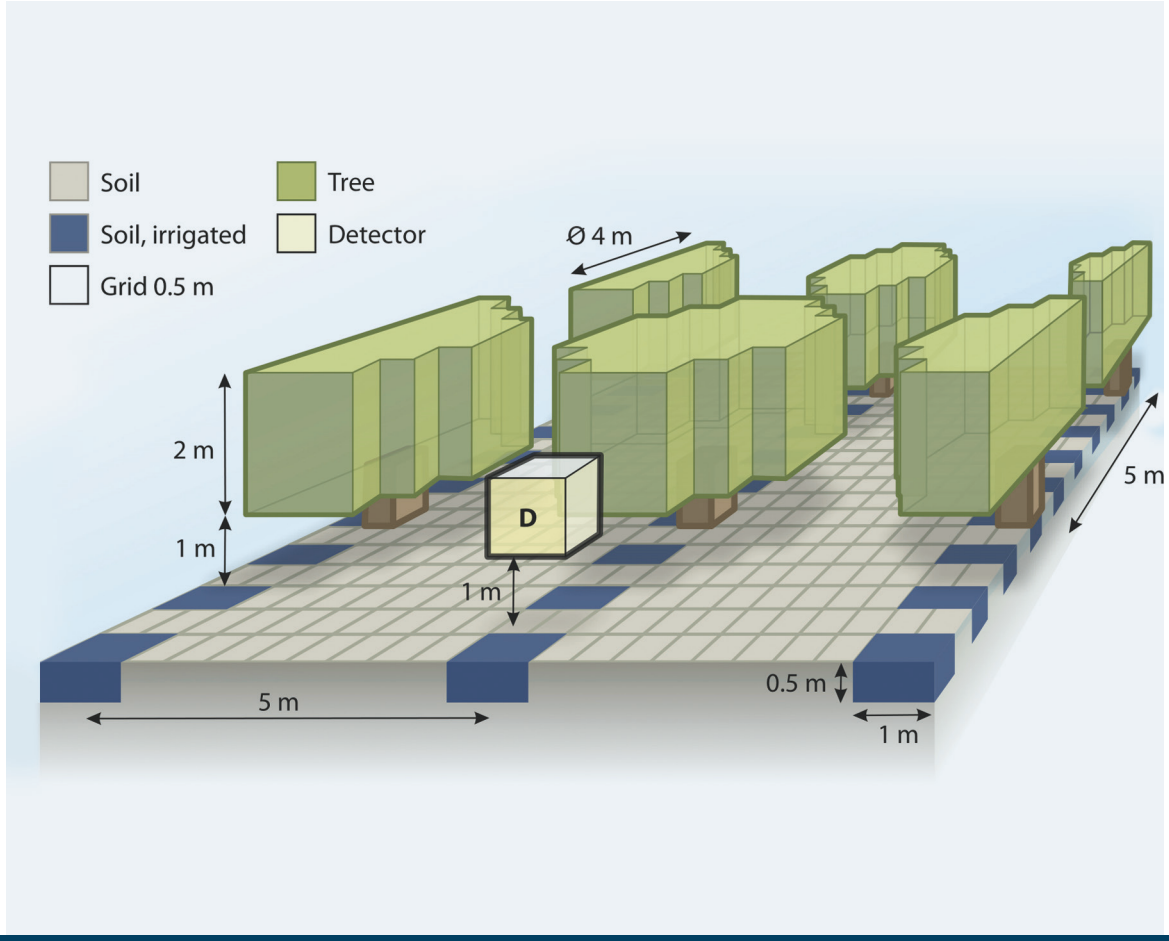

Towards a new real-time irrigation scheduling method: observation, modelling and their integration by data assimilation

Dazhi Li

Energie & Umwelt / Energy & Environment
Band / Volume 505
ISBN 978-3-95806-492-8

Mitglied der Helmholtz-Gemeinschaft

JÜLICH
Forschungszentrum

Schriften des Forschungszentrums Jülich
Reihe Energie & Umwelt / Energy & Environment Band / Volume 505

Forschungszentrum Jülich GmbH
Institut für Bio- und Geowissenschaften
Agrosphäre (IBG-3)

Towards a new real-time irrigation scheduling method: observation, modelling and their integration by data assimilation

Dazhi Li

Schriften des Forschungszentrums Jülich
Reihe Energie & Umwelt / Energy & Environment Band / Volume 505

ISSN 1866-1793 ISBN 978-3-95806-492-8

Bibliografische Information der Deutschen Nationalbibliothek.
Die Deutsche Nationalbibliothek verzeichnet diese Publikation in der
Deutschen Nationalbibliografie; detaillierte Bibliografische Daten
sind im Internet über http://dnb.d-nb.de abrufbar.

Herausgeber und Vertrieb:	Forschungszentrum Jülich GmbH Zentralbibliothek, Verlag 52425 Jülich Tel.: +49 2461 61-5368 Fax: +49 2461 61-6103 zb-publikation@fz-juelich.de www.fz-juelich.de/zb
Umschlaggestaltung:	Grafische Medien, Forschungszentrum Jülich GmbH
Druck:	Grafische Medien, Forschungszentrum Jülich GmbH
Copyright:	Forschungszentrum Jülich 2020

Schriften des Forschungszentrums Jülich
Reihe Energie & Umwelt / Energy & Environment, Band / Volume 505

D 82 (Diss. RWTH Aachen University, 2019)

ISSN 1866-1793
ISBN 978-3-95806-492-8

Vollständig frei verfügbar über das Publikationsportal des Forschungszentrums Jülich (JuSER)
unter www.fz-juelich.de/zb/openaccess.

Contents

List of Figures

List of Tables

List of Acronyms

CLM	Community Land Model
CESM	Community Earth System Model
CRNS	Cosmic-ray Neutron Sensing
DA	Data Assimilation
DSMW	Digital Soil Map of the World
EnKF	Ensemble Kalman Filter
ET	Evapotranspiration
FDR	Frequency Domain Reflectometry
FAO	Food and Agriculture Organization
fPAR	fraction of Photosynthetically Active Radiation
GRACE	Gravity Recovery and Climate Experiment
GFS	Global Forecast System
GLDAS	Global Land Data Assimilation System
GLEAM	Global Land Evaporation: the Amsterdam Methodology
IVIA	Instituto Valenciano de Investigaciones Agrarias
IMD	India Meteorology Department
ISWP	Integrated Stem Water Potential
KGE	Kling-Gupta Efficiency
LETKF	Local Ensemble Transform Kalman Filter
LAI	Leaf Area Index
LAS	Large Aperture Scintillometer
MODIS	Moderate Resolution Imaging Spectroradiometer
NCEP	National Center for Environmental Prediction
NDVI	Normalized Difference Vegetation Index
PFT	Plant Functional Types
RMSE	Root Mean Square Error

SWC	Soil Water Content
SCADA	Supervisory Control and Data Acquisition system
SWP	Stem Water Potential
SIPI	Seasonal Irrigation Performance Indicator
SMOS	Soil Moisture and Ocean Salinity
SMAP	Soil Moisture Active Passive
SAI	Stem Area Index
SEBS	Surface Energy Balance System
T	Transpiration
TDT	Time Domain Transmissivity
TerrSysMP	Terrestrial System Modeling Platform
USDA	United States Department of Agriculture
URANOS	Ultra Rapid Neutron-Only Simulation
WRF	Weather Research and Forecasting model

Abstract

Irrigated agriculture is very important in securing food production for an increasing population over the next decades. Given the scarcity of water resources, optimal irrigation management is needed to reduce water usage while maintaining maximal crop productivity. The irrigation scheduling methods are normally based on soil water content (SWC) measurements, e.g. from soil moisture sensors. Meanwhile land surface models such as the Community Land Model (CLM) have been commonly used to simulate SWC, crop status and hydrological processes. Data assimilation (DA) can combine different measurement data with a numerical model to get optimal estimation of model states. The integration of SWC measurements and Community Land Model using a sequential data assimilation method is promising to improve the real-time prediction of SWC and the calculation of irrigation demand. One of the aim of this PhD work is to introduce a new CLM-DA based real-time irrigation scheduling method and test it in a real world case, to explore the possibility of using other sources of SWC measurements (e.g. Cosmic-ray Neutron Sensing) for irrigation scheduling and to conduct the uncertainty analysis of irrigation modelling with CLM.

In the first study of this PhD thesis, we conducted a real-time irrigation scheduling campaign in a drip irrigated citrus field of Picassent, Spain. The SWC observations from soil sensors and CLM modelling were combined using a sequential data assimilation method to get real-time prediction of soil water deficit and irrigation demand. In addition, the weather forecasts by the Global Forecast System were used as atmospheric forcing data for CLM to predict soil water deficit for the next few days and schedule irrigation accordingly. The performance of the CLM-DA irrigation scheduling was investigated and compared with other irrigation scheduling approaches including the FAO water balance method and traditional farmers' experience. The comparison of the methods was based on the applied irrigation amounts, vegetation water stress measurements and citrus production. Results suggest that the CLM-DA based irrigation scheduling approach has better water saving potential compared to traditional irrigation scheduling methods. With less irrigation water, the citrus fields using CLM-DA method showed no significant production loss or water stress. Another finding from this study is that the observation of SWC is an important factor for the irrigation estimation with CLM-DA method.

In the second study of this thesis, the Cosmic-ray Neutron Sensing (CRNS) method was used to investigate its potential for monitoring SWC and scheduling drip irrigation. The CRNS probe can determine root zone SWC based on measured neutron intensity at the scale of tens of hectares. For the Picassent site in Spain, the footprint SWC was derived through soil sampling in the field and a calibration function. The overall SWC for the CRNS footprint was well characterized, but the experimental results also indicated the limitations of CRNS to detect drip water input. We found that the CRNS failed to sense the SWC variation caused by drip irrigation. In order to better interpret the results of the field experiment, the neutron transport model URANOS was used to simulate the neutron response to drip irrigation at the

CRNS location. Both the CRNS measurements and the neutron transport simulation results suggest that a standard CRNS probe is insufficient to detect the neutron response to drip irrigation in our specific case, because of the small area of irrigated patches, short irrigation time and weak SWC changes. Although the precise scheduling of drip irrigation is not feasible with a traditional CRNS probe, CRNS would perform better in drier case or with more intense irrigation events. New CRNS instruments like the cosmic-ray rover could be used to increase the sensitivity and to detect small-scale drip irrigation.

In the third study of this PhD thesis, we investigated the uncertainties of simulating irrigation demand by a land surface model. The lack of information on irrigation frequency, irrigation factor and the spatiotemporal variation of irrigation intensities affect the irrigation estimation by land surface models, especially for large-scale applications. Different model simulation scenarios were used to evaluate the impact of these uncertainties on the simulated irrigation demand, land surface fluxes and water balance over the Indian domain. This was done with the Community Land Model for the year of 2010. The daily-irrigated cases with default irrigation factor had the highest irrigation amounts, evapotranspiration and runoff throughout the year. The modelled irrigation requirement and surface runoff increased with the irrigation frequency and irrigation factor. It indicates that the irrigation factor should be calibrated to avoid water loss through runoff and to better model the irrigation for regional scale. The land surface fluxes modelled by CLM if a season-specific irrigation map was used as input, showed a similar trend as remote sensing based evapotranspiration. Using season-specific irrigation maps resulted in a higher transpiration-evapotranspiration ratio in the pre-monsoon season compared to other irrigation strategies, which means higher irrigation efficiency. It indicates that more accurate spatial and temporal information on irrigation will improve land surface modelling results. However, the resolution of irrigation modelling should be increased to improve the estimation of soil water deficit and irrigation demand.

Overall, our results show that the CLM-DA method provides a promising approach for irrigation scheduling by combining SWC observations and a land surface model using data assimilation, with the ability of real-time on-line control and the possibility to ingest different types of measurement data. Data assimilation turns out to be a promising method to integrate many kinds of observation data into a dynamic model and to improve the real-time water deficit prediction and irrigation allocation. SWC measurements from local (e.g. FDR sensor) to medium scale (e.g. CRNS) and large scale (e.g. remote sensing) along with modelling scales from local to large, will extend the feasibility of the CLM-DA method to different scales of irrigation management. The accurate information of spatiotemporal irrigation intensity is necessary for better large-scale irrigation modelling and characterization of land-atmosphere exchange fluxes and water balance.

Zusammenfassung

Die Bewässerungsfeldwirtschaft spielt eine entscheidende Rolle dabei, den steigenden Nahrungsmittelbedarf der wachsenden Weltbevölkerung in den nächsten Jahrzehnten zu decken. Angesichts der zunehmenden Wasserknappheit ist ein optimales Bewässerungsmanagement erforderlich, um den Wasserverbrauch bei gleichzeitiger Beibehaltung maximaler Pflanzenproduktivität zu reduzieren. Die Bewässerungsplanung basiert in der Regel auf die Messung von Bodenwassergehalten (Soil Water Content: SWC), zum Beispiel mit Hilfe von Bodenfeuchtesensoren. Zur Simulation von SWC, Erntezustand und hydrologischen Prozessen kommen derzeit Landoberflächenmodelle wie das Community Land Model (CLM) häufig zum Einsatz. Mit Hilfe von Datenassimilation (DA) können unterschiedliche Messdaten in ein numerisches Modell integriert werden, um daraus optimale Vorhersagen zu erzielen. Die Kombination von SWC-Messungen und CLM mit einer sequenziellen Datenassimilationsmethode verspricht eine Verbesserung der Echtzeit-Vorhersage des Bodenwassergehaltes und somit des Bewässerungsbedarfs. Eines der Ziele dieser Doktorarbeit ist es, eine neue CLM-DA-basierte Echtzeit-Bewässerungsplanungsmethode zu entwickeln und anhand eines realen Fallbeispiels, die Nutzungsmöglichkeit von anderen SWC-Produkten (beispielsweise aus Cosmic-ray Neutron Sensing) im Hinblick auf die Bewässerungsplanung zu überprüfen und die Unsicherheiten der Bewässerungsmodellierung mit CLM zu analysieren.

Die erste Studie dieser Doktorarbeit umfasst eine Kampagne, in der eine Echtzeit-Bewässerungsplanung in einem tropfbewässerten Zitrusfeld in Picassent, Spanien, durchgeführt wurde. Gemessene SWC mit Bodensensoren und CLM-Modellierung wurden mit einer sequenziellen Datenassimilationsmethode kombiniert, um das Bodenwasserdefizit und den Bewässerungsbedarf in Echtzeit vorherzusagen. Darüber hinaus wurden die Wettervorhersagen des Global Forecast System als atmosphärische Antriebsdaten für das CLM verwendet, um daraus Bodenwasserdefizit für die nächsten Tage vorherzusagen und die Bewässerung entsprechend zu planen. Die Leistung der Bewässerungsplanung durch CLM-DA wurde untersucht und mit anderen Ansätzen wie der FAO-Wasserbilanzmethode und den Erfahrungen traditioneller Bauern verglichen. Der Vergleich basierte auf der aufgebrachten Wassermenge, dem Wasserstress der Pflanzen und der Zitrusproduktion. Die Ergebnisse deuten darauf hin, dass die CLM-DA-basierte Bewässerungsplanung im Vergleich zu herkömmlichen Planungsansätzen ein besseres Wassereinsparpotenzial aufweist. Trotz weniger Bewässerungswasser zeigten die mit CLM-DA geplanten Zitrusfelder keinen signifikanten Produktionsverlust sowie keinen Wasserstress. Ein weiteres Ergebnis dieser Studie besteht darin, dass die Beobachtung des Bodenwassergehalts ein wichtiger Faktor für die Schätzung der Bewässerungsmenge mit der CLM-DA-Methode darstellt.

In der zweiten Studie dieser Arbeit wurde das Potenzial der Cosmic-ray Neutron Sensing (CRNS)-Methode für die Überwachung des Bodenwassergehalts und der Planung der Tropfenbewässerung untersucht. Die CRNS-Sonde kann den SWC der Wurzelzone, basierend auf der gemessenen Neutronenintensität, für eine Fläche bis zu mehreren Zehnern von Hektaren bestimmen. Für den Standort Picassent in Spanien wurde der Footprint des SWC durch Bodenprobenahmen im Feld und eine Kalibrierfunktion abgeleitet. Der gesamte SWC für den CRNS-Footprint konnte gut charakterisiert werden, jedoch zeigten die experimentellen Ergebnisse auch die Grenzen von CRNS bei der Erkennung von Tropfwassereintrag. Wir fanden heraus, dass CRNS die SWC-Variation, welche durch die Tropfenbewässerung verursacht wurde, nicht wiedergeben konnte. Um die Ergebnisse des Feldexperiments besser interpretieren zu können, wurde mit dem Neutronentransportmodell

URANOS die Neutronenreaktion auf die Tröpfchenbewässerung am CRNS-Standort simuliert. Sowohl die CRNS-Messungen als auch die Ergebnisse der Neutronentransportsimulation deuten darauf hin, dass eine Standard-CRNS-Sonde dafür nicht ausreicht, die Neutronenreaktion auf die Tröpfchenbewässerung in unserem speziellen Fallbeispiel zu erfassen. Gründe dafür sind die geringen bewässerten Flächen, die kurze Bewässerungszeit und die niedrigen Änderungen des Bodenwassergehaltes. Obwohl die genaue Planung der Tröpfchenbewässerung mit einer herkömmlichen CRNS-Sonde nicht möglich ist, würde CRNS im trockeneren Fall oder bei intensiveren Bewässerungsereignissen besser funktionieren. Neue CRNS-Geräte wie der Cosmic-ray Rover könnten eingesetzt werden, um die Empfindlichkeit zu erhöhen und Tropfenbewässerungen auf kleineren Skalen zu erkennen.

In der dritten Studie wurden die Unsicherheiten der Simulation des Bewässerungsbedarfs mittels eines Landoberflächenmodells untersucht. Der Mangel an Informationen über die Bewässerungshäufigkeit, den Bewässerungsfaktor und die räumlich-zeitliche Variation der Bewässerungsintensitäten beeinflusst die Bewässerungsschätzung durch Landoberflächenmodelle, insbesondere für Großanwendungen. Verschiedene Modellsimulationsszenarien wurden verwendet um die Auswirkungen dieser Unsicherheiten auf den simulierten Bewässerungsbedarf, die Landoberflächenflüsse und den Wasserhaushalt in Indien zu bewerten. Dies geschah mit dem Community Land Model für das Jahr 2010. Die täglich bewässerten Flächen mit dem Standard-Bewässerungsfaktor hatten das ganze Jahr über den höchsten Abfluss, die höchste Bewässerungs- und Evapotranspirationsraten. Der modellierte Bewässerungsbedarf und der Oberflächenabfluss nahmen mit der Bewässerungshäufigkeit und dem Bewässerungsfaktor zu. Es zeigt sich, dass der Bewässerungsfaktor kalibriert werden sollte, um Wasserverlust durch Abfluss zu vermeiden und die Bewässerung für den regionalen Maßstab besser zu modellieren. Die Landoberflächenflüsse, die durch das CLM-Modell, das als Input die saisonabhängigen Bewässerungskarten nahm, modelliert wurden, zeigten einen ähnlichen Trend wie die durch Fernerkundung ermittelte Evapotranspiration. Die Verwendung saisonabhängiger Bewässerungskarten führte zu einem höheren Transpiration-Evapotranspiration-Verhältnis im Vormonsun im Vergleich zu anderen Bewässerungsstrategien, was zu einer höheren Bewässerungseffizienz führt. Es zeigt sich, dass genauere räumliche und zeitliche Informationen über die Bewässerung die Ergebnisse der Landoberflächenmodellierung verbessern können. Allerdings sollte die Auflösung der Bewässerungsmodellierung erhöht werden, um die Schätzung des Bodenwasserdefizits und des Bewässerungsbedarfs zu verbessern.

Insgesamt zeigen die Ergebnisse, dass die CLM-DA-Methode einen vielversprechenden Ansatz für die Bewässerungsplanung bietet, indem sie SWC-Messungen und Landoberflächenmodell mit Datenassimilation kombiniert. Die Datenassimilation erweist sich als eine vielversprechende Methode, um unterschiedliche Beobachtungsdaten in ein dynamisches Modell zu integrieren und die Echtzeit-Vorhersage des Wasserdefizits zu verbessern. SWC-Messungen von lokaler (z. B. FDR-Sensor), mittlerer (z. B. CRNS) bis großer (z. B. Fernerkundung) Skala sowie Modellierungsskalen von lokal bis groß werden die Anwendung der CLM-DA-Methode auf verschiedene Ebenen des Bewässerungsmanagements erweitern. Genaue Informationen über die räumlich-zeitliche Bewässerungsintensität sind notwendig, um eine bessere Modellierung und Charakterisierung der Austauschflüsse zwischen dem Land und der Atmosphäre und des Wasserhaushalts im großen Maßstab zu ermöglichen.

Chapter 1 : Introduction

Irrigated agriculture, which accounts for 40% of the food production, is important in securing the food for an increasing world population (Playán and Mateos 2006; McLaughlin and Kinzelbach 2015). Meanwhile irrigation is responsible for 70% of the fresh water withdrawals (Vereecken et al. 2009). Given the scarcity of water resources especially in arid and semi-arid areas, more efficient irrigation scheduling is needed to save water resources and to fulfil crop requirements. Depending on the availability of water stress information, the irrigation scheduling methods can be based on: soil water content (SWC) measurements, evapotranspiration (ET) and/or plant water stress (e.g. stem water potential) (Evans et al. 1991; Jones 2004; Pardossi and Incrocci 2011). The SWC based irrigation scheduling approach is normally applied on the basis of the difference between root-zone SWC and a target SWC that is related to the crop type (Evans et al. 1991).

Many sensors can measure soil water content, such as Time Domain Transmissivity (TDT), Frequency Domain Reflectometry (FDR) (Peters et al. 2013), tensiometers (Smajstrla and Locascio 1996) and capacitance probes (Fares and Alva 2000). The advantages of SWC sensors compared with the traditional gravimetric method are lower costs, less time intensive and less invasive. However, SWC sensors are limited by their spatial representativeness. In order to obtain SWC information at a larger scale, many TDT or FDR-probes can be connected in a wireless sensor network, which can achieve SWC characterization at a larger scale and in real-time (Vellidis et al. 2008; Bogena et al. 2010). Cosmic-ray Neutron Sensing (CRNS) is a cosmic-ray neutron intensity based device that can monitor SWC at an intermediate scale and non-invasively (Zreda et al. 2012). Remote sensing can also provide regional SWC information, like the Soil Moisture and Ocean Salinity (SMOS) (Kerr et al. 2001) and Soil Moisture Active Passive (SMAP) missions (Entekhabi et al. 2010; El Sharif et al. 2015).

The traditional irrigation scheduling method was often based on a simple water production function or water balance model, while ignoring the complex interactions between soil and vegetation (Barrett and Skogerboe 1980; Sammis et al. 2012). Land surface models such as the Community Land Model (CLM) have been widely used in climate and hydrological research to describe ecological and hydrological processes (Oleson et al. 2010). The Community land model is the land model of the Community Earth System Model, and it can simulate the soil water content of the root zone from a single point to the global scale (Oleson

et al. 2010; 2013). There have been several studies on irrigation modelling by a land surface model at the regional and global scale (Döll and Siebert 2002; Lawston et al. 2017; Leng et al. 2013; Lu et al. 2015; Xie et al. 2017; Zeng et al. 2017). The performance of the irrigation simulation by CLM4 and CLM4.5 and the interactions between climate and irrigated area have been evaluated (Leng et al. 2013; Lu et al. 2015; Xie et al. 2017; Zeng et al. 2017). The combination of a land surface model and weather forecast allows the simultaneous simulation of ET and crop yield, as well as the irrigation water demand (Linker et al. 2016). Meanwhile various new modelling, controlling and decision support methods were introduced into irrigation scheduling (Shang and Mao 2006; Geerts et al. 2010); with help of multiple mathematical optimization algorithms like simulated annealing (Brown et al. 2010), genetic algorithms (Irmak and Kamble 2009; Wardlaw and Bhaktikul 2004) and computational neural networks (Pulido-Calvo and Gutiérrez-Estrada 2009).

Sequential data assimilation (DA) is the optimal merging of model predictions on one hand and measurement data on the other hand (Evensen 2003). Data assimilation can improve the characterization of initial soil water contents (compared to measurement alone or model simulations alone) and therefore also improve the irrigation scheduling (Han et al. 2016a). To predict short or medium time scale soil water balance conditions, weather forecast data are also important (Lorite et al. 2015). If weather forecast information is used as model forcing, the dynamic model can provide a forecast of soil water content and crop states. Previous study has shown that DA based combination of SWC information from sensors and predictions by CLM allows calculating the future water deficit and the real-time automatic control of irrigation (Han et al. 2016a).

However, the application of the CLM-DA based irrigation scheduling method for a real-world case was not conducted and verified before, which will be one objective of this PhD work. To assist crop monitoring and irrigation management at different spatial scales, the CLM-DA based real-time irrigation scheduling scheme should be tested for smaller fields but also over a larger domain. Two major components of the CLM-DA irrigation scheduling system are real-time SWC observation and land surface modelling, which all can be conducted at different spatial and temporal resolutions.

In order to have SWC observation at different spatial scales, a network of dielectric probes (e.g. FDR) covering the field scale or the CRNS probe measuring at the intermediate scale are needed. The CRNS technique is promising for irrigation management as the measurement

footprint is representative for the root-zone SWC at the intermediate scale of tens of hectares (Zreda et al. 2012). If we can estimate soil water deficit at the intermediate scale using a single sensor like CRNS, the costs associated with the construction of a large SWC network can be avoided. The possibilities of using CRNS to schedule drip irrigation have not been studied in a real world case before and need to be further explored.

Irrigation significantly changes the interaction between land and atmosphere, causing high impact on the water and energy budget of the land surface (Ozdogan et al. 2010). The effect of irrigation cannot be neglected when conducting land surface modelling over large areas like India, which has large proportion of land being irrigated (Kumar 2003). Although there has been plenty research on irrigation modelling by CLM and other land surface models, most studies ignored the effect of temporal variable irrigation areas and irrigation intensity, as well as uncertainty of soil texture (Döll and Siebert 2002; Leng et al. 2013; Lawston et al. 2017; Zeng et al. 2017). In India, the irrigation demand is strongly decided by the unevenly distributed precipitation throughout the year. It is therefore very important to assess the impact of the uncertainty of temporal variable irrigation areas (seasonal-variable irrigation map) and frequency.

The objectives of this PhD thesis are to:

(1) introduce an alternative irrigation scheduling approach based on the CLM-DA method with the ability of real-time control and integration of soil water content observations, and evaluate the performance of this approach in real-time irrigation scheduling. This is done at a drip irrigated field site with citrus trees near Picassent (Spain). The water saving capability of the CLM-DA approach is compared with other irrigation scheduling methods like the FAO (Food and Agriculture Organization) water balance method and a traditional approach used by framers according their experience.

(2) explore the potential of using the CRNS technique to monitor water deficit and schedule irrigation. This is also tested at the drip irrigated Picassent site. Moreover, to better interpret the experimental data, neutron transport simulation was used to mimic the Picassent site and simulate the effect of drip irrigation on the cosmic-ray neutron counts.

(3) investigate the uncertainties associated with calculating irrigation by a land surface model, which are caused by uncertainty concerning the temporal variability of irrigation intensity, irrigation frequency and irrigation factor (related the target soil water content when irrigation

stops). The influence of those factors on land surface fluxes and water balance modelling are further explored over a large model domain over India.

Chapter 2 gives an overview of the land surface model and data assimilation method being used in our work. Furthermore, this chapter introduces the basic knowledge of CRNS observation, calibration, as well as the neutron transport modelling.

In chapter 3 we apply the method integrating SWC measurements and CLM using sequential DA to improve the prediction of soil water status and design the real-time drip irrigation scheduling strategies for the citrus fields in Picassent, Spain. SWC measured by FDR was assimilated into CLM by the Local Ensemble Transform Kalman Filter (LETKF) to improve the characterization of the soil moisture condition. Atmospheric input data from the Global Forecast System (GFS) were used to force CLM to predict the short-term evolution of the SWC. The irrigation amount was then calculated on the basis of the difference between predicted and targeted root zone SWC. During the real-time irrigation campaigns in 2015 and 2016, there were 6 fields irrigated according the CLM-DA approach, 2 further fields according the FAO water balance method and also 2 fields according the farmers experience. The corresponding amount of irrigation water for each citrus field was applied by SCADA (supervisory control and data acquisition system). After the harvest, the efficiency of the different irrigation scheduling methods was compared in terms of the overall applied irrigation amount, measured stem water potential, deep root zone SWC and citrus yield.

Chapter 4 evaluates the measurement precision of the CRNS at the Picassent drip-irrigated field and evaluates whether it is sufficient to support drip irrigation management. The work relies on both field experimentation and modelling of neutron intensity. A soil sampling was carried out to determine the relationship between footprint SWC and neutron intensity measured by the CRNS probe. Also multiple FDR-sensors were installed in the CRNS-footprint to be used as verification. The neutron transfer simulation model URANOS (Ultra Rapid Neutron-Only Simulation) was used to model the neutron response for the drip irrigated citrus fields and to explore the potential of the CRNS method to detect drip irrigation events.

Chapter 5 investigates how the temporal variation of irrigated areas (as reflected in an irrigation map), irrigation frequency and irrigation factor affect calculations with a land surface model in terms of irrigation and water flux modelling. By using the CLM model, the irrigation demand and land-atmosphere exchange fluxes over the Indian model domain were

reconstructed for the year of 2010 at a resolution of 10 km × 10km. The uncertainties with respect to time-variable irrigation area, irrigation frequency and irrigation factor were explored by different simulation scenarios. The results in terms of irrigation and land surface flux modelling for different simulation scenarios were then compared and validated by large-scale remote sensing data.

Finally, chapter 6 summarizes the main results and provides an outlook for future research.

Chapter 2 : Theory

2.1 Community Land Model

The Community Land Model (CLM) is the land surface model of the Community Earth System Model (CESM) developed by the American National Center for Atmospheric Research. CLM describes the ecological and hydrological processes relevant for irrigation optimization and the interaction between the atmospheric boundary layer, soil and vegetation, and is widely used in climate, hydrology and other environmental research (Oleson et al. 2010; 2013). The CLM has been constantly updated with new versions, with version 4.0 and 4.5 being used in this thesis. The version 4.0 of CLM was released in 2010 to include the biogeochemistry components in the model including the coupled carbon and nitrogen cycles (Oleson et al. 2010). The update from version 4.0 to version 4.5 in 2013 included modifications regarding the representation of canopy process, lakes, snow cover and hydraulic properties of frozen soil (Oleson et al. 2013).

Land surface heterogeneity is represented in CLM by 3 levels of sub-grid hierarchy including land units (urban, glacier, lake, wetland and vegetated), columns and 16 plant functional types (PFT). The plant functional types are: evergreen needle leaf (boreal or temperate), deciduous needle leaf (boreal), evergreen broadleaf (temperate or tropical), deciduous broadleaf (boreal, temperate or tropical), deciduous shrub (boreal, temperate), evergreen shrub (temperate), grass (C3 Artic, C3 and C4), and crop (C3 rainfed, C3 irrigated) (Oleson et al. 2010). The multiple columns within one land unit make it possible to divide one land unit into vegetated irrigated column and non-irrigated bare soil column.

In CLM, soil water storage and vertical water fluxes in the soil are governed by different processes, including rainfall infiltration, surface and subsurface runoff, root water uptake (canopy transpiration), and interaction with the below-lying aquifer (Oleson et al. 2010). The vertical soil profile in CLM is divided into 15 layers, while only for the upper 10 layers soil water content is calculated. The thickness of the CLM layers varies between 1.75 cm for the first layer and 1.51m for the 10^{th} layer (Oleson et al. 2010).

The most important hydrology part in CLM for irrigation management is the calculation of soil water content. A modified Richards equation was used to simulate the soil water flow:

$$\frac{\partial \theta_i}{\partial t} = \frac{\partial}{\partial z}\left[k_i\left(\frac{\partial(\psi_i - \psi_{e,i})}{\partial z}\right)\right] - Q \qquad (2.1)$$

where θ_i is the volumetric soil water content (cm^3/cm^3) in layer i, t is time, ψ_i (mm) is the soil matric potential, k_i (mm/s) is hydraulic conductivity, z_i represents the soil depth, $\psi_{e,i}$ (mm) is the equilibrium soil matric potential of the i^{th} soil layer, and Q is the soil water removed by root water uptake (Decker and Zeng 2009; Oleson et al. 2013).

Soil hydraulic parameters like hydraulic conductivity are calculated from the Clapp-Hornberger pedotransfer function (Clapp and Hornberger 1978; Cosby et al. 1984) using sand and clay content, as well as organic properties of each soil layer as input (Lawrence and Slater 2008; Oleson et al. 2010):

$$k_{s,i} = \left(1 - f_{p,i}\right)\left[\frac{1-f_{om,i}}{0.0070556 \cdot 10^{(-0.884+1.53 f_{sd,i})}} + \frac{f_{om,i}-f_{p,i}}{k_{s,om}}\right]^{-1} + f_{p,i} k_{s,om} \quad (2.2)$$

where $k_{s,i}$ (mm/s) is the saturated hydraulic conductivity; $f_{sd,i}$ and $f_{om,i}$ are the percentages (%) of sand and organic matter; the fraction $f_{p,i}$ is zero when $f_{om,i}$ is less than 0.5, otherwise $f_{p,i} = 1.101 \times f_{om,i}(f_{om,i} - 0.5)^{0.139}$; $k_{s,om}$ is the saturated hydraulic conductivity of organic matter (Oleson et al. 2013).

Soil water content is also strongly determined by evapotranspiration (Q in Equation 2.1). The simulation of land-atmosphere exchange fluxes is based on Monin-Obukhov similarity theory (Oleson et al. 2013). The evapotranspiration from the vegetation column was divided into three parts: ground evaporation, interception evaporation and vegetation transpiration. For each column, the canopy evaporation and transpiration are the sum from all PFTs sharing the same soil column. For the vegetated soil column (without canopy interception water), the evapotranspiration includes the water vapor flux from vegetation E_v and from ground soil E_s (Oleson et al. 2013):

$$E_v = -\frac{\rho_{atm}(q_s - q_{sat}^{T_v})}{r_{total}} \quad (2.3)$$

$$E_s = -\frac{\rho_{atm}\beta_{soil}(q_s - q_{soil})}{r'_{aw} + r_{litter}} \quad (2.4)$$

where r_{total} (s/m) is the total aerodynamic resistance to water vapor transfer from the canopy to canopy air including contributions from leaf boundary layer and stomata; r'_{aw} (s/m) is the aerodynamic resistance to water vapor transfer between the ground and canopy air; r_{litter} (s/m) is the resistance from plant litter layer; $q_{sat}^{T_v}$ (kg/kg) is the saturated specific humidity at the vegetation temperature T_v; q_s (kg/kg) is the canopy specific humidity; q_{soil} (kg/kg) is the

specific humidity of soil; β_{soil} is an empirical function of soil water content (Oleson et al. 2013).

The difference between the predicted soil water content and the target soil water content is the water deficit, and irrigation scheduling is planned on the basis of the calculated water deficit. In CLM, the target soil water content can be defined for the irrigation needs of different crops (Oleson et al. 2010):

$$\theta_{\text{target}} = (1 - 0.7) \cdot \theta_{\text{min}} + 0.7 \cdot \theta_{\text{max}} \tag{2.5}$$

where θ_{min} is the minimum needed soil water content to sustain completely open stomata and θ_{max} is soil saturation. They are defined separately for each soil layer. The empirical parameter 0.7 was set in CLM to match the calculated global irrigation demand for the year 2000 with the observation data (Oleson et al. 2010).

The irrigation amount (W_{deficit}) is calculated by the integrated water deficit over the root zone (Oleson et al. 2010):

$$W_{\text{deficit}} = \sum_i^N R_i \cdot \max\left(\theta_{\text{target}} - \theta_i, 0\right) \tag{2.6}$$

where θ_i is the soil water content for layer i, R_i is the root fraction for that layer, and N is the number of CLM-layers with roots, which are dependent on the plant functional type (PFT) in CLM.

$$R_i = \begin{cases} 0.5 \left[\begin{matrix}\exp(-r_a Z_{h,i-1}) + \exp(-r_b Z_{h,i-1}) \\ -\exp(-r_a Z_{h,i}) + \exp(-r_b Z_{h,i})\end{matrix}\right] & 1 \le i < N_{\text{levsoi}} \\ 0.5\left[\exp(-r_b Z_{h,i-1}) + \exp(-r_b Z_{h,i-1})\right] & i = N_{\text{levsoi}} \end{cases} \tag{2.7}$$

where $Z_{h,i}$ (m) is the depth from the surface to the interface between soil layers i and $i+1$; r_a and r_b are root distribution parameters for different plants (Zeng 2001).

2.2 Data assimilation

Data assimilation (DA) combines direct and/or indirect measurements and dynamic models to get optimal estimates of model state variables (Reichle 2008). In this PhD work, data assimilation is applied to use available soil water content data to correct predictions by CLM in a probabilistic manner. It updates the current system states and should give better estimates

of future system states, together with a characterization of the uncertainty of the estimates (Evensen 2003).

Ensemble Kalman Filter (EnKF) is the Monte Carlo approximation of the Kalman filter that estimates state variables through a forecast and analysis process, where the model covariance matrix is estimated from a limited number of ensemble members which avoids the very expensive explicit computation of the model covariance matrix (Evensen 2003). In the work of chapter 3, the Local Ensemble Transform Kalman Filter (LETKF) is used, which is a variant of the Ensemble Kalman Filter. It has been widely used by scientists in land surface hydrology and meteorology (Hunt et al. 2007; Miyoshi et al. 2007; Han et al. 2014a; Han et al. 2015). More details of LETKF can be found in Hunt et al. (2007).

Compared with traditional ensemble Kalman filters, LETKF is more efficient. In LETKF, the global state and observation matrices are only prepared once in a forecast step, then each model grid is updated separately along with the local analysis error covariance matrix, avoiding the calculation of a large error covariance matrix (Han et al. 2014a). By dividing the global model grid into separate local patches, each grid cell of the model is updated separately which can be easily exploited in parallel computations (Miyoshi et al. 2007).

In the global operation step of LETKF, two global matrices $\mathbf{X}^{\mathrm{b}}$ and $\mathbf{Y}^{\mathrm{b}}$ are constructed based on soil moisture modeled by CLM for each grid cell.

$$\mathbf{X}^{\mathrm{b}} = [\mathbf{x}_1^{\mathrm{b}} - \bar{\mathbf{x}}^{\mathrm{b}}, \dots, \mathbf{x}_{\mathrm{M}}^{\mathrm{b}} - \bar{\mathbf{x}}^{\mathrm{b}}] \tag{2.8}$$

$$\mathbf{Y}^{\mathrm{b}} = [\mathbf{y}_1^{\mathrm{b}} - \bar{\mathbf{y}}^{\mathrm{b}}, \dots, \mathbf{y}_{\mathrm{M}}^{\mathrm{b}} - \bar{\mathbf{y}}^{\mathrm{b}}] \tag{2.9}$$

$$\mathbf{y}_{\mathrm{i}}^{\mathrm{b}} = \mathbf{H}(\mathbf{x}_{\mathrm{i}}^{\mathrm{b}}) \tag{2.10}$$

where $\mathbf{x}_1^{\mathrm{b}} \dots \mathbf{x}_{\mathrm{M}}^{\mathrm{b}}$ contain the modeled states for the *M* ensemble members, $\bar{\mathbf{x}}^{\mathrm{b}}$ is the ensemble mean; $\mathbf{y}_1^{\mathrm{b}} \dots \mathbf{y}_{\mathrm{M}}^{\mathrm{b}}$ are vectors containing the model states at the observation locations for each of the *M* ensemble members, $\bar{\mathbf{y}}^{\mathrm{b}}$ is the vector of the corresponding ensemble means and $\mathbf{H}$ is the observation operator that maps between the model space and the observation space, which is identity matrix in our case because of the direct observation. The model state vector $\mathbf{x}^{\mathrm{b}}$ is constructed as:

$$\mathrm{x}^{\mathrm{b}} = [\theta_1, \theta_2 \dots \theta_{10}]^{\mathrm{T}} \tag{2.11}$$

where $\theta_1, \theta_2 \dots \theta_{10}$ are modeled soil moisture contents for the ten CLM layers.

In the local analysis step, the analysis error covariance matrix $\widetilde{\mathrm{P}}^{\mathrm{a}}$ is calculated as:

$$\widetilde{\mathbf{P}}^{a} = \left[(M-1)\mathbf{I} + \left(\mathbf{Y}^{\mathrm{b}}\right)^{\mathrm{T}}\mathbf{R}^{-1}\mathbf{Y}^{\mathrm{b}}\right]^{-1} \tag{2.12}$$

where **R** is the observation error matrix, **I** is the identity matrix.

The perturbations matrix $\mathbf{W}^{a}$ and analysis mean $\bar{\mathbf{w}}^{a}$ are calculated as:

$$\mathbf{W}^{a} = [(M-1)\widetilde{\mathbf{P}}^{a}]^{1/2} \tag{2.13}$$

$$\bar{\mathbf{w}}^{\mathrm{a}} = \widetilde{\mathbf{P}}^{\mathrm{a}}\left(\mathbf{Y}^{\mathrm{b}}\right)^{\mathrm{T}}\mathbf{R}^{-1}(\mathbf{y}^{0} - \bar{\mathbf{y}}^{\mathrm{b}}) \tag{2.14}$$

where $\mathbf{y}^{0}$ is the observation vector containing soil moisture measured by the FDR sensors and for the different layers.

Finally the new analysis matrix $\mathbf{X}^{\mathrm{a}}$ that contains the updated ensemble members in model space is obtained by:

$$\mathbf{X}^{\mathrm{a}} = \bar{\mathbf{x}}^{\mathrm{b}} + \mathbf{X}^{\mathrm{b}}(\mathbf{W}^{\mathrm{a}} + \bar{\mathbf{w}}^{\mathrm{a}}) \tag{2.15}$$

Section 2.1 and 2.2 are adopted from Li et al. (2018).

2.3 Cosmic-ray Neutron Sensing

In chapter 4, the measurement precision of Cosmic-ray Neutron Sensing (CRNS) was tested in a drip-irrigated field in order to explore whether it is sufficient to support drip irrigation management. Cosmic radiation originates in outer space and penetrates the Earth atmosphere. This interaction creates high-energy neutrons which further collide with atoms in the air, soil, and vegetation to produce medium-energy neutrons (Zreda et al. 2012). Those neutrons can be efficiently moderated towards lower energies by nuclear collisions with hydrogen. Therefore, the intensity of medium-energy neutrons is an indication for the amount of hydrogen atoms at the land surface and its temporal variation. The Cosmic-ray Neutron Sensing probe can be used to measure soil water content up to depths of 80 cm and with a footprint radius ranging from 130 m to 240 m at sea level (Köhli et al. 2015)

The CRNS probe needs to be calibrated with soil samples during a field campaign while neutron intensity is simultaneously measured by the CRNS probe. The so-called N_0 method was developed by Desilets et al. (2010) to estimate soil water content θ_{v} in the CRNS footprint as function of the neutron count rate N_{pih} through a simple calibration function. To

calibrate the N_0 parameter, a single field calibration campaign was conducted as described in chapter 4.

$$\theta_{\mathrm{v}} = (a_0 \cdot \rho_{\mathrm{bd}}) \left(\frac{N_{\mathrm{pih}}}{N_0} - a_1\right)^{-1} - (a_2 \cdot \rho_{\mathrm{bd}}) - \theta_{\mathrm{lat}} - \theta_{\mathrm{org}} \tag{2.16}$$

where N_0 stands for the neutron intensity over dry soil at a specific test site and needs to be calibrated once; a_0=0.0808, a_1=0.372 and a_2=0.115 are constant fitting parameters. ρ_{bd} is soil bulk density (g/cm^3) averaged from all the soil samples taken on the calibration day (1.3 g/cm^3), it was calculated with an iterative method along with the weighting of soil water content for each layer. θ_{lat} is the volumetric lattice water (cm^3/cm^3) and θ_{org} is soil organic water equivalent (cm^3/cm^3).

The neutron transfer model called Ultra Rapid Neutron-Only Simulation (URANOS) was used to model the neutron response to the drip irrigated citrus fields in Picassent and to explore the potential of the CRNS method to detect drip irrigation events. The URANOS model simulates neutron interactions in a Monte Carlo framework, and was originally aimed for applications in nuclear physics (Köhli et al. 2018). Recently it has been used to model the interaction of cosmic-ray neutrons with air, soil and vegetation in order to understand neutron intensity measured by CRNS probe (Köhli et al. 2015).

Section 2.3 is adopted from “Li et al., 2019. Can drip irrigation be scheduled with Cosmic-ray Neutron Sensing? Vadose Zone Journal, 18(1). doi: 10.2136/vzj2019.05.0053”.

Chapter 3 : Evaluation of an operational real-time irrigation scheduling scheme for drip irrigated citrus fields in Picassent, Spain

*adapted from: Li, D., Hendricks Franssen, H.-J., Han, X., Jiménez-Bello, M. A., Alzamora, F. M., and Vereecken, H., 2018. Evaluation of an operational real-time irrigation scheduling scheme for drip irrigated citrus fields in Picassent, Spain. Agricultural Water Management, 208, 465-477. https://doi.org/10.1016/j.agwat.2018.06.022

3.1 Introduction

3.1.1 Water scarcity and irrigation scheduling

The world's population has exceeded 7 billion and will continue to increase with a high rate (https://en.wikipedia.org/wiki/World_population). To feed the increasing population, our agriculture must produce more food. Irrigated agriculture accounts for 40% of food production, and 70% of fresh water withdrawals are used by irrigation (Vereecken et al. 2009; Playán and Mateos 2006). Irrigation is important for the food security of the world (McLaughlin and Kinzelbach 2015). Given climate change and increased groundwater pollution, we are facing a global water crisis and stronger constraints on water resources (Vörösmarty et al. 2000; Iglesias and Garrote 2015). Groundwater recharge in semi-arid areas is usually limited, resulting in unsustainable groundwater use for irrigation and groundwater depletion (Scanlon et al. 2012). Therefore, efficient water use by irrigation scheduling is needed to allocate irrigation water rationally.

Irrigation scheduling aims to minimize water use while maintaining the agricultural production (Evans et al. 1991). Scheduling efforts can have a long-term focus or short-term focus, which includes real-time scheduling (Ticlavilca et al. 2013). Real-time scheduling of irrigation is usually based on calculated daily water allocation (Pham et al., 2013). With irrigation scheduling we decide when and how much to irrigate. When to irrigate is related to the sensitivity of crops to water stress, which determines the threshold when yield and quality reduction occur under water shortage. How much should be irrigated depends on the water deficit between the current and targeted water status (Evans et al. 1991). In order to make decisions regarding irrigation scheduling, the water stress condition needs to be known. Depending on the type of water stress information available, the irrigation scheduling approaches can be divided into: soil moisture measurements based, evapotranspiration (ET)

based and plant water stress based (Evans et al. 1991; Jones 2004; Pardossi and Incrocci 2011).

Many devices can give information on soil moisture status including dielectric sensors using Time Domain Transmissivity (TDT) and Frequency Domain Reflectometry (FDR) (Peters et al. 2013), tensiometers (Smajstrla and Locascio 1996), capacitance probes (Fares and Alva 2000), neutron probes and cosmic-ray probes (Zreda et al. 2012). The combination of soil moisture information from sensors and predictions by a given model allows to calculate the future water deficit (Blonquist et al. 2006). Evapotranspiration is defined as the sum of evaporation from the soil surface and transpiration from the crop (Allen et al. 1998). The ET based irrigation scheduling calculates the irrigated water amount by the difference between daily actual ET and precipitation (Davis and Dukes 2010). Water stress information from crops can be obtained by different indicators like sap flow (Fernández et al. 2001), stem water potential (Choné et al. 2001; Fernández and Cuevas 2010), trunk diameter fluctuation (Moriana et al. 2010), leaf stomata pressure, canopy temperature (Clawson and Blad 1982) and crop water stress index (Moran et al. 1994).

3.1.2 Drip Irrigation scheduling for citrus

Compared with all the major types of surface irrigation (furrow, flood, or large scale sprinkler irrigation), drip irrigation is seen as the most water-efficient and precise method (Provenzano 2007). Lots of irrigation scheduling methods were tested on drip irrigated fields on the base of measuring soil or plant water status and evapotranspiration (Dabach et al. 2013). For the drip irrigation of citrus trees, there are plenty of different indicators of plant water stress like stem water potential and soil capacitance, and also several ways to determine evapotranspiration like the FAO method, lysimeter and eddy covariance method (Jiménez-Bello 2015). Stem water potential (Sdoodee and Somjun 2008) and daily trunk shrinkage (Velez et al. 2007) were used to schedule irrigation for citrus orchards world widely. Also the water balance method for drip irrigation scheduling is popular. For example, Sammis et al. (2012) used a two-dimensional soil water balance model for drip irrigation scheduling.

The traditional way of drip irrigation scheduling was often based on a simple water production function or water balance model, while ignoring the complex interaction between soil and vegetation (Barrett and Skogerboe 1980). A new development is the use of complex models and weather data, combined with mathematical optimization methods (Shang and Mao 2006). Advanced modelling and programing technology offers a new possibility to

calculate soil water status. Various controlling and decision support methods were introduced into irrigation scheduling. Simulated annealing (Brown et al. 2010), genetic algorithms (Irmak and Kamble 2009; Wardlaw and Bhaktikul 2004) and computational neural networks (Pulido-Calvo and Gutiérrez-Estrada 2009) were used to support decisions concerning the irrigated water amount. To predict short or medium scale soil water balance conditions, weather forecast data are also important (Lorite et al. 2015; De Jager and Kennedy, 1996).

In this work, the Community Land Model (CLM) (Oleson et al. 2010) is used to estimate soil and crop water states. Data assimilation (DA) combines direct and/or indirect measurements and dynamic models to get optimal estimates of model states (Reichle 2008). Han et al. (2016a) already illustrated the potential of sequential DA to improve irrigation scheduling with CLM model predictions. In the past already hydrological models like HYDRUS (Autovino et al. 2018) and simpler water balance models (Rallo et al. 2017) were used for irrigation scheduling, but not a land surface model that couples the water and energy cycles. The use of data assimilation in this context is also a novel contribution for the irrigation scheduling of citrus or other fruit trees.

The main objective of this paper is to provide a new approach for irrigation scheduling by introducing the combination of data assimilation and land surface modelling, with the possibility of real-time on-line control and the possibility to ingest different types of measurement data. The CLM-DA method combines model predictions by a land surface model, weather prediction and soil moisture data measured by capacitance probes. We illustrate our approach for the near real-time irrigation scheduling of citrus trees near Picassent, Valencia (Spain). During the irrigation campaign for the Picassent site from July to October in 2015 and June to October in 2016, three different irrigation scheduling methods were tested for 10 citrus fields, including the CLM-DA method proposed in this paper, the FAO water balance model and a traditional method based on farmer's experience. The CLM-DA method combines model predictions by a land surface model, weather prediction and soil moisture data measured by capacitance probes. These information sources are optimally combined using sequential data assimilation, to predict drought stress for the next days and schedule irrigation accordingly. The applied irrigation amounts were measured by a water meter, and then divided by the irrigation area to get the water depth. Stem water potential and citrus production indicating the possible water stress were also measured.

3.2 Materials and methods

3.2.1 Research site and experimental set-up

The research site is located near Picassent in Spain (39.38° N, 0.47° E), in a semi-arid region. Precipitation is concentrated in spring, autumn and winter, and the yearly average precipitation amount is 453 mm, with an annual average daily maximum temperature of 22.3 °C and an annual average daily minimum temperature of 13.4 °C (https://en.wikipedia.org/wiki/Valencia#Climate). The crop growing at the test site is citrus, with major management procedures like fertilization and weeding carried out by the orchard owners. Although the citrus varieties differ between the fields, there are no significant differences in crop management, fertilization and tree ages. Information on field-specific tree ages were lacking, but all the trees were mature (older than 15 years) and in full-production stage. As precipitation during the main growing period of citrus in summer is rare, the water demand of the citrus trees almost entirely depends on irrigation. Drip irrigation is being used in these citrus tree fields, with two pipelines and 8~10 emitters for each tree. Detailed information about the types of citrus plant, spacing, and vegetative growth character can be found in Table 3.1.

Within the area of Picassent, the meteorology observatory of IVIA (Instituto Valenciano de Investigaciones Agrarias) provides meteorological data (http://riegos.ivia.es/). Twelve FDR probes were installed in the context of the EU-project AGADAPT since 2013, spreading over the irrigation plots (see Figure 3.1), measuring soil water content at four depths (10 cm, 30 cm, 50 cm, and 70 cm). During June and July 2015, 12 more FDR probes were installed in the field to enhance the observation density. The FDR probes were installed close to drip emitter and a representative tree of average size in the orchard. The FDR soil water content measurements (10 cm and 30 cm) in the irrigated area were used in the DA system for irrigation scheduling, because most roots of citrus trees are located in the top 50 cm. FDR measurements at 50 cm and 70 cm depth were later used as independent verification data for possible water depletion. During the irrigation period, the stem water potential was also measured for each field, covering the different irrigation scheduling methods.

Three different irrigation scheduling schemes were compared for this site: irrigation scheduling according (i) CLM-DA calculation (CLM fields), (ii) the FAO water balance model (FAO fields) and (iii) farmers' experiences (Farmer fields). The irrigation scheduling

schemes were assigned to different fields in the following way: (1) CLM-DA method: fields CLM-A, CLM-B, CLM-C, CLM-D, CLM-E and CLM-F; (2) FAO water balance: fields FAO-A, FAO-B; (3) farmers' experience: fields Farmer-A, Farmer-B. In June drip irrigation was applied on Monday, Tuesday, Wednesday, Friday and Saturday night (five times per week). In July and August also on Thursday there was irrigation. From September and October onwards, depending on the weather and fruit maturation process, irrigation frequency was reduced and finally stopped. All the experimental fields share the same irrigation frequency while only CLM-DA and FAO fields got suggested irrigation time from the calculations of different methods. The irrigation at the Farmer fields was conducted according the farmer's experience. The irrigation time of Farmer fields ranged from 1 to 2 hours depending on the flow speed and technician's evaluation of water demand for trees.

For the CLM-DA method, there are six fields involved in the irrigation scheduling in 2015 and 2016. Compared with the experiment of 2015, the data assimilation and irrigation controlling process of 2016 were slightly modified to avoid problems which occurred in 2015. As the applied irrigation water amounts in 2015 were affected by the variable flow velocity of the drip line, in 2016 the flow velocity data were retrieved every 3 days, which allowed more accurate irrigation duration so that the truly applied irrigation amount was closer to the scheduled irrigation amount. The needed irrigation amount (which was converted in an irrigation duration) was sent to the technicians in Valencia twice per week to do the real-time control of drip irrigation (period July 7 – October 31 2015). In 2016, the irrigation scheduling was from June 1 to October 31 and the corresponding irrigation time was applied directly through SCADA (Supervisory Control And Data Acquisition system) for each CLM-DA field. In 2016 the truly applied irrigation amounts were available shortly after the irrigation was done.

Table 3.1 The types of citrus tree, spacing, and vegetative growth characters for the different fields involved in the study (CLM-DA, FAO and Farmer)

Fields	Area (m^2)	Citrus variety	Ground Cover	Row distance(m)	Tree distance(m)	Emitters per tree	Q(l/h)
CLM-A	8210	Valencia Late	0.33	3.5	3.5	8	2.5
CLM-B	12375	Hernandina	0.70	4.5	5	10	3.5
CLM-C	4502	Clemenules	0.67	4.5	5	10	3.32
CLM-D	3031	Clemenules	0.48	5	5	12	5.6
CLM-E	9573	Navelina	0.45	6	5	10	1.9
CLM-F	8978	Hernanadina	0.46	6	4	10	3.7
FAO-A	3288	Lane Late	0.49	4.5	3.5	10	3.9
FAO-B	5340	Orogrande	0.60	5	5	10	4.5
Farmer-A	10583	Orogrande	0.60	5	5	10	4.4
Farmer-B	8670	Hernandina	0.60	5	5	10	2.3

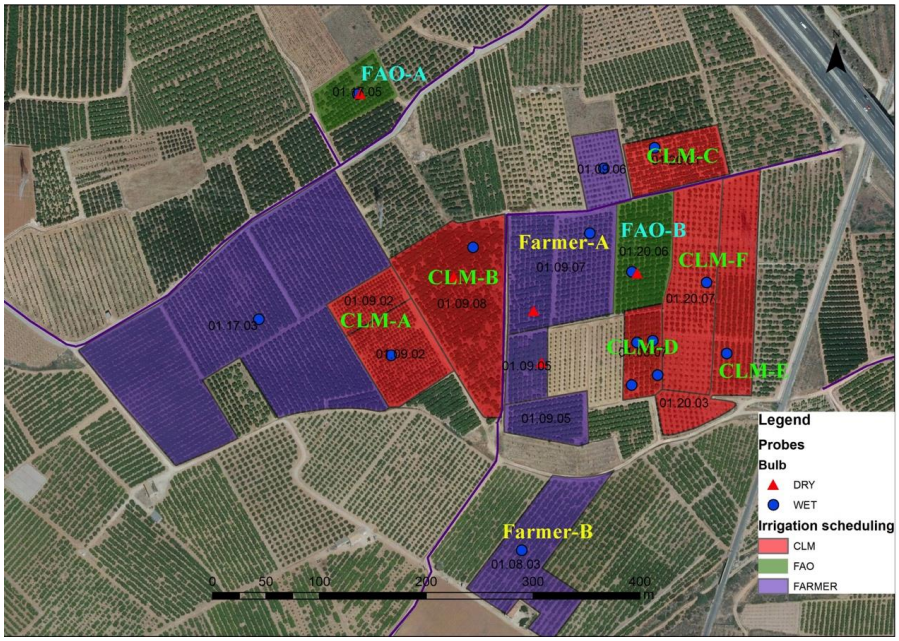

Figure 3.1 The distribution of the fields (with their numbers listed) and indication of the irrigation scheduling method applied (red fields: CLM, green fields: FAO, purple fields: Farmer) for each of the fields. The blue dots and red triangles are symbols of FDR probes, which were installed in the irrigated and not irrigated area.

3.2.2 FAO Soil water balance based irrigation scheduling

The FAO56 procedure uses the following basic water balance model (Rallo et al. 2011):

$$D_i = D_{i-1} + ET_C - P_i - I_i + R_i + DP_i \quad (3.1)$$

where D_i is the water depletion at day i, D_{i-1} is water depletion at the previous day i-1, ET_C is crop evapotranspiration, P_i is precipitation, I_i is irrigation, R_i is net runoff and DP_i is deep percolation. Ideally, runoff can be neglected in flat terrain, and deep percolation is set to zero to avoid water losses (Davis and Dukes 2010).

The actual crop evapotranspiration (ET_{C}) can be calculated from the reference evapotranspiration (ET_0) and the crop coefficient (K_{C}).

$$ET_{\mathrm{C}} = K_{\mathrm{C}} \cdot ET_0 \quad (3.2)$$

Reference evapotranspiration is calculated by the FAO Penmann-Monteith method (Allen et al. 1998). The crop coefficient may change as function of the vegetation development and the evolution of ground cover, the values of which are available from field experiments or remote sensing (Bausch 1995).

For the FAO water balance method applied in our fields, the irrigation amount was set equal to the water depletion at previous day (D_{i}), and the K_{C} was taken to calculate ET_{C} (Castel 2000):

$$K_{\mathrm{C}} = K_{\mathrm{cavg}} \cdot f_{\mathrm{cmonth}} \quad (3.3)$$

$$K_{\mathrm{cavg}} = 0.274 + GC \cdot 0.005 \quad (20\% < GC < 70\%) \quad (3.4)$$

where K_{cavg} depends on ground cover GC and the f_{cmonth} is a correction factor which depends on the month of year and is used by the Irrigation Advisory System of Valencia for fruit trees (http://riegos.ivia.es/).

3.2.3 Real-time drip irrigation scheduling with CLM and data assimilation

3.2.3(a) Land surface model

The Community land model (CLM4.0) is the land surface model of the Community Earth System Model (CESM1.1.2), which describes the ecological and hydrological processes relevant for irrigation optimization and the interaction between the atmospheric boundary

layer, soil and vegetation, and is widely used in climate, hydrology and other environmental research (Oleson et al. 2010). A modified Richards equation and Monin-Obukhov similarity theory are used to simulate the soil water flow and land-atmosphere exchange fluxes. The land surface heterogeneity of CLM is represented by 3 levels of sub-grid hierarchy including land units (urban, glacier, lake, wetland and vegetated), columns and 16 plant functional types (PFT) (Oleson et al., 2010).

In this study, in order to use the irrigation model in CLM, each grid cell has two columns: a bare soil non-irrigated column (67 %) and a vegetated irrigated column (33 %). The plant functional type chosen to represent the citrus tree in our model is evergreen broadleaf tree, which has many similarities with citrus trees. The root distribution parameters were modified as described by Han et al. (2016a) so that most roots are located within 50 cm soil depth, which is in correspondence with the shallow rooting of irrigated citrus trees as detected by experimental data.

The vertical soil profile in CLM is divided into 15 layers, while only for the upper 10 layers soil water content is calculated. Only these 10 layers will be considered for state updating by data assimilation. The thickness of the CLM layers varies between 1.75 cm for the first layer and 1.51 m for the 10^{th} layer (Han et al. 2014a). We took the bottom of the third layer (9.06 cm depth) and 5th layer (28.91 cm depth) as the counterparts for FDR measurements at 10 cm and 30 cm depth.

In CLM, soil hydraulic parameters and soil matric potential are calculated from the sand and clay fractions. In-situ measurement data of soil texture were used for the site (silty clay: silt 33 %, clay 32 % and sand 35 %). The soil hydraulic parameters like saturated hydraulic conductivity are calculated from the Clapp-Hornberger pedotransfer function using as input sand and clay content, as well as organic properties of each soil layer.

3.2.3(b) Data assimilation

Data assimilation is applied in this work to use available soil moisture data to correct predictions by the Land Surface Model CLM in a probabilistic manner. It updates the current system states and should give better estimates of future system states, together with a characterization of the uncertainty of the estimates (Evensen 2003). In this work, the Local Ensemble Transform Kalman Filter (LETKF) is used, which is a deterministic variant of the Ensemble Kalman Filter. It has been widely used by scientists in land surface hydrology and

meteorology (Hunt et al. 2007; Miyoshi et al. 2007; Han et al. 2014a; 2015). More detailed description of LETKF can be found in chapter 2.

In LETKF, localization implementation implies that each model grid cell is only updated by the closest FDR sensor observation. Ensemble inflation is also used in LETKF to prevent filter divergence (Han et al. 2014a). In this work, only the model grid cells with FDR observations were updated by data assimilation while soil and vegetation parameters are pre-defined and taken from in-situ measurements and LAI data respectively. The LAI values were calculated based on the ground coverage and an empirical function derived from field measurements. More details of the data assimilation with LETKF and CLM can be found in Han et al (2015; 2016a).

$$\mathrm{LAI} = -1.3 \cdot \log\left(\frac{(1-GC)}{1+GC}\right) \tag{3.5}$$

3.2.3(c) CLM-DA based irrigation scheduling

After the data assimilation analysis, the updated initial model states in the form of soil water content values are used as input for predicting the evolution of soil water content values for the next 3 or 4 days. This is done for each of the model ensemble members so that also the uncertainty of the predictions can be characterized. These predictions use weather forecasts as input. On the other hand, a target soil water status is defined to sustain crop growth and yield. The difference between the predicted soil water status and the target soil water status is the water deficit, and irrigation scheduling is planned on the basis of the calculated water deficit. In CLM, the target soil water content can be defined for the irrigation needs of different crops (Oleson et al. 2010):

$$\theta_{\mathrm{target}} = (1 - 0.7) \cdot \theta_{\mathrm{min}} + 0.7 \cdot \theta_{\mathrm{max}} \tag{3.6}$$

where θ_{min} is the minimum needed soil water content to sustain completely open stomata and θ_{max} is soil saturation. They are defined separately for each soil layer. The empirical parameter 0.7 was set in CLM to match the calculated global irrigation demand for the year 2000 with the observation data (Oleson et al. 2010).

The irrigation amount (W_{deficit}) is calculated by the integrated water deficit over the root zone (Oleson et al. 2010):

$$W_{\mathrm{deficit}} = \sum_i^N R_i \cdot \max\left(\theta_{\mathrm{target}} - \theta_i, 0\right) \tag{3.7}$$

where θ_i is the soil water content for layer i, R_i is the root fraction for that layer, and N is the number of CLM-layers with roots, which are dependent on the plant functional type (PFT) in CLM.

$$R_i = \begin{cases} 0.5 \begin{bmatrix} \exp(-r_a Z_{h,i-1}) + \exp(-r_b Z_{h,i-1}) \\ -\exp(-r_a Z_{h,i}) + \exp(-r_b Z_{h,i}) \end{bmatrix} & 1 \le i < N_{\text{levsoi}} \\ 0.5\left[\exp(-r_b Z_{h,i-1}) + \exp(-r_b Z_{h,i-1})\right] & i = N_{\text{levsoi}} \end{cases} \quad (3.8)$$

where $Z_{h,i}$ (m) is the depth from the surface to the interface between soil layers i and $i+1$, r_a and r_b (both are 8.992 for citrus) are root distribution parameters for different plants (Zeng 2001).

Forecasted weather data were used as input to the land surface model for soil water status predictions. The T1534 Semi-Lagrangian grid weather forecast data (0.25°) were downloaded from the Global Forecast System (GFS) product inventory twice per week (http://www.nco.ncep.noaa.gov/pmb/products/gfs/). For land surface model predictions and irrigation scheduling from Monday to Wednesday the GFS-forecast from Sunday was used, whereas for land surface model predictions and irrigation scheduling from Thursday to Sunday the forecast from Wednesday was taken. One GFS-pixel covers our complete simulation domain and was therefore applied to all CLM grid cells. The original GFS data were interpolated from 3-hour intervals to 1-hour intervals. In the irrigation scheduling campaign of 2016, irrigation was not applied if the forecasted precipitation amount was larger than 5 mm.

3.2.4 Stem water potential, deep soil water content measurements and production data

We had three independent data sources to evaluate water stress by the trees: (i) stem water potential measurements, (ii) deep soil water content measurements, and (iii) production data. These sources of information will be discussed in addition.

During the irrigation campaign, stem water potential (SWP) was measured with pressure chamber equipment (Model 600 Pressure Chamber, PMS Instrument Company, Albahy, USA) by following the method descried by Turner (1981). Even though the stem water potential has no direct quantitative relation with the soil water content, it is a sensitive indicator of crop water stress and can be used to evaluate the water deficit condition of the fields. In the irrigation periods, stem water potential was measured every 2 weeks at noon with a sample of

5 trees per field and 4 leaves per tree. They were chosen from at least three different emitter lines and always including the tree where the FDR probe was placed. After 2 hours in the plastic bag, leaf water potential will be equal to the stem water potential. Then the leaves were sealed into the air chamber with a part of petiole exposed outside. The increased air pressure that makes water coming out from the cut surface of petiole is considered as the water tension within the leaves. The measured value of water potential is normally negative, which symbolizes the level of water stress and water deficit of the plants. Low stem water potential may cause the closure of stomata, the commonly used threshold is -1.5 MPa (Blonquist et al. 2006).

Soil water content measured by FDR sensors at 50 cm and 70 cm depth was not used in the data assimilation, but was used as a further indicator of possible water stress. The drop of deep soil water content in the irrigation season is linked to the possibility that not enough drip irrigation is applied.

The fruit production data for each field were also collected at the end of the season to support the evaluation. The production is the commercial yield that farmers sold to cooperatives. Unfortunately, not for all fields production data could be obtained as not all farmers collected this information. Reduced fruit production can be another indicator of the existence of water stress during the past growing season, but there are other possible explanations for a relatively small fruit production not related to drought stress.

3.2.5 Statistical analysis of the performance of the irrigation scheduling methods

The predictions by the models were evaluated by the Root Mean Square Error (RMSE) according to:

$$\mathrm{RMSE} = \sqrt{\frac{\sum_{t=1}^{n}(\theta_m - \theta_s)^2}{n}} \tag{3.9}$$

where θ_m is the CLM modeled soil water content, θ_s soil water content measured by FDR probes and n is the number of time steps within the modelling period.

In order to explore the efficiency of the CLM-DA based irrigation, the irrigation amounts for the different fields (CLM-DA method, FAO-method and Farmer approach) were compared. The applied water volume was divided by the area (m^2) of each field, and the water depth (mm) for each irrigation day was calculated. Possible drought stress was analysed with help

of the data from the stem water potential campaigns, fruit production measured at the end of the season and measured soil water content at 50 cm and 70 cm depth, which were not assimilated.

Integrated stem water potential (ISWP) was calculated based on the following function (García-Tejero et al. 2010):

$$\text{ISWP} = \sum_{i=1}^{i=t} P_{i+1}(n_{i+1} - n_i) + \frac{1}{2}(P_i - P_{i+1})(n_{i+1} - n_i) \quad (3.10)$$

where P_i and P_{i+1} are midday stem water potential measurements at day i and day i+1 day, $(n_{i+1} - n_i)$ is the interval in days between two measurements (14 days for our fields).

We also calculated the Seasonal Irrigation Performance Indicator (SIPI) for the period July-September, which is potentially most affected by drought stress, for the years 2015 and 2016. SIPI is an indicator for the water saving performance of each irrigation method. It was calculated as ratio between actual evapotranspiration (ET_C) and the incoming water flux (irrigation water and rainfall) in the same period. Therefore, irrigation amount and ET_0 and ET_C were determined for these periods, with K_C factor derived by the method in section 3.2.2.

A statistical analysis was performed on the basis of measured integrated stem water potentials, soil water contents, irrigation amount, commercial fruit production and irrigation performance index. We calculated Pearson correlation coefficients between variables, and analysed (linear) relationships between variables.

3.3 Results and discussion

3.3.1 Selection of the fields for evaluation in 2015 and 2016

Three CLM fields (CLM-D, CLM-E, CLM-F) were excluded from the analysis in 2015, as for those fields the scheduled irrigation scheme was not followed. Figure 3.2 illustrates the comparison between scheduled and real-applied irrigation amounts, including the three inconsistent CLM fields. In two cases the farmers did not follow the recommended irrigation amount, and in one case flow velocity in the irrigation system differed significantly from the anticipated value. In all cases, more irrigation was applied than planned as shown in Figure 3.2.

For the irrigation period 2016, again three CLM fields (CLM-A, CLM-C, CLM-F) were excluded from the analysis. The soil moisture sensor for field CLM-C showed permanently saturated conditions and the FDR sensor for field CLM-A broke one month after the start of irrigation scheduling. The experiment in field CLM-F was aborted by the request of the field owner in the middle of August, as he was worried that our irrigation scheduling scheme could compromise the production. However, neither stem water potential measurements nor visual inspections at site indicated drought stress. The other three CLM fields (CLM-B, CLM-D, CLM-E) followed the CLM-DA irrigation scheduling scheme, with applied irrigation amounts close to the calculated amounts most of the time. This is also related to the fact that in 2016 water flow speeds were re-calculated on the basis of a near real-time comparison of scheduled and applied irrigation amounts, and corrected if necessary. The real applied irrigation amounts for field CLM-D in June and July were smaller than the calculated one, as the administrator of the irrigation system accidentally stopped the irrigation on some days in this period.

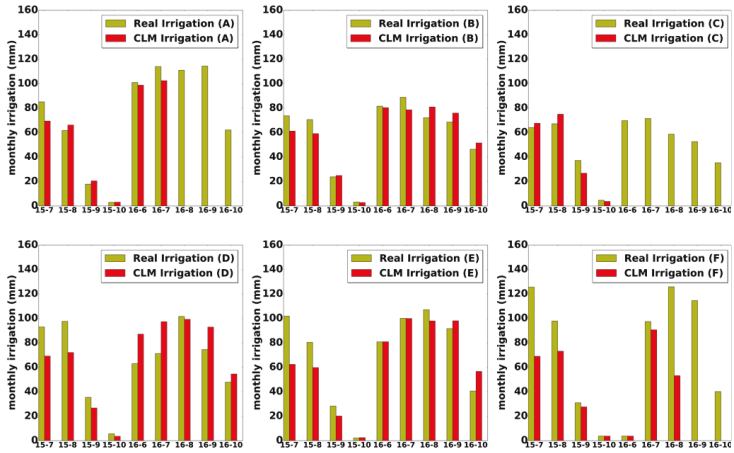

Figure 3.2 Comparison of irrigation amounts calculated for CLM-DA and truly applied irrigation amounts for all CLM-DA (A~F) fields in 2015 and 2016.

3.3.2 The forecasted precipitation

The irrigation prediction for the next few days is also dependent on the accuracy of the weather forecast, in particular the amount of precipitation. Figure 3.3 compares the forecasted and observed precipitation for the site. Mostly, the forecasted precipitation is higher than the observed one. Nevertheless, most of the precipitation events were predicted by GFS. In the irrigation period from July to October in 2015, the sum of the forecasted precipitation amount was 328mm, compared to a measured amount of 193mm. From June to October 2016, the sum of the forecasted precipitation amount was 156mm, compared to a measured amount of 100mm.

In October (both in 2015 and 2016) the forecasted precipitation was much higher than the observed one. The forecast biases in 2015 and 2016 were mainly related to October. In October, larger precipitation amounts are related to mesoscale systems which form over the relatively warm Mediterranean Sea and it seems that the prediction of the precipitation associated with those systems was more difficult.

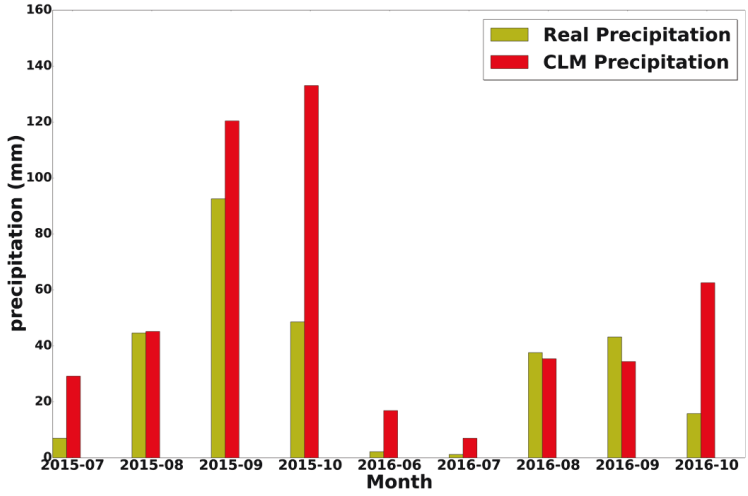

Figure 3.3 Comparison of forecasted (CLM Precipitation) and measured (Real Precipitation) monthly precipitation for 2015 and 2016.

3.3.3 Stem water potential and deep layer soil water content data for the evaluation of water stress

Previous research for citrus trees suggested that the minimum water potential value at wilting point can be down to -1.7 MPa for young leaves, and -1.9 MPa to -2.6 MPa for mature leaves (Syvertsen et al. 1981; Syvertsen 1982). It is also reported that citrus trees under regulated deficit irrigation can have a threshold stem water potential of -1.84 MPa (Ballester et al. 2014). So we got the conclusion that if stem water potential is lower than -1.8 MPa a negative impact on citrus trees is expected. As shown in Figure 3.4, in 2015 two of the CLM-DA fields (CLM-A, CLM-B) may have experienced water stress at one measurement day in August, and this was also the case for one FAO field (FAO-B). This water stress might be related to the high water vapor pressure deficit that day, which might have resulted in stomata closure irrespective of irrigation amount and soil water status (Ballester et al. 2011). From June to October in 2016, Figure 3.4 indicates the possible water stress in July for field CLM-D, related to irrigation scheduling which did not follow the CLM-DA suggestions and was too low. At the end of October, with the harvest season coming for some fields and given predicted precipitation events, the irrigation was stopped by the technicians resulting again in drought stress. In all other cases there was no drought stress according to these measurements.

As shown in Figure 3.5, soil water measured at 50 cm and 70 cm depth for the three CLM fields did not show a decreasing trend over the irrigation season in 2016, which implies that irrigation was not too small, which would cause decrease of soil water contents. Soil water contents measured at 50 cm and 70 cm depth for the fields irrigated according the FAO and Farmer methods did not show a decreasing trend either.

3.3.4 Statistical analysis

3.3.4(a) Validation of the CLM-DA system

The observed and modelled soil water contents (SWC) at 10 and 30 cm depth for one of the CLM fields are shown in Figure 3.6. The assimilation of FDR measurements significantly improved the SWC-characterization at 10 and 30 cm depth. Table 3.2 illustrates that the RMSE for SWC at 10 and 30 cm depth is smaller than 0.04 cm^3/cm^3 for all the 6 fields in 2015. However, some of the fields show a relatively high RMSE compared to others. As only states but no parameters were updated, a systematic bias of soil properties can be expected, affecting also soil water contents.

Unfortunately, for the experiments in 2016 three CLM-DA experiments could not be considered in the analysis as discussed in section 3.3.1. Therefore, the RMSE of SWC for those fields could not be calculated and is symbolized as N.A. in Table 3.2.

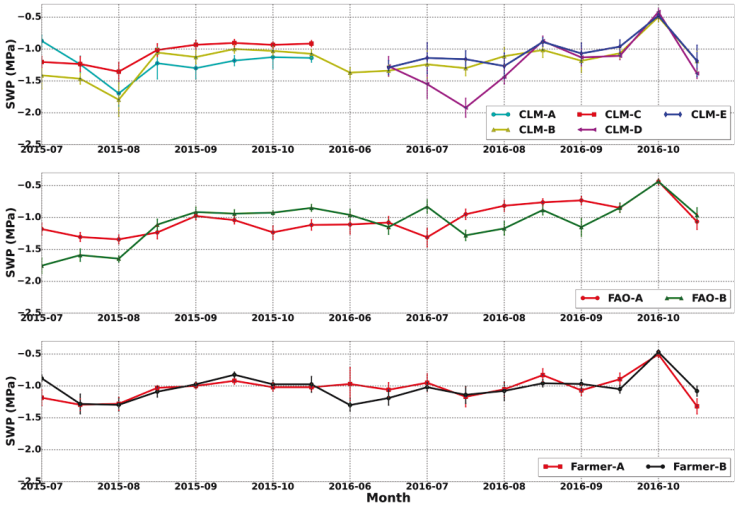

Figure 3.4 Stem water potential measurements (including error bars for standard deviation) for CLM fields, FAO fields and Farmer fields in 2015 and 2016.

Table 3.2 Comparison of RMSE (cm^3/cm^3) between simulated and measured SWC for the CLM fields (N.A. is no data).

Fields	CLM-A	CLM-B	CLM-C	CLM-D	CLM-E	CLM-F
2015	0.02	0.022	0.04	0.034	0.03	0.025
2016	N.A.	0.037	N.A.	0.021	0.031	N.A.

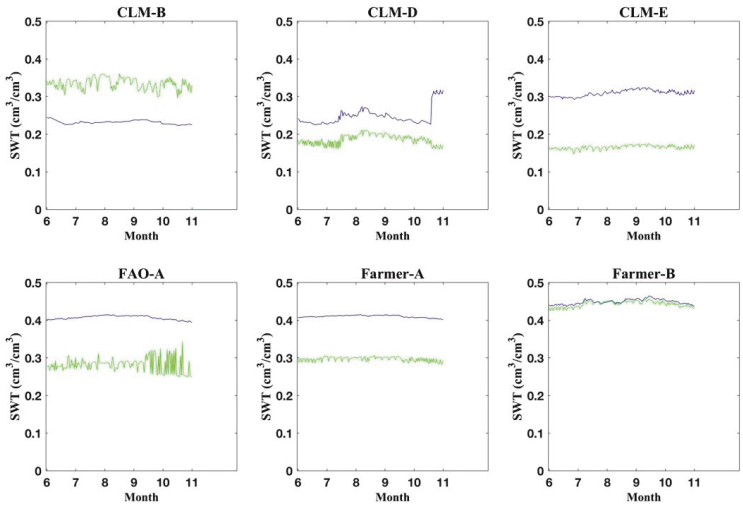

Figure 3.5 Soil water content (SWC) measurements at 50 cm (green line) and 70 cm (blue line) depth for the CLM fields, FAO fields and Farmer fields in 2016. These measurements were not used in the assimilation.

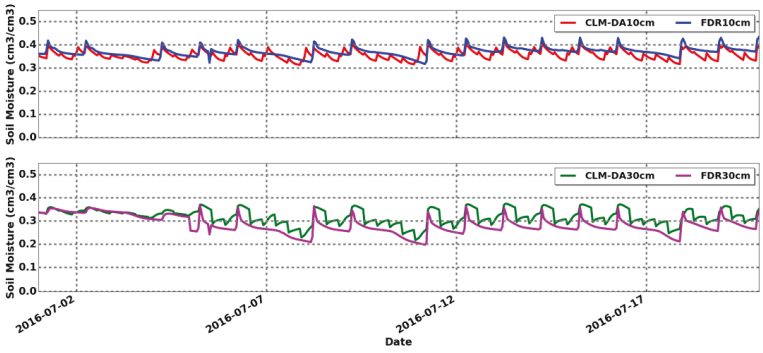

Figure 3.6 Comparison of soil water content modelled by CLM and measured by FDR (field CLM-B) at 10 cm and 30 cm depth for the year 2016.

3.3.4(b) Water consumption data and irrigation performance

Irrigation records for the three irrigation scheduling methods are presented in Table 3.3 and Figures 3.7 and 3.8. Overall, the CLM fields were irrigated with a smaller water amount than the Farmer fields. In 2015 the water saving performance was even better than the FAO

method (9% less irrigation water for CLM than for FAO and 21% less for CLM than for Farmer fields). Table 3.3 shows that in average the accumulated irrigation depths in 2016 are slightly larger for the CLM-DA fields (341 mm) than for the fields following the FAO method (337mm), but again smaller than for the Farmer fields (424 mm). The averaged seasonal irrigation performance index (SIPI) for 3 CLM fields in 2015 was larger than for the FAO fields (0.71 for CLM and 0.64 for FAO), suggesting better water saving performance. In 2016 the averaged SIPI for CLM and FAO fields showed no differences (both are 0.66), and were both larger than for the Farmer fields (0.56).

Taking the average over both years and the three months of July, August and September, the CLM fields received 24% less irrigation water than the fields irrigated according the Farmer method, while the FAO fields were irrigated with 22% less water than the Farmer method. Meanwhile, the fruit production data showed that the CLM fields had a slightly smaller production, but given the large variation between the fields this is not significant. In 2016, due to heavy precipitation and strong winds in the harvest period (November and December), all the fields suffered production loss irrespective of the irrigation method.

Figure 3.7 shows that the irrigation amounts vary less between the different months for the CLM fields than for the FAO fields. Although the differences in irrigation amount between the fields are large, all the fields show a similar trend in the monthly irrigation amounts, with largest irrigation amounts for the months of June until August.

The temporal dynamics of irrigation depth, ET_0, ET_C and precipitation for the different fields which are irrigated according different methods are displayed in Figure 3.8 (except CLM-fieds which were excluded from the analysis, see section 3.3.1). The daily maximum temperature (T_{max}), minimum temperature (T_{min}), ET_C and precipitation were also shown in Figure 3.8. The ET_C was calculated by meteorological data assuming a K_C factor of 0.68, a typical value for citrus tree. Precipitation amounts were lower in 2015 resulting in a higher irrigation demand than in 2016 for all fields, irrespective of the irrigation method. In particular the larger amounts of precipitation in September and October 2015 resulted in a temporary irrigation stop and the overall smaller applied irrigation amounts than in 2016.

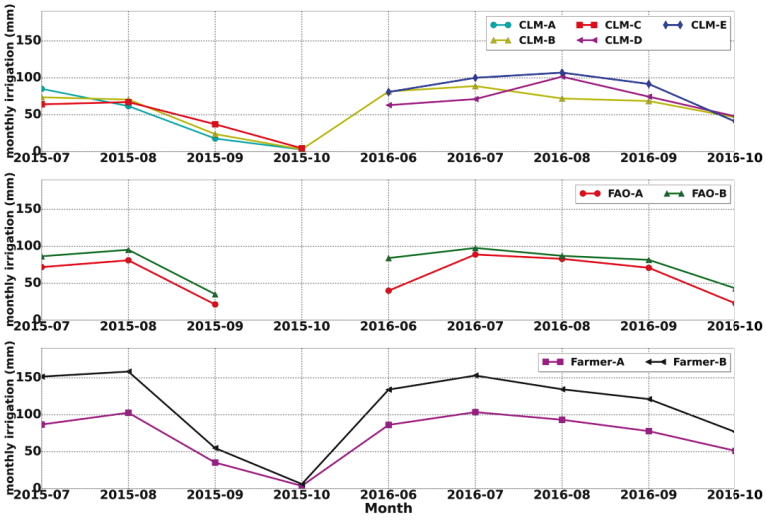

Figure 3.7 Comparison of monthly applied irrigation amounts for the different fields according different irrigation scheduling methods in 2015 and 2016.

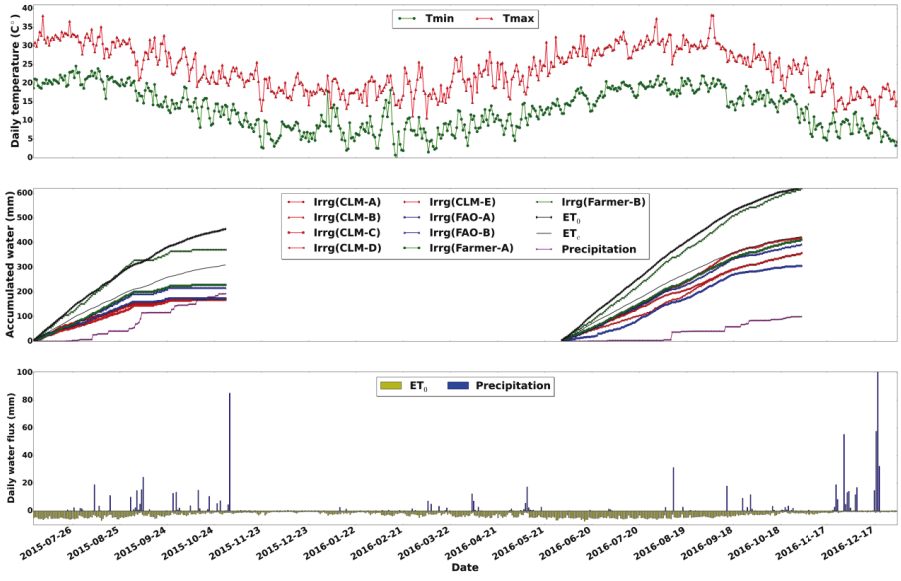

Figure 3.8 Temporal variation of maximum (T_{max}) and minimum (T_{min}) daily temperature of 2015 and 2016 (upper); accumulated irrigation depth (Irrg), ET_0, ET_c and precipitation for CLM fields, FAO fields and other Farmer fields during the irrigation scheduling periods of 2015 and 2016 (middle); daily ET_c and precipitation (bottom).

Table 3.3 The summary of accumulated water depth (including irrigation and precipitation), integrated stem water potential (ISWP), FDR soil water content averaged by 10 cm and 30 cm measurements (SWC), seasonal irrigation performance index (SIPI) and commercial fruit production (yield) for 3 CLM fields, 2 FAO fields and 2 Farmer fields in both year of 2015, 2016.

Fields	SWC15 (cm^3/cm^3)	SWC16 (cm^3/cm^3)	ISWP15 (MPa)	ISWP16 (MPa)	water depth15 (mm)	water depth16 (mm)	SIPI 15	SIPI 16	yield (ton/h)15	yield (ton/h)16
CLM-A	0.29	0.28	-90.78	-83.80	308.96	421.41	0.56	0.42	43.85	35.32
CLM-B	0.3	0.32	-93.06	-92.01	312.42	311.57	0.79	0.81	38.78	14.54
CLM-C	0.36	0.37	-78.29	-74.75	312.74	264.8	0.77	0.93	29.32	28.88
CLM-D	0.21	0.25	-88.94	-104.71	370.35	329.44	0.55	0.64	11.55	N.A.
CLM-E	0.22	0.23	-90.70	-86.49	354.9	380.86	0.56	0.53	19.54	N.A.
CLM-F	0.34	0.35	-60.66	-68.98	398.76	419.95	0.5	0.49	27.53	25.85
FAO-A	0.28	0.31	-83.61	-69.91	318.37	324.87	0.65	0.65	36.5	35.01
FAO-B	0.2	0.22	-92.54	-83.88	361.15	348.48	0.63	0.67	50.37	N.A.
Farmer-A	0.36	0.37	-79.21	-80.71	369.03	356.58	0.61	0.65	30.61	30.71
Farmer-B	0.34	0.36	-76.96	-83.40	509.16	490.77	0.45	0.48	27.68	14.99

3.3.4(c) Validation of the CLM-DA system

Table 3.4 shows the correlations between different variables determined at the irrigated fields. The table shows that only two pairs of variables show larger absolute correlation coefficients: (i) SWC and ISWP, and (ii) SIPI and accumulated water depth, simply because SIPI was calculated based on incoming water depth and ET.

We could not find significant correlations between fruit production and other environmental variables. This shows that SWC and ISWP were still in a range without or very limited drought stress, so that production is not affected by those conditions. In addition, commercial fruit production was affected by other conditions like heavy rain and wind late in the season in 2016, which might have impacted the different fields to a different degree, and which adds additional noise in the relation between fruit production and other variables. Further variables of relevance are the citrus variety and the management by the farmers which differed between

the fields and also might have affected production. In summary, it can be concluded that irrigation according the CLM-DA methodology did not reduce fruit production, and fruit production showed larger variations between fields related to other variables than SWC and ISWP.

Table 3.4 Correlation matrix between different variables determined at the irrigated fields: average FDR soil water content measured at 10 cm and 30 cm depth (SWC), integrated stem water potential (ISWP), accumulated incoming water depth, seasonal irrigation performance index (SIPI) and commercial fruit production (yield).

	SWC	**ISWP**	**water depth**	**SIPI**	**yield**
SWC	1.00	0.61	-0.26	0.37	-0.07
ISWP	0.61	1.00	0.26	-0.12	-0.09
water depth	-0.26	0.26	1.00	-0.87	-0.11
SIPI	0.37	-0.12	-0.87	1.00	-0.03
yield	-0.07	-0.09	-0.11	-0.03	1.00

3.3.4(d) Soil water content - Stem water potential relation

As shown in Figure 3.9, the soil water contents at 10 cm and 30 cm depth, show a significant linear correlation ($r = 0.61$) with integrated stem water potential. This implies that plant water stress can be monitored with help of soil water content measurements at 10 cm and 30 cm depth.

3.3.4(e) Soil water content - Incoming water depth relation

The incoming water depth is the applied irrigation plus the precipitation and it is calculated for each field. Figure 3.10 shows that for the CLM and FAO-fields there is a relation between average SWC and incoming water depth. The incoming water depth is higher for fields with a low SWC, which illustrates that irrigation is especially needed for drier fields. It also illustrates that the irrigation amount was not too large, as the fields which are most intensively irrigated still have an average SWC smaller than other fields. This is not the case for the Farmer fields where average SWC is very high and the incoming water depth is also very high. It is clear that for those fields the high irrigation amounts resulted in high SWC reaching saturation.

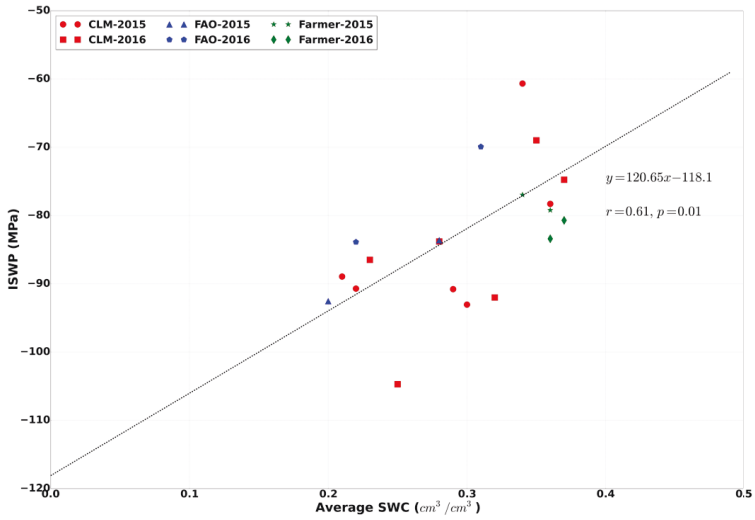

Figure 3.9 Relation between integrated stem water potential (ISWP) and soil water content measurements at 10 cm and 30 cm (Average SWC) depth for all fields and both the years 2015 and 2016.

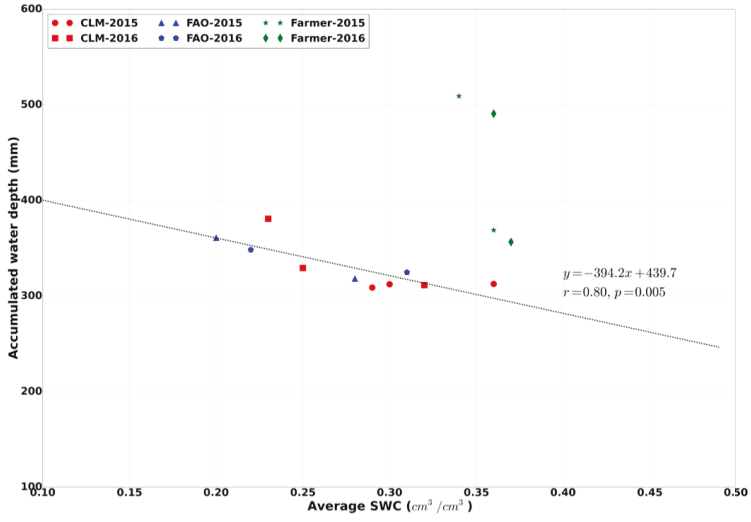

Figure 3.10 Relation between accumulated water depth (irrigation + rainfall) and average soil water content measurements at 10 cm and 30 cm depth (Average SWC) for all fields and both the years 2015 and 2016.

3.4 Conclusions and outlook

During the irrigation campaign for the Picassent site (near Valencia, Spain) from July to October in 2015 and June to October in 2016, three different irrigation scheduling methods were tested for 10 citrus fields, including the CLM-DA method proposed in this paper, the FAO water balance model and a traditional method based on farmer's experience. The CLM-DA method combines model predictions by a land surface model, weather prediction and soil moisture data measured by capacitance probes. These information sources are optimally combined using sequential data assimilation, to predict drought stress for the next days and schedule irrigation accordingly.

The applied irrigation amounts were measured by a water meter. Stem water potential and citrus production indicating the possible water stress were also measured. The results illustrate the water saving potential of the CLM-DA method compared to traditional irrigation by farmers. The data from the different fields indicate that 24 % less irrigation water was needed than the irrigation scheduling according the Farmer method. The stem water potential and deep soil water content data showed that during most of the irrigation period, CLM fields were not suffering from water stress. Although using less water than the farmer fields, no significant production loss was detected. The FAO method is also an efficient irrigation scheduling approach but it is highly dependent on site-specific empirical parameters.

A statistical analysis of all data collected in the field campaign revealed a positive correlation between SWC and integrated stem water potential data. This illustrates that SWC-data measured at 10 cm and 30 cm depth are useful to detect plant drought stress and can be used as basis to schedule irrigation. It was also found that for the CLM and FAO-fields, the applied amount of irrigation correlated negatively with SWC, illustrating that drier fields needed more irrigation and that it was the low SWC that governed irrigation amounts. On the contrary, for the fields that were irrigated according the Farmers method high average SWC was associated with very high irrigation amounts, indicating that for those fields the causal relation was different from the CLM- and FAO-fields; for the Farmer fields the high irrigation resulted in high SWC close to saturation. The statistical analysis also revealed no significant relation between SWC and ISWP on one hand and fruit production on the other hand, indicating that for the range of SWC and ISWP in this study, SWC and drought stress were not limiting factors for fruit production.

Comparing the CLM-, and FAO-methods, a similar performance was found in this study. It should be taken into account that the FAO-method was an established methodology for these fields and parameter settings were already tuned for this approach. Therefore the performance of the CLM-DA approach can be considered satisfying. The main differences between the two methods are the more complex and biophysically based model used in the CLM-DA method, the use of measurements in near real time to actualize the model state (while the FAO-method does not include those) and the use of a weather forecast. It is expected that the CLM-DA method will outperform the FAO-method if more measurements and better weather forecast data are available, if weather conditions are less stable and if the model is well calibrated on the basis of locally available data.

In summary, a rational, automated approach for irrigation scheduling was formulated with high potential in terms of integrating on-line data from sensors. The advantage of the CLM-DA method is automatic remote control, real time response, and the possibility to integrate all kinds of soil moisture and other data into a model. For example, this approach would also allow the integration of land surface temperature measured at high resolution by drones.

Nevertheless, the real-world application of this method is challenging. The accurate application of the calculated irrigation water to the fields was one of the challenges requiring intensive cooperation with farmers and continuous maintenance of the measurement infrastructure (e.g. soil moisture sensors). Irrigation scheduling could have been further improved with additional data which would have allowed the estimation of parameters specific for citrus trees as well as a better definition of the critical soil moisture threshold.

Chapter 4 : Can drip irrigation be scheduled with Cosmic-ray Neutron Sensing?

*adapted from: Li, D., Schrön, M., Köhli, M., Bogena, H., Weimar J., Jiménez-Bello, M. A., Han, X., Martínez Gimeno, M. A., Zacharias, S., Vereecken, H., and Hendricks Franssen, H.-J., 2019. Can drip irrigation be scheduled with Cosmic-ray Neutron Sensing? Vadose Zone Journal, 18(1). doi: 10.2136/vzj2019.05.0053.

4.1 Introduction

Irrigated agriculture plays a vital role in the food production to support the increasing world population. Irrigation is responsible for 70 % of the fresh water consumption by mankind (Vereecken et al. 2009). In order to save water resources and to fulfil future crop production requirements, more efficient irrigation scheduling is needed. The irrigation scheduling approach can be applied based on the difference between root-zone soil water content (SWC, cm^3/cm^3) and a target soil water content that is related to the specific plant preferences (Evans et al. 1991).

Many devices can provide information about soil water content, such as Time Domain Transmissivity (TDT), Frequency Domain Reflectometry (FDR) (Peters et al. 2013), tensiometers (Smajstrla and Locascio 1996), capacitance probes (Fares and Alva 2000) and Cosmic-ray Neutron Sensing probe (Zreda et al. 2012). The Cosmic-ray Neutron Sensing (CRNS) probe can be used to measure soil water content up to depths of 80 cm and with a footprint radius ranging from 130 m to 240 m at sea level (Köhli et al. 2015). Cosmic radiation originates from extrasolar sources and penetrates the atmosphere of the Earth. This interaction creates high-energy neutrons which further collide with atoms in the air, soil, and vegetation to produce medium-energy neutrons (Zreda et al. 2012). Those neutrons can be efficiently moderated towards lower energies by collisions with hydrogen. Therefore, the intensity of medium-energy neutrons is an indication for the amount of hydrogen atoms at the land surface and its temporal variation. The medium-energy neutrons, which can be detected by the CRNS probe, travel hundreds of meters in air and tens of decimeters in the soil. Hence, the advantage of the CRNS method is its ability to determine soil water states over larger areas and deeper soil layers, non-invasively, with low maintenance, and at a smaller cost compared to traditional soil moisture sensors.

To properly understand the neutron signal and its dependence on the integral soil water content, many attempts have been made to model the neutron response with Monte Carlo

codes (Desilets et al. 2010; Zreda et al. 2012; Franz et al. 2013). In 2015, the neutron transport model URANOS (Ultra Rapid Neutron-Only Simulation) (Köhli et al. 2015; 2018) was developed to reduce the number of model assumptions and make easy-to-use neutron simulations available for hydrological and soil science communities. Since then, the revised model results have been confirmed in many experimental studies (Heidbüchel et al. 2016; Schattan et al. 2018; Schrön et al. 2017; 2018a; 2018b; Fersch et al. 2018). The footprint is a function of air pressure, soil moisture, and air humidity, and is also slightly affected by the vegetation cover (Köhli et al. 2015). For typical wet soils the measurement depth is about 15 cm, while 86 % of the measured neutrons originate from within a circle with a diameter of about 400 m (Köhli et al. 2015). In dry soils, the measurement depth can go down to 80 cm and the diameter to more than 500 m at sea level. The above-ground neutron density is affected by changes of cosmic-ray intensity and by additional hydrogen sources, such as biomass and lattice water (Andreasen et al. 2017; Schreiner-McGraw et al. 2016; Baatz et al. 2015). Standard procedures are available to correct these effects.

The accuracy of CRNS retrieved soil water content has been verified in many investigations (Zreda et al. 2012; Han et al. 2014b; Zhu et al. 2015; Hawdon et al. 2014; Schrön et al. 2018b). Earlier work allowed improving the interpretation of measured neutron signals by CRNS for wet ecosystems, which showed that soil water content could be estimated with an error of 0.03 cm^3/cm^3 (Bogena et al. 2013; Baatz et al. 2014). Other studies demonstrated, that reliable estimates of soil moisture with standard CRNS probes under humid conditions at sea level can only be achieved for integration times equal or larger than 6 hours (Schrön et al. 2018b).

Drip irrigation is a localized irrigation method that allows water to drip slowly to the plant roots to save water and fertilizer input. Drip irrigation is associated with strongly heterogeneous soil water content, with relatively small irrigated wet patches and larger non-irrigated dry area. The research of Li et al. (2018) has demonstrated the possibility of drip irrigation scheduling based on FDR soil water content measurements in the irrigated part. The limited number of FDR sensors and the FDR sensor's limited measurement volume (FDR footprint) has imposed considerable uncertainties regarding soil water content estimates for the small wet patches, so that the estimate of soil water deficit for the whole field is also uncertain. This in turn makes it challenging to schedule the amount of drip irrigation water needed for the plants located on the wet patches.

As CRNS is able to estimate soil water change for a relatively large footprint, some past research was dedicated to the use of the CRNS for irrigation scheduling. Barker et al. (2017) investigated the optimal number and locations of CRNS probe for irrigation management. Han et al. (2016b) tested the assimilation of synthetic neutron intensity data to improve land surface modelling with the Community Land Model (CLM) and to do real-time drip irrigation scheduling. None of these studies applied CRNS data in a real-world case study for drip irrigation scheduling.

Our research question is to what extent the CRNS can be used for the scheduling of drip irrigation amounts by using measured neutron intensity as a proxy for root-zone soil water content. This work aims to test the measurement precision of the CRNS in a drip-irrigated field and to evaluate whether it is sufficient to support drip irrigation management. The work relies on both, field experimentation and modelling of neutron intensity. A field calibration campaign was carried out for the drip irrigated Picassent site in Spain. The neutron transfer model (URANOS) was used to model the neutron response to the drip irrigated citrus fields and to explore the potential of the CRNS method to detect drip irrigation events.

4.2 Materials and methods

4.2.1 Research sites and measurements

The research site is an area with drip irrigated citrus fields located close to Picassent in Spain (39.38° N, 0.47° E), which is a semi-arid region. Precipitation is concentrated in the autumn, winter and spring, and the yearly average precipitation is 453 mm (Li et al. 2018). Citrus is one of the most productive fruit plants in the world. The growing of citrus needs abundant sunlight and adequate rainfall or irrigation. Citrus trees flower in spring; fruits develop afterwards and ripen in fall or early winter. Precipitation during the main growth period of citrus fruit in summer is rare and therefore the water demand of the trees almost entirely depends on irrigation.

Drip irrigation is being used to schedule irrigation for these citrus tree fields, with two pipelines (1 m distance) and 10 emitters for each tree. The emitters in the study area are mostly integrated pressure compensating type, with a common flow rate of 4 L/h. All the emitters are surface placed every meter without mulch cover. The trees are separated by 5 m from each other, both along the planted lines and between these lines, see also descriptions in Li et al. (2018). The meteorology observatory of IVIA (Instituto Valenciano de

Investigaciones Agrarias) provides meteorological data and is located 2868m from the CRNS-probe (http://riegos.ivia.es/). During most irrigation periods, drip irrigation was applied five or six times per week. From October onwards, depending on the weather and fruit maturation process, irrigation frequency was reduced and finally stopped. Due to drip irrigation, the soil water status of the land surface is very heterogeneous. The field can be divided into wet patches (irrigated parts) and dry patches (the rest of the field). The areal contribution of the drip irrigated part to the whole area is small and thus the SWC identification poses a challenge to the integral CRNS method.

As shown in Figure 4.1, we have installed a CRNS probe in the dry patch between two drip lines (CRS1000, HydroInnova LLC, 2009) and various FDR probes at the test site. FDR probes (factory calibrated ENVIROSCAN Water-Content-Profile Probe, Campbell Scientific, Inc.) were installed in six irrigation plots within the footprint of the CRNS probe, measuring soil water content at four depths (10 cm, 30 cm, 50 cm, and 70 cm). Within a distance of 200 m from the CRNS probe, 4 FDR probes were installed to measure soil water content in the non-irrigated part of the area and 9 FDR probes were installed in the irrigated part of the area.

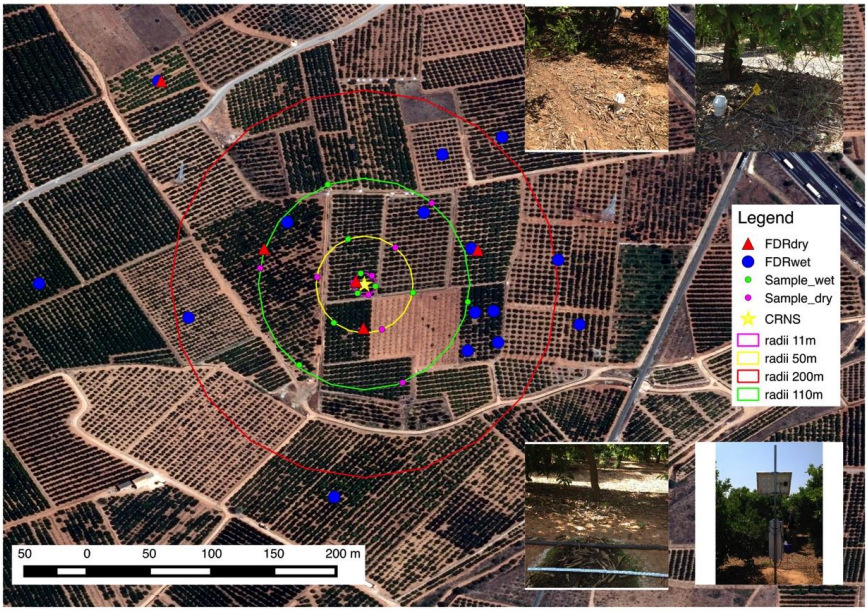

Figure 4.1 The distribution of FDR probes (for irrigated and non-irrigated area respectively), 18 soil samples for the CRNS-calibration and CRNS probe in the Picassent field, Spain. The radii of the circles are 11, 50, 110 and 200 meters. The small photographs show the installation of FDR in non-irrigated (upper left) and irrigated (upper right) area, as well as the shape of irrigated patch (lower left) and the installation position of CRNS (lower right).

4.2.2 Field sampling for CRNS calibration in Picassent

The CRNS probe needs to be calibrated with soil samples during a field campaign while neutron intensity is simultaneously measured by the CRNS probe. According to the new findings by Köhli et al. (2015) and Schrön et al. (2017), the area within a radius of less than 50 m from the CRNS probe has about the same contribution to the neutron signal as the remaining area beyond 50 m. In accordance with suggestions by Schrön et al. (2017), sampling radii for this study were chosen as 11 m, 50 m, and 110 m, where six sampling locations were evenly distributed along each circle. At each location, the soil was sampled at six layers separated by 5 cm between 0 cm and 30 cm depth.

Samples were taken using a soil corer of 30 cm length and 5 cm diameter (HUMAX, Martin Burch AG, Rothenburg, Switzerland) on June 1st, 2015. Half of the samples were taken in the wet and irrigated area (the green dots in Figure 4.1), and the other half in the dry, non-irrigated area (red dots in Figure 4.1). Each 30 cm long soil core was frozen and cut by 5 cm intervals, in order to obtain 6 layers for each sampling location. All the 108 samples were dried in the oven for over 36 hours until the sample weight became stable. These samples have been averaged to get footprint soil water content taking into account their distance to the CRNS probe by using a weighting function that corresponds to the neutron transport theory (see section 4.2.3).

Six soil samples (10 g), containing material from all six layers were also analysed in the lab for contents of lattice water and soil organic material. The lab analysis gave the organic and the inorganic carbon content (C_{org}, C), and the hydrogen content (by using a heat conductivity detector) and nitrogen content. The analysed hydrogen content was converted to water equivalents by multiplying with a ratio value of 9 (H_2:H_2O=1:9). From the analysed hydrogen content, all the weight of lattice and organic water was calculated and converted to volumetric content using the average soil bulk density value. The average volumetric lattice water and organic water content were found to be 0.04 cm^3/cm^3 in total.

4.2.3 Footprint soil water content from soil sampling and FDR sensor network

In order to obtain soil water content time series from CRNS probe, the FDR soil water content measurements need to be vertically and horizontally averaged using the weighting function from Schrön et al. (2017). The footprint soil water content from gravimetric

sampling was derived to do the calibration. Meanwhile the FDR sensors were also area averaged to get footprint SWC, which was used as verification data.

Our research site is composed of non-irrigated fields, which are typically drier, and areas that exhibit a heterogeneous soil moisture pattern due to drip irrigation. In order to account for this heterogeneous soil moisture pattern, we introduced the fraction of the irrigated area Fr_{wet} and calculated the weighted SWC for the wet part θ_{wet} and dry part θ_{dry} separately. Assuming the wet part fraction Fr_{wet} is the same across the whole CRNS footprint, the soil water content for the footprint θ_{total} can then be obtained as:

$$\theta_{\mathrm{total}} = \theta_{\mathrm{wet}} * Fr_{\mathrm{wet}} + \theta_{\mathrm{dry}} * (1 - Fr_{\mathrm{wet}}) \tag{4.1}$$

The measurements to determine the extent of the wet fraction were made before the soil sampling campaign. For each tree, there are two drip lines separated by 1 m in space. The dripping points along the drip line are separated with 1 m distance. Since the row distance and tree distance are 5 m, each tree occupies an area of 5 m × 5 m, among which there are 10 emitters. The average diameter (D) defines the wetted area for each dripping point. The fraction of the total drip-irrigated area (Fr_{wet}) is given then by:

$$Frg_{\mathrm{wet}} = 10 \cdot \frac{\pi \cdot (0.5 \cdot D)^2}{5 \cdot 5} \tag{4.2}$$

The weighting method proposed by Schrön et al. (2017) was used to obtain a weighted average soil moisture value from the point samples and FDR sensors. The vertical weight W_{d} for different soil layers at depth d can be calculated with the following empirical function (Schrön et al. 2017; Köhli et al. 2015):

$$W_{\mathrm{d}}(r, \theta) \propto e^{-2d/D_{86}(r,\theta)} \tag{4.3}$$

where the effective measurement depth D_{86} can be calculated from the distance to CRNS probe (r) and soil water content θ. Then the weighted average soil water content $< \theta_{\mathrm{k}} >$ from all the measurements (1~k) can be obtained by the weighting function (Köhli et al. 2015):

$$< \theta_{\mathrm{k}} > = \frac{\sum_k W_{\mathrm{k}} \cdot \theta_{\mathrm{k}}}{\sum_k W_{\mathrm{k}}} \tag{4.4}$$

An iterative approach was used to calculate the vertical weight of each layer, which means that the initial vertical soil water content was set equal to the average over all the six soil

samples taken by the HUMAX soil corer, and in case of FDR, to the average over the first two soil layers (10 cm and 30 cm depth). The representative depth of each soil sample was considered as the middle of this segment (e.g. 2.5 cm is the representative depth for the first segment).

The horizontal weights for each of the soil sampling points or FDR probes depend on the distance between the FDR probes and the CRNS probe, as well as the air humidity and soil water status in the footprint (Schrön et al. 2017). The average over all the profile soil samplings or FDR measurements using Equation 4.1 was taken as the initial soil water content for the footprint, and then the horizontal weights along with Equation 4.4 were used to get the new soil water content for the footprint in an iterative fashion.

4.2.4 Soil water content estimation from CRNS probe

The data used in the analysis are hourly neutron intensities measured by CRNS probe from June 1 2015 to December 31 2016 in Picassent. Besides neutron intensity, CRNS probe also records time, temperature, relative humidity and air pressure, which is used for data quality control and data pre-processing. Epithermal neutron count data have to be corrected for external influencing factors that are not related to soil water content. Neutron intensity data are normalized to reference air pressure (Zreda et al. 2012). In our case, it is the air pressure at the calibration day (June 1st, 2015).

The variation in the incoming neutron flux also needs to be corrected using the concurrent and reference high-energy neutron count rate during the research period (Zreda et al. 2012), which were provided by the Jungfraujoch neutron monitor station of the University of Bern (3-NM64, http://cosray.unibe.ch). The reference high-energy neutron count rate is the averaged value during the calibration day. The effect of atmospheric water vapor on epithermal neutron intensity was then corrected using the method described in (Rosolem et al. 2013), the reference absolute humidity value was set equal to the average value on the calibration day.

The so-called N_0 method was developed by Desilets et al. (2010) to estimate soil water content θ_v in the CRNS footprint as function of the neutron count rate N_{pih} through a simple calibration function. To calibrate the N_0 parameter, a single field calibration campaign was conducted as described in section 4.2.2.

$$\theta_{\mathrm{v}} = (a_0 \cdot \rho_{\mathrm{bd}}) \left(\frac{N_{\mathrm{pih}}}{N_0} - a_1\right)^{-1} - (a_2 \cdot \rho_{\mathrm{bd}}) - \theta_{\mathrm{lat}} - \theta_{\mathrm{org}} \quad (4.5)$$

where N_0 stands for the neutron intensity over dry soil at a specific test site and needs to be calibrated once; a_0=0.0808, a_1=0.372 and a_2=0.115 are constant fitting parameters. ρ_{bd} is soil bulk density (g/cm^3) averaged from all the soil samples taken on the calibration day (1.3 g/cm^3), it was calculated with an iterative method along with the weighting of soil water content for each layer. θ_{lat} is the volumetric lattice water (cm^3/cm^3) and θ_{org} is soil organic water equivalent (cm^3/cm^3).

4.2.5 Modelling of the neutron response to drip irrigation

The neutron response was simulated with URANOS (version 0.99rho) for the drip-irrigated field in Picassent to test the effect of drip irrigation on the neutron intensity at the CRNS location. The URANOS model simulates neutron interactions in a Monte Carlo framework, and was originally aimed for applications in nuclear physics (Köhli et al. 2018). Recently it has been used to model the interaction of cosmic-ray neutrons with air, soil and vegetation in order to understand neutron intensity measured by CRNS probe (Köhli et al. 2015).

URANOS was applied here on the SWC pattern caused by drip irrigation with a model resolution of 0.5 m. As shown in Figure 4.2, a typically irrigated domain of size 500 m × 500 m around the CRNS probe was divided into wet and dry grids as a simplified scenario, with wet grids of 1 m width interrupted by every 0.5 m (to mimic the irrigated wet patches) and larger dry patches of 4 m width between trees. The CRNS probe is located in the dry grid within the wet stripe.

The domain was further divided into two vertical layers; the bottom layer was 0.5 m thick soil and the above layer was vegetation with air in the canopy space. The canopy was described as blocks with 4 m diameter and 2 m thickness, while the stem height was 1 m. The biomass density in the upper layer was 10 kg/m^2, and the air humidity was 1.4 g/m^3, which were typical values for the study domain and based on measurements.

The URANOS model used two main scenarios for the non-irrigated area: SWC value of 0.14 cm^3/cm^3 and 0.05 cm^3/cm^3 for the non-irrigated part (with the 0.04 cm^3/cm^3 lattice water and organic carbon taking into consideration). Meanwhile the SWC values range between 0.10 cm^3/cm^3 and 0.45 cm^3/cm^3 for the irrigated part with steps of 0.05 cm^3/cm^3. Given this model set-up, we analysed the spatial distribution of neutron density and observed intensity with

regard to changing water content in the irrigated patches. The latter scenario is to test whether CRNS results differ under more arid conditions.

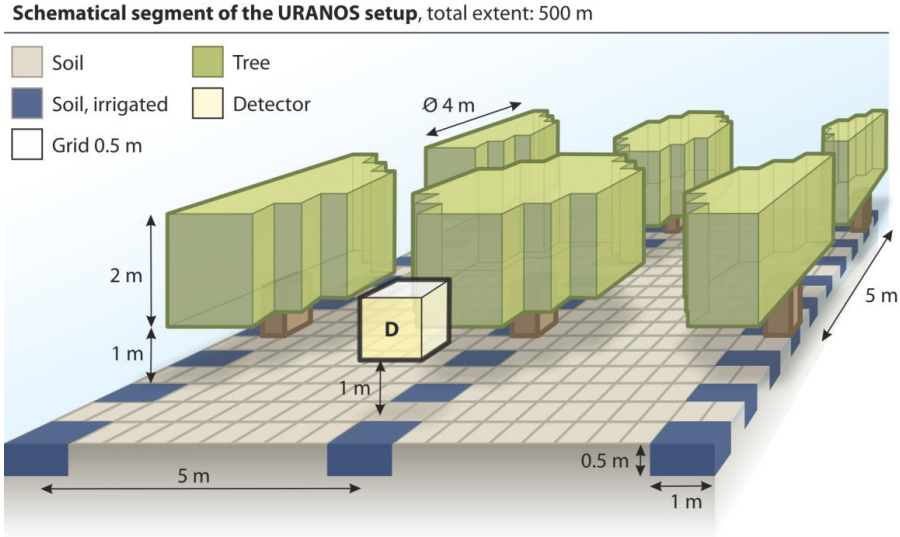

Figure 4.2 Neutron transfer model settings for the typical condition in Picassent, the blue grids correspond to the irrigated patches and gray grids correspond to the non-irrigated area; the green layer on the top is the simplified representation of the citrus vegetation cover including canopy and stem; the yellow cube symbolizes the CRNS detector.

4.2.6 Statistical analysis

The two time series (from June 1, 2015 to December 31, 2016 for Picassent) of footprint soil water content, calculated from neutron intensity data and derived from FDR probes, were compared by the Root Mean Square Error (RMSE), Pearson correlation coefficient (r) and Kling-Gupta efficiency (KGE) (Gupta et al. 2009):

$$RMSE = \sqrt{\frac{\sum_{t=1}^{n}(X_{1,t}-X_{2,t})^2}{n}} \tag{4.6}$$

$$r(X_1, X_2) = \frac{cov(X_1,X_2)}{\sigma_{X_1}\sigma_{X_1}} \tag{4.7}$$

$$KGE = 1 - \left[(r(X_1, X_2) - 1)^2 + \left(\frac{\sigma_{X_1}}{\sigma_{X_1}} - 1\right)^2 + \left(\frac{\mu_{X_1}}{\mu_{X_1}} - 1\right)^2\right]^{0.5} \tag{4.8}$$

where $X_1$is the soil water content estimated from neutron intensity measured by the CRNS probe, X_2 is the average soil water content in the CRNS footprint calculated from the FDR-probes, n is the number of time steps with measurements, and t indicates time step, $cov(X_1, X_2)$ is the covariance between X_1 and X_2, μ and σ represent the means and standard deviations of X_1 and X_2. In the ideal case, the best fit between X_1 and X_2 would reach RMSE = 0, r =1 and KGE = 1 (Gupta et al. 2009).

The daily maximum variation (*DEF*) of FDR soil water content was calculated on drip irrigation days to demonstrate the effect of irrigation on soil water content measured by FDR sensors.

$$DEF = \max\{\max(X_{\mathrm{d}}) - \min(X_{\mathrm{d}})\} \tag{4.9}$$

where $\max(X_{\mathrm{d}})$ and $\min(X_{\mathrm{d}})$ are the maximum and minimum daily soil water content averaged over all FDR sensors in the footprint, the average has been calculated every 10 minutes.

In addition, the normalized Standard Deviation (N_{std}) of CRNS neutron intensity was calculated to determine the CRNS measurement error. The hourly neutron intensity *N* and its uncertainty σ have a relation as described in Bogena et al. (2013) and Schrön et al. (2018b). σ is the standard deviation of *N* using Gaussian statistics; and N_{std} is the hourly normalized standard deviation of neutron count rate:

$$\sigma(N) = \sqrt{N} \tag{4.10}$$

$$N_{\mathrm{std}} = \sigma(N)/N = 1/\sqrt{N} \tag{4.11}$$

Also a statistical analysis was performed to analyse the linear correlation between measured soil water content and neutron intensity. The Pearson correlation coefficients were calculated for each month of 2016 to explore under which conditions the soil water content shows a stronger correlation with the CRNS measurements.

4.3 Results and discussion

4.3.1 Soil water content measurements from field sampling and FDR sensors

4.3.1(a) Area averaged soil water content from soil sampling and FDR

Table 4.1 illustrates that a typical wet patch created by drip irrigation has an average diameter (*D*) of 0.50 m. Given the measured dimensions of a typical wet patch, the overall percentage of wet fraction (Fr_{wet}) within the larger field is around 8 %. The wet fraction of 8 % is used for CRNS calibration using data from the soil sampling campaign in June 2015.

The vertical and horizontal weighted SWC for the irrigated and non-irrigated parts are shown in Figure 4.3, which demonstrates the effect of drip irrigation and precipitation on soil water content as measured by FDR sensors. For averaging soil water content horizontally, the relative proportions of the wet and dry fractions within the CRNS footprint are needed. Figure 4.3 shows the influence of the relative proportion of the irrigated, wet fraction (Fr_{wet}) on the spatial average of the FDR soil water content measurements. If the fraction of the wet, irrigated part in the CRNS footprint were larger, the apparent average soil water content of the CRNS footprint would also increase. The temporal evolution of soil water content for the CRNS footprint coincides with the soil water content for the non-irrigated dry part, and is strongly related to precipitation events. Due to the failure of FDR data from September to December in 2015, there was a data gap for this period.

Figure 4.4 demonstrates that the measured gravimetric soil water content for the dry, non-irrigated part is lower than the soil water content measured by FDR probes. It suggests the existence of a systematic bias between the gravimetric soil water content measurements and the FDR data. This can be related to the sampling volume as the gravimetric soil water content for the upper 10 cm has been determined by two sections of sampling profiles. For the non-irrigated part, the soil of the upper 5 cm is much drier than the soil at 5~10 cm depth based on soil sampling results, so that the FDR-based footprint soil water content (the shallowest layer measured at 10 cm depth) is higher than the gravimetric soil water content determined over the upper 10 cm. The found biases were constant so that a correction of -0.05 cm^3/cm^3 was added to the FDR derived foot print soil water content time series for the non-irrigated part and +0.01 cm^3/cm^3 for the irrigated part.

Table 4.1 Measurements of diameters of drip irrigated patches (and their average) in June 2015 in the close vicinity of the installed CRNS probe.

	Patch 1	Patch 1	Patch 3	Patch 4	Average
Diameter (cm)	50	49	46	54	50

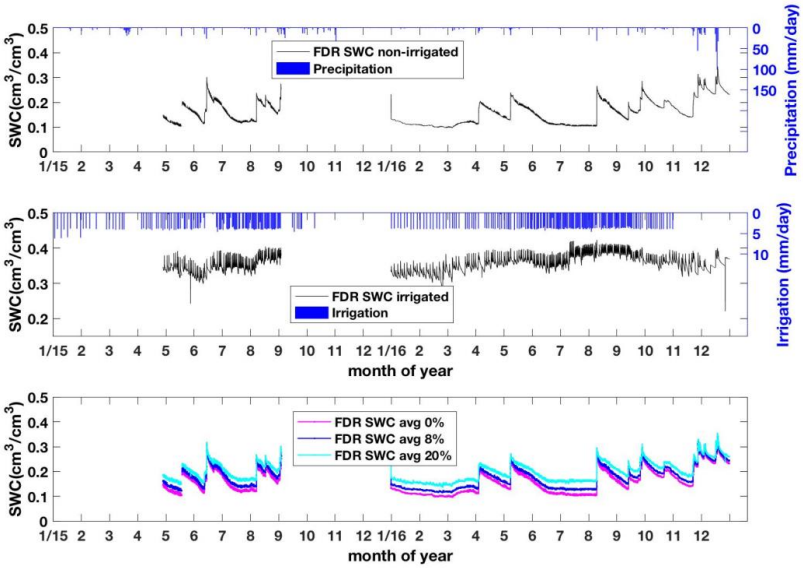

Figure 4.3 Area averaged soil water content of FDR sensors installed in the non-irrigated part (upper) and irrigated part (middle) for 2015 and 2016, together with precipitation and irrigation depths (cubic water amount divided by field area) of the field where CRNS was installed. The lower graph shows the averaged FDR soil water content in the CRNS footprint as function of different values for the wet (drip irrigated) fraction (0, 8 %, 20 %) within the footprint.

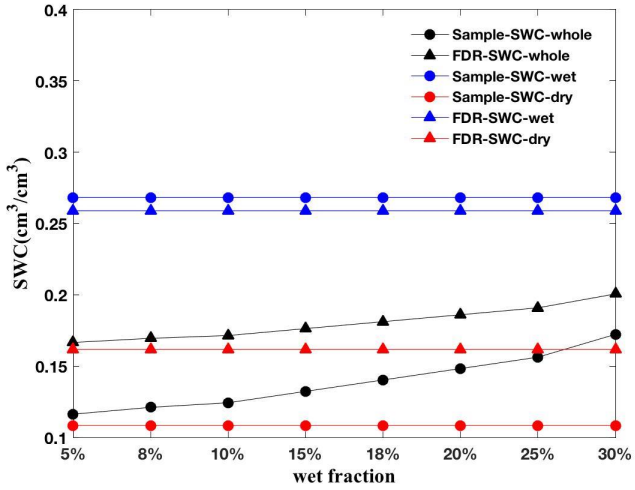

Figure 4.4 The footprint soil water content (black line) at the CRNS-calibration day in Picassent, calculated from both the soil sampling campaign and the installed FDR sensors. The averaged SWC for the irrigated part (blue) and non-irrigated part (red), from both the soil sampling and corresponding FDR data are also shown. The wet fraction on the X-axis is the drip-irrigated percentage in CRNS footprint.

4.3.1(b) FDR response to drip irrigation

Figure 4.5 shows the hourly soil water content averaged over all FDR sensors measured in the irrigated wet part. There is a daily cycle of soil water content on irrigation days for each month in 2016. The soil water content increased fast when irrigation started in the late night, but dropped to lower values close to pre-irrigation afterwards with a daily maximum variation smaller than 0.05 cm^3/cm^3 as shown in Table 4.2.

Table 4.2 The daily maximum variation range (*DEF*) of FDR soil water content (cm^3/cm^3) measured in the drip irrigated area during irrigation days, then averaged for each month, N.A. means no data.

	Jan	**Feb**	**Mar**	**Apr**	**May**	**Jun**	**Jul**	**Aug**	**Sep**	**Oct**	**Nov**	**Dec**
***DEF*(SWC)**	0.043	0.042	0.048	0.054	0.041	0.052	0.055	0.045	0.034	0.027	0.027	N.A.

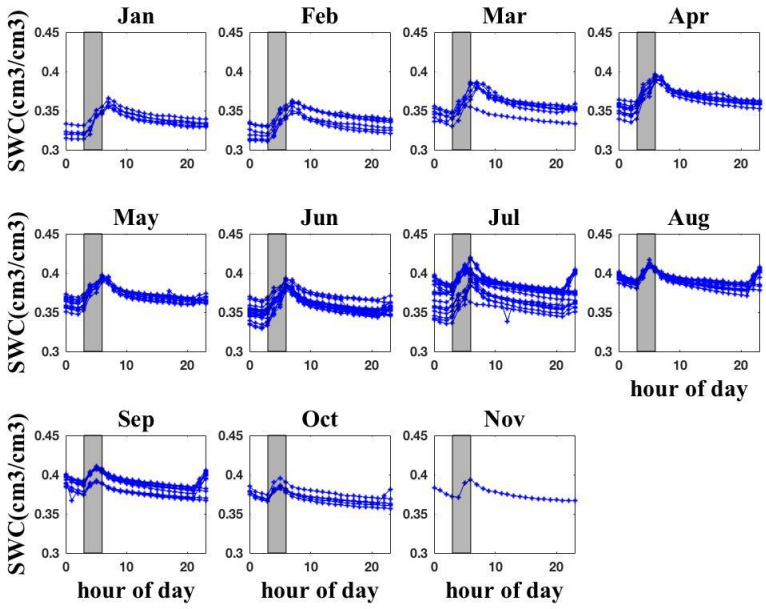

Figure 4.5 Hourly records of area averaged soil water content measured by FDR sensors installed in the irrigated wet part for all irrigation days and for different months (2016). The shadow area highlights the irrigation period (starts from 3 am and lasts 1~2 hours).

4.3.2 Soil water content inversion from CRNS for drip irrigated field

4.3.2(a) Neutron intensity measured by CRNS

The measured hourly and 12 hourly averaged neutron intensity data from June 2015 to December 2016 in Picassent were corrected for fluctuations in air pressure, variations in incoming neutron intensity, and variations in water vapor pressure of the air. Figure 4.6 shows the temporal evolution of the corrected neutron intensity and also illustrates that neutron intensity and precipitation are inversely correlated. Major rainfall events are associated with a rapid drop in neutron counting rate.

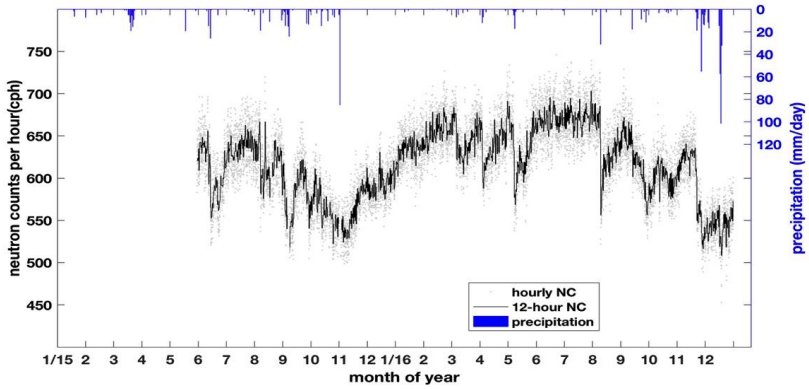

Figure 4.6 The corrected neutron intensity averaged for 1 hour and 12 hour intervals and daily precipitation amounts (meteorological data from IVIA) at the Picassent site in Spain from June 2015 to December 2016.

4.3.2(b) Relation between CRNS data and footprint soil water content

Figure 4.7 shows the correlation between the footprint soil water content calculated from FDR measurements (assuming a wet (irrigated) fraction of 8 %) and measured neutron intensity. Measured neutron intensity was averaged over a 24-hour interval. The results show weaker correlation coefficients between SWC and neutron count intensity (larger than -0.5) in February, March, June and July, when SWC is generally lower than in other months. The possible reason is that the effect of irrigation on neutron intensity is neutralized by strong evaporation in summer days resulting in limited SWC-fluctuations over time. The months with stronger (more negative) correlation exhibit days with higher SWC and therefore more variation in SWC, which is related to higher precipitation amounts in those months (Figure 4.6). This also indicates that the calibration curve will be better determined if data are available from days with more different SWC as suggested in previous research (Iwema et al. 2015).

As the duration of the drip irrigation was normally 1~2 hours, we also explored the relation between CRNS measurements and drip irrigation in an hourly time interval. However, the measured hourly neutron intensity did not show a clear trend related to applied drip irrigation (see Figure 4.8). The sampling fluctuations are also large, related to the short time period (hourly) for averaging neutron intensities. In order to determine the uncertainty of CRNS measurements, the hourly standard deviations (N_{std}) of CRNS measurements on irrigation days are shown in Table 4.3.

4.3.2(c) Inversion of CRNS soil water content by soil sampling calibration

The fitted calibration curve based on the N_0 method is given in Figure 4.9, and can be used to estimate soil water content from the measured neutron intensity. This curve is based on neutron intensity measurements averaged over 12-hour intervals. The footprint SWC calculated from the gravimetric soil sampling on June 1st 2015, was used to carry out the N_0 calibration, assuming the wet part fraction is 8 %. The FDR derived footprint SWC, over the years 2015 and 2016, were used as verification.

Figure 4.9 illustrates that the calibration curve fits well with FDR derived footprint SWC and corresponding neutron intensity. Figure 4.10 shows the estimated soil water content for the CRNS footprint for the years 2015 and 2016 with this method. The RMSE between CRNS and FDR derived footprint SWC is 0.025 cm^3/cm^3. The calibrated N_0 is close to 876 cph for a wet part fraction of 8 %. The Pearson correlation coefficient and KGE value between calibrated CRNS SWC and FDR derived footprint SWC during the research period are 0.848 and 0.842. Those values are all close to 1, suggesting a good fit between the CRNS calibration results and FDR observation.

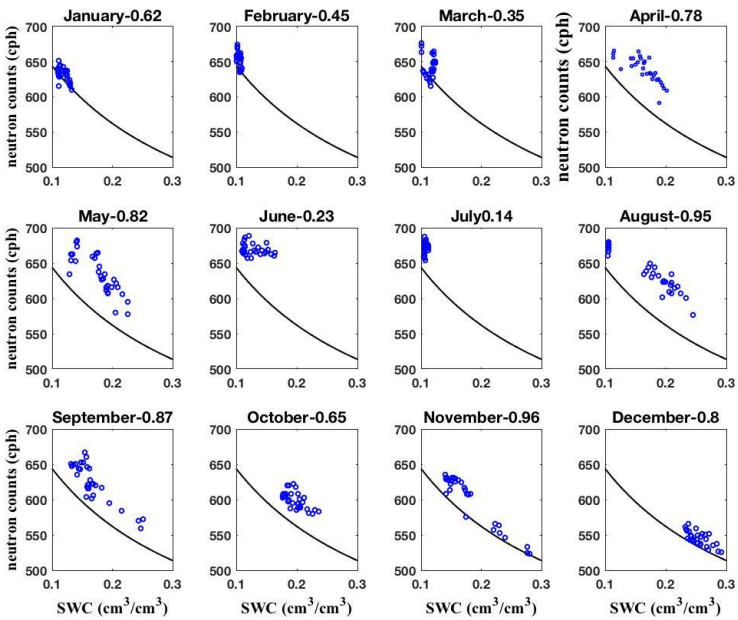

Figure 4.7 Correlation between daily averaged CRNS neutron counts and footprint soil water content (SWC) for all months of 2016. The line in the background is the calibration curve.

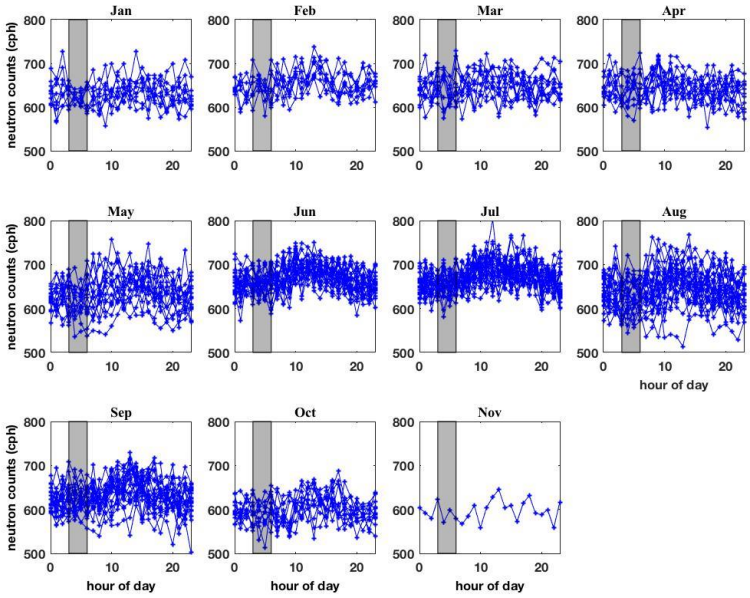

Figure 4.8 Hourly neutron intensity during drip irrigation days at the Picassent site from January to December 2016, each line symbolizes the hourly variations for one day. The shadow area highlights the irrigation period (starts from 3 am and lasts 1~2 hours).

Table 4.3 Hourly normalized standard deviation (N_{std}) of neutron intensity measured on drip irrigation days (averaged for each month).

	Jan	**Feb**	**Mar**	**Apr**	**May**	**Jun**	**Jul**	**Aug**	**Sep**	**Oct**	**Nov**
N_{std}	0.040	0.039	0.039	0.039	0.040	0.039	0.039	0.040	0.040	0.041	0.041

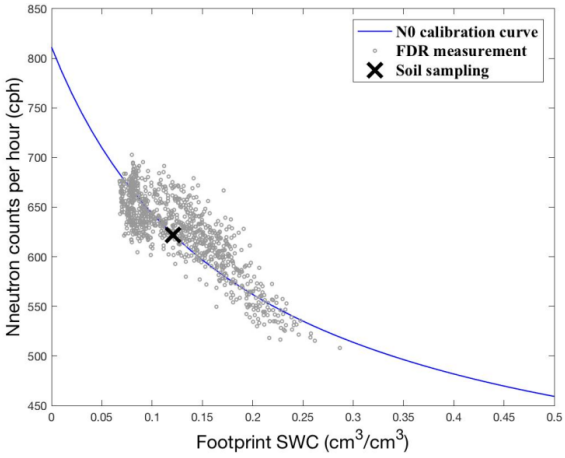

Figure 4.9 N_0 calibration curve showing the site-specific relationship between footprint SWC and measured neutron intensity. The cross corresponds to the gravimetric sampling campaign on the calibration day. The grey dots are the FDR derived footprint SWC and corresponding neutron intensity.

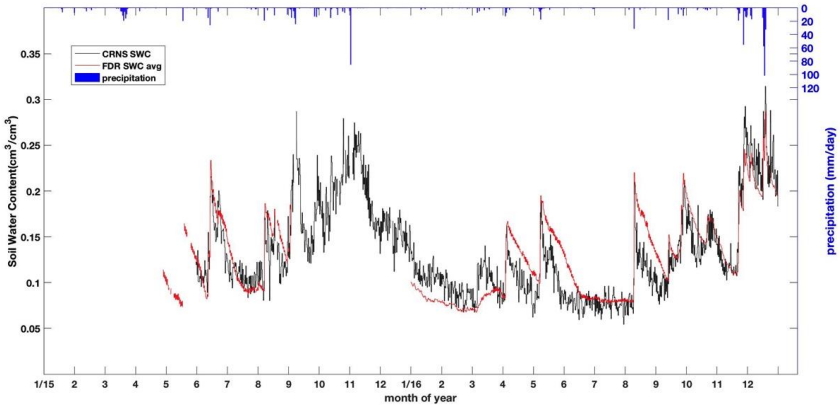

Figure 4.10 Soil water content derived by the N_0 method (CRNS SWC) after bias correction of the FDR sensors. Displayed are also the FDR averaged footprint SWC (FDR SWC avg) and daily precipitation.

4.3.3 Neutron modelling with URANOS model

In section 4.3.2 we found that SWC can be estimated for the CRNS-footprint with a relatively small RMSE. However, drip irrigation does not cause a large increase in the SWC of the

footprint as shown in section 4.3.1. In order to further explore this, the detectable neutron density was simulated with URANOS for the whole field to test the effect of drip irrigation on the neutron intensity.

The URANOS simulation result (see Figure 4.11) shows the highest neutron density for tree canopies, suggesting the canopy locally dominates the whole pattern. The reason is that the canopy acts as an additional moderator, slowing neutrons of higher energies down to detectable medium-range energies. This effect is stronger than the moderation of medium-energy neutrons down to thermal energies, to which the sensor is mostly insensitive (Köhli et al. 2018).

As shown in Figure 4.12, it is evident that the neutron intensity decreases when the irrigated soil becomes wetter. However, the FDR sensors located in the wet patches show SWC (cm^3/cm^3) increases by a maximum of 0.05 related to irrigation (see Figure 4.5 and Table 4.2). And the neutron count limit that can be detected by the CRNS in 1 hour is approximately 4 % relative intensity change, as shown in Table 4.3. For a wetter case (0.14 SWC for the non-irrigated soil), the change of 0.05 SWC by irrigation decreases the neutron intensity by not more than 1-3 neutrons per hour, or less than 1 % (see Figure 4.12). The total SWC change from 0.14 to 0.45 modelled with URANOS corresponds to a decrease of total neutron intensity change by 4.5 %, which can be visible for CRNS. For drier non-irrigated soil, the total neutron intensity change is steeper as shown in Figure 4.12. The additional 0.05 SWC caused by irrigation corresponds to a 2.1 % neutron intensity change. This change in the neutron intensity could be visible for more efficient CRNS detectors or with higher integration time. But in both cases a SWC change from 0.30 to 0.35 for irrigated soil cannot be resolved.

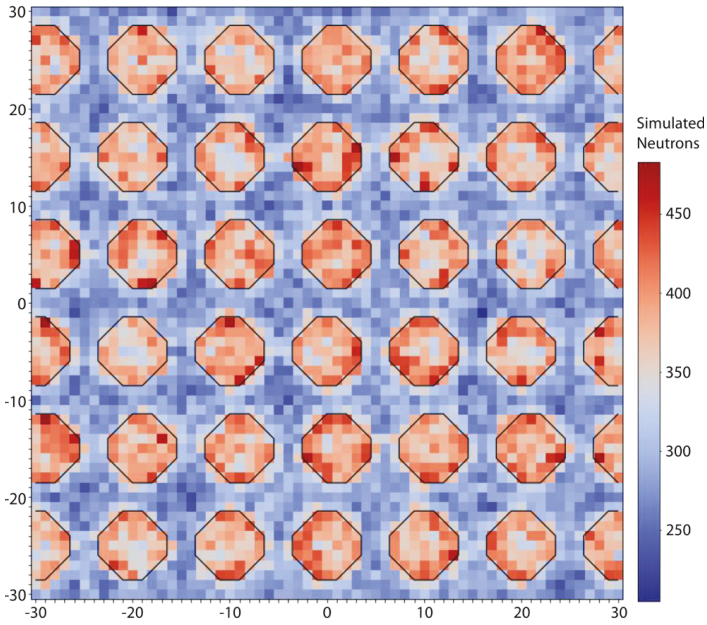

Figure 4.11 Birds-eye view at a central 30 m × 30 m slice of the research domain showing the modelled distribution of neutron intensity at 0.5 m resolution. Black contours indicate the location of the trees.

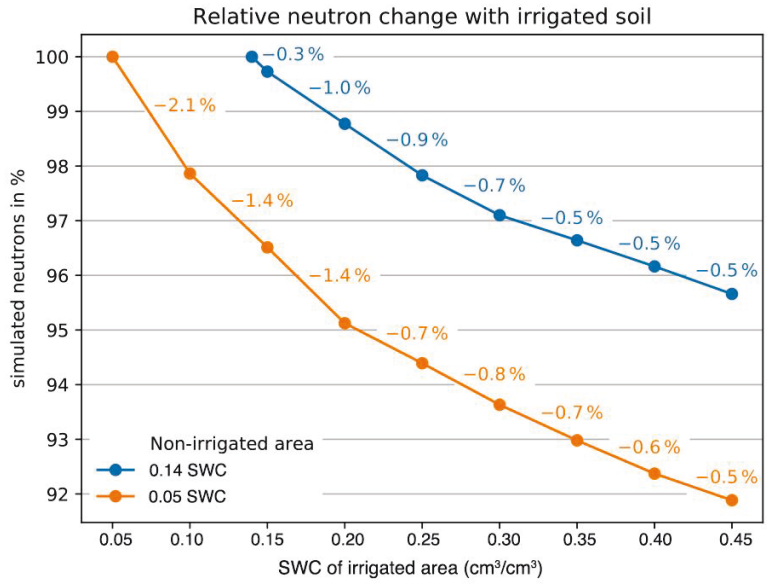

Figure 4.12 Relative change of modelled neutrons as a response to drip irrigation for actual soil conditions at our site (blue) and for dryer conditions (orange) of the non-irrigated soil.

4.4 Conclusions

The drip-irrigated site near Picassent, Spain was used for investigating how well soil water content can be estimated with a CRNS probe and whether this can be used to reliably schedule irrigation amounts. Measurements of neutron intensity by the CRNS probe were made from June 2015 to December 2016 and soil water content for the CRNS footprint was calculated for the same period. A soil sampling campaign was used to calibrate the N_0 parameter, as suggested in the CRNS literature.

The results indicate that in spite of limited calibration data, still a relatively good estimate of the CRNS footprint soil water content could be obtained. Nevertheless, the soil water status of the wet, irrigated area could not be estimated precisely. Simulations by the URANOS neutron transport model confirmed that a standard CRNS probe does not allow for accurate estimation of the soil water content of the irrigated area at our specific site. The modelled neutron intensity changes caused by drip irrigation were lower than the statistical fluctuations of the CRNS measurement. The performance of CRNS technique is mainly limited by the following conditions:

1. The irrigated area is only 8 % of the total area. Since CRNS has an area-averaging footprint, the small patches of irrigation are hardly visible and interpretable in the neutron detector signal. We suppose that irrigation of larger areas could have a more significant influence on the CRNS signal. For example, this effect was actually observed during rain events.

2. Changes of soil water content due to irrigation are small (+0.05 cm^3/cm^3) under rather wet conditions (about 0.35 cm^3/cm^3 SWC). The above-ground neutron density is much more sensitive to changes of SWC at the lower, dry end of the SWC spectrum. Hence we suppose that the sensor would perform better in more arid regions (see also Figure 4.12).

3. The irrigation period is only active for a few hours. The statistical uncertainty of such a short-term neutron measurement is not sufficient to resolve changes below 3 %. The employed CRNS detector can resolve small changes of water content only with longer integration periods of about 12 hours. We suppose that larger and more sensitive detectors could be able to resolve shorter periods.

We conclude that the precise scheduling of drip irrigation is not feasible with a traditional CRNS device in our specific case. But CRNS would perform better in cases where drier soil

is irrigated, during a longer time period or with a more intense irrigation method. The sensitivity of CRNS should also be improved to get a much higher signal to noise ratio in order to detect small-scale drip irrigation. Non-standard CRNS probes, such as the Cosmic-ray Rover (Desilets et al. 2010; Schrön et al. 2018a) are comprised of larger proportional counter tube and hence feature shorter integration times, allowing for higher count rates in the same time interval (Köhli et al. 2018). Multiple CRNS probes at the same field would also increase the total detected neutron intensity and decrease the statistical noise (Schrön et al. 2018b; Jakobi et al. 2018). These new instruments and measurement strategies could be further tested to observe the soil water content variation caused by drip irrigation.

Chapter 5 : Assessment of the uncertainties related to irrigation modelling by a land surface model across India

*adapted from: Li, D., Han, X., Dhanya, C. T., Siebert, S., Vereecken, H., and Hendricks Franssen, H.-J., 2020. Assessment of the uncertainty related to irrigation modelling by a land surface model across India, In preparation for submission to Journal of Hydrology.

5.1 Introduction

Irrigated agriculture is crucial for feeding the increasing population around the world (Carruthers et al., 1997; McLaughlin and Kinzelbach, 2015). Human activities have put extra pressure on the water resources through water withdrawals, especially for agricultural purpose. In order to assess the water balance situation in the past, present and future, it is necessary to model the irrigation requirement (Döll and Siebert, 2002). Irrigation modelling is also needed for understanding land-atmosphere interaction over agricultural areas (Lawston et al., 2017). Irrigation will affect both the energy and water budgets of the land surface (Ozdogan et al., 2010). Several studies illustrated that irrigation increases evapotranspiration (ET) and decreases land surface temperature (Leng et al., 2013; Huang et al., 2016; Shah et al., 2019). Considering irrigation modelling in land surface models could therefore give an improved description of the water and energy balance variations, also in relation to climate change and human activities. Some land surface modelling studies analysed the impact of irrigation at the regional and global scales (Döll and Siebert, 2002). Both land surface models and hydraulic models have been widely used for simulating irrigation and water storage variations under conditions of climate change (Sacks et al., 2009; Fowler et al., 2018; Shah et al., 2019).

Leng et al. (2013) evaluated the performance of irrigation simulation by the Community Land Model (CLM4) considering the spatial distribution and intensity of applied irrigation. Lu et al. (2015) coupled a crop model (CLM4crop) with the Weather Research and Forecasting model (WRF) to represent the interactions between climate and irrigated agriculture, showing an improved surface flux partitioning at irrigated agricultural sites compared to model simulations without dynamic crop growth. Xie et al. (2017) and Zeng et al. (2017) developed a system based on CLM 4.5 considering human water withdrawal and lateral groundwater flow incorporated. Their simulations over the Heihe River Basin of northwestern China showed that irrigation and other anthropogenic exploitation have caused 2 m groundwater depletion (Zeng et al., 2016; 2017).

According to a UN report (UN: World Population Prospects 2017), the population of India has exceeded 1.3 billion and will continue to increase with a high rate of over 1% per year. The increased food demand will increase the need for agricultural production. As irrigated agriculture accounts for 70% of India's food production, water resources are critical for sustaining the huge population (Kumar, 2003). India has frequently been affected by droughts and drought frequency and severity is expected to increase in the context of climate change (Prabhakar and Shaw, 2008; Kumar et al., 2013; Mallya et al., 2016). Given the frequently dry conditions in India, the irrigation requirement will also further increase, which implies increased pressure on groundwater resources (Murray, 2013). GRACE (Gravity Recovery and Climate Experiment) satellite data have shown that India is affected by severe groundwater depletion (Rodell et al., 2009). Groundwater depletion is likely to increase in the future with increasing temperatures and the projected increase of severe droughts (Scanlon et al., 2012).

In parts of India, the impact from human activities on water resources is larger than the impact of global warming (Haddeland et al., 2014). Given the sensitivity of the Indian subcontinent to water stress, the reconstruction of changes in water storage and the water cycle over the subcontinent have gained importance. For India and the Indian subcontinent, the research of Shah et al. (2019) shows the influence of irrigation on the water budget and the land surface temperature by applying the hydrological model VIC. Fowler et al. (2018) have shown the impact of irrigation on precipitation by using the irrigation enabled Community Land Model (CLM4). Previous research also suggested that the effect of irrigation on the land surface fluxes is larger than the uncertainties of the global land cover product over the irrigated area of India (Madhusoodhanan et al., 2017).

In India, the spatiotemporal pattern of crop and irrigation requirement is strongly decided by the unevenly distributed precipitation within the monsoon season. However, most of the previous studies (Haddeland et al., 2014; Fowler et al. 2018; Shah et al. 2019) ignored the temporal variability of varying irrigation areas and frequency throughout the year. The seasonal change of the irrigation area and the effect of irrigation frequency have not been considered in the past researches. Therefore, it is important to explore the influence of a time-variable irrigation map and irrigation frequency on the irrigation modelling with land surface models. By using the CLM model, the irrigation requirement and land surface flux of each grid cell in the model domain over India have been reconstructed for the year of 2010 at a resolution of 10 km × 10 km. The uncertainties of time-variable irrigation area and irrigation

frequency were explored by different simulation scenarios. In addition, the role of the irrigation factor, which determines the target soil water content and therefore the needed amount of irrigation to compensate the water deficit, were tested. The modelled irrigation requirement was calculated for each scenario to determine the role of these uncertainties in irrigation modelling. The land surface fluxes (total evapotranspiration, transpiration) for different modelling scenarios were calculated and compared with large-scale remote sensing data. The ratio of transpiration to total evapotranspiration was also calculated to explore the effect of irrigation on the partitioning of evapotranspiration.

5.2 Data and methods

5.2.1 Study area

Our research area is the India Subcontinent covering the spatial domain of 8˚N-38˚N and 68˚E-98˚E. India has a large proportion of farmland and 90% of water use is for agricultural purpose (Kumar, 2003). Indian summer monsoon rainfall contributes to around 80% of the annual precipitation (Paul et al., 2016). The whole year is divided into three seasons, namely Zaid (pre-monsoon: March to May), Kharif (monsoon: June to October), and Rabi (post-monsoon: November to February), in accordance to the uneven distribution of precipitation in time.

Northern and southern India have different onset and durations of the monsoon season, and farmers select crop types and crop schedule according to the agricultural water availability. Groundwater from aquifers is extracted extensively for irrigation, especially during the non-monsoon season, which is reflected in the GRACE gravity data over Northern India (Asoka et al., 2017). Such declination in not evident over Southern India, however (Asoka et al., 2017). In this study, Northern and Southern India will be considered separately. The validation of the irrigation modelling result will be focused on Northern India. The division line is set at the latitude of 23 degrees, which divides the research domain into two equal parts.

5.2.2 Methods

5.2.2(a) Community land model

The Community land model (CLM4.5) is the land model of the Community Earth System Model (Oleson et al., 2013). It has been widely used in climate and hydrological research, to

model ecological and hydrological processes. In CLM, the soil water flow and land-atmosphere exchange fluxes are simulated by using a modified Richards equation and Monin-Obukhov similarity theory (Oleson et al., 2013).

The soil profile in CLM has 15 vertical layers, while soil hydrological states and fluxes are calculated only for the upper 10 layers (Oleson et al., 2010). The soil hydraulic parameters are calculated from the sand and clay fractions (Oleson et al., 2013) using the Clapp-Hornberger pedotransfer function in combination with the Brooks-Corey parameterization. Spatial land surface heterogeneity of CLM is represented by 3 levels of sub-grid hierarchy including land units, snow/soil columns and plant functional types (PFT) (Oleson et al., 2010). Each grid cell may have multiple land units including urban, glacier, lake, wetland and vegetated, as well as multiple columns and PFTs (Oleson et al., 2013).

In this study, the modelling domain for whole India was composed by 360 × 360 grid cells, at an average resolution of 10 km × 10 km. In order to avoid heterogeneity within a single model grid cell, each grid cell has only one soil column and one plant functional type, representing the most dominant plant type. The plant functional types are derived from MODIS (Moderate Resolution Imaging Spectroradiometer) land cover data (MCD12Q1) with the help of world climate classification data (Ke et al., 2012). The detailed description of the method can be found in in Ke et al. (2012).

The monthly LAI (Leaf Area Index) for each PFT in CLM was obtained from the MODIS LAI 8-day composite product (MOD15A2). The original 500 m data was regridded to 10 km using Nearest Neighbor sampling method. The monthly SAI (Stem Area Index) for each PFT was derived from monthly LAI values by using the method of Lawrence and Chase (Lawrence and Chase, 2007).

5.2.2(b) Irrigation scheme

In CLM, the irrigation scheduling is planned on the basis of the calculated water deficit, which is the difference between the model predicted and target soil water content. The target soil water content is defined for each soil layer as described in Equation 5.1 (Oleson et al. 2010):

$$\theta_{\text{target}} = (1 - F_{\text{irrig}}) \cdot \theta_{\min} + F_{\text{irrig}} \cdot \theta_{\max} \quad (5.1)$$

where $\theta_{\min}$ is the minimum soil water content to keep stomata completely open and $\theta_{\max}$ is soil saturation. The irrigation factor F_{irrig} (default value is 0.7) was derived empirically to let the calculated global irrigation amount match with the gross agricultural water withdrawal around the year of 2000 (Oleson et al. 2010). Since the default factor was calibrated without specifying the irrigation frequency, the impact of the value for the irrigation factor should be assessed along with irrigation frequency.

The irrigation amount is calculated by the integrated water deficit (W_{deficit}) over the root zone (Oleson et al. 2010):

$$W_{\text{deficit}} = \sum_i^N R_i \cdot \max\left(\theta_{\text{target}} - \theta_i, 0\right) \tag{5.2}$$

where θ_i is the soil water content for layer i, R_i is the root fraction, and N is the number of CLM-layers with roots.

The irrigation amount was calculated with the help of a Python code, coupled with CLM, to integrate different irrigation maps, irrigation frequencies and other irrigation parameters. Irrigation was only applied to the model pixels with crop cover and non-zero LAI.

5.2.3 Datasets

5.2.3(a) Soil texture

We used the global soil texture data from FAO (Food and Agricultural Organization of United Nations), which were transformed from vector maps to raster files (see Figure 5.1). The FAO Digital Soil Map of the World (DSMW) is the digital version of the FAO-UNESCO Soil Map of the World at a scale of 1:5 million, with soil types classified according to the FAO-UNESCO legend.

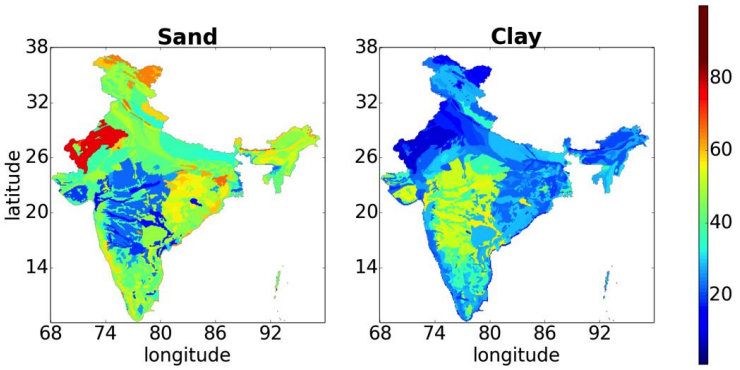

Figure 5.1 The sand (left) and clay (right) percentages of the FAO-based soil map.

5.2.3(b) Atmospheric forcing

Previous research has shown that global reanalysis products are valuable for drought assessment during the Indian monsoon season (Shah and Mishra 2014). In our simulation experiments, the meteorological forcings being used by CLM were generated by combining reanalysis data from NCEP (National Center for Environmental Prediction), GLDAS (Global Land Data Assimilation System) and rain gauge measured precipitation data. The GLDAS_NOAH025 forcing data is 3-hourly and with a spatial resolution of 0.25˚ × 0.25˚ (Rodell et al. 2004). Meteorological variables like wind speed, relative humidity, air pressure, air temperature, incoming long wave and short wave radiation from GLDAS were used as input for the CLM model.

Since precipitation is the major influencing meteorological variable for the water balance with the largest uncertainty, the precipitation amounts from GLDAS were not used but replaced by daily gridded rain gauge observations from IMD (India Meteorology Department) (Pai et al. 2014). The daily rainfall data (IMD4) have a resolution of 0.25˚ × 0.25˚ and are available for a long period (1901-2010) (Pai et al. 2014). The daily precipitation amounts from IMD4 were divided by 24 and used as hourly input data for CLM.

5.2.3(c) Irrigation map

Two irrigation maps were used in the CLM model simulations, which are a time-fixed irrigation map and a season-specific irrigation map. The time-fixed irrigation map was a high resolution irrigation map (250m, from the year of 2000 to 2015) created by remote sensing data was chosen to derive the irrigated area (Ambika et al., 2016). The high-resolution

irrigated area data were created based on the differences between normalized difference vegetation index (NDVI) for irrigated and non-irrigated crops, making use of the NDVI product and land cover data from MODIS (Ambika et al., 2016). In addition, the percentage of irrigated area in each model grid cell of 10 km × 10 km was calculated. In order to simplify the computation while maintaining the irrigated area equal to the irrigated area from the original irrigation map (approximately 850,000 km^2), model grids with over 35 % land being irrigated were considered as irrigated pixel, as shown in Figure 5.2.

For creating the second season-specific irrigation map, another irrigation dataset (GEOSHARE pilot project- Crop Science Bonn) with a spatial resolution of 0.5˚ × 0.5˚ was used, including the spatial distribution of cereal crops (including maize, wheat and rice) under irrigation in each of the three seasons (Zaid, Kharif and Rabi). The seasonal maps for irrigated cropping areas were created by integrating land cover data, crop calendars and census data of the year 2005 (Zhao and Siebert, 2015). In order to create the season-specific irrigation map with resolution of 10 km × 10 km, the coarse resolution (0.5˚ × 0.5˚) and the previous time-fixed irrigation map with higher resolution (10 km × 10 km) were combined together, with irrigation only applied to model grids that are irrigated in both maps as shown in Figure 5.3.

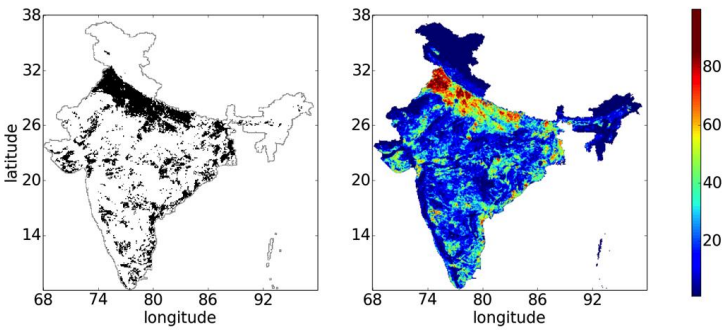

Figure 5.2 The time-fixed irrigation map with resolutions of 10 km × 10 km (left) and corresponding irrigation percentage (right) in each model grid.

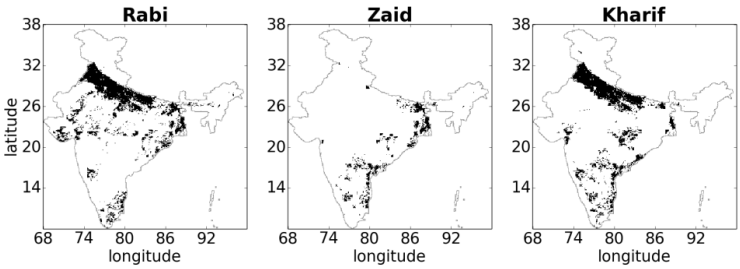

Figure 5.3 The distribution of the irrigated areas in the three seasons (Rabi, Zaid and Kharif) according to the combination of irrigated maps with two resolutions (0.5˚ × 0.5˚ and 10 km × 10 km).

5.2.3(d) Global ET products as model validation

Evapotranspiration (ET), which includes soil evaporation, plant transpiration (T) and canopy evaporation, represents an important process for the global water and energy cycles (Wei et al. 2017). The spatiotemporal patterns of ET are the consequence of complex interactions between soil, vegetation, and lower atmosphere (Zhang et al. 2009; Wu et al. 2017). Many approaches are being used for the observation of ET, such as lysimeters, the eddy covariance technique and the LAS (Large Aperture Scintillometer) (Meijninger et al. 2002). Global ET estimates have been also been acquired by remote sensing based methods, examples are SEBS (Surface Energy Balance System) (Su 2002), GLEAM (Global Land Evaporation: the Amsterdam Methodology) (Miralles et al. 2011), and the MODIS ET product (Mu et al. 2011).

GLEAM ET data (v3: 0.25˚ × 0.25˚) and MODIS ET (MOD16A2: 500 m) were used to compare with CLM modelled ET. The GLEAM ET product is based on the Priestley and Taylor equation and microwave remote sensing data, without considering the parameterization of stomata conductance and aerodynamic resistance (Miralles et al. 2011). The MODIS ET product is derived from a remote sensing based Penman-Monteith method and Priestley-Taylor equation with aerodynamic resistance taken into consideration, with various input data like land cover (MOD12), albedo (MCD43) and Leaf Area Index/fraction of Photosynthetically Active Radiation (LAI/fPAR, MOD15A2) from MODIS (Mu et al. 2011). Both products were resampled to the CLM resolution (10 km × 10 km) using Nearest Neighbour sampling method.

5.2.4 Experiment design and analysis

In this study, six numerical experiments were conducted as shown in Table 5.1. The irrigation requirement and hydrological fluxes over India were reconstructed with help of the CLM model for the year 2010. Different scenarios were tested to explore the role of time-variable irrigation area, irrigation frequency and irrigation factor. The different model scenarios included the control case without irrigation and the cases with weekly irrigation and default irrigation factor of 0.7. In addition, for the weekly and daily irrigation scenario, a time-variable seasonal irrigation map was used. Moreover, the irrigation factor (F_{irrig}) was set to 0.7, 0.6 and 0.5 for the daily-irrigated cases, in order to test the influence of irrigation factor on the modelled irrigation and surface runoff. The duration of irrigation was set to 4 hours for all the simulation scenarios.

The model validation was conducted separately for Northern and Southern India, for the model grids that were irrigated. The averages of irrigation amount and ET for the irrigated grid cells in Northern India were calculated. In order to explore the effect of ignoring heterogeneity within the 10 km × 10 km model grid cells, the averages ratio of transpiration to total evapotranspiration was separately calculated for grid cells with more than 50 % of the area being irrigated and grid cells with only 35-50 % being irrigated. Due to the lack of verification data, the irrigation modelling for the different scenarios was compared and the impact of the different input data was evaluated. The modelled ET over all grids with irrigation was compared with the satellite-based GLEAM and MODIS ET products.

Table 5.1 Summary of simulation experiments with different model setups.

Experiment	Description
noIR	Model run without irrigation
weekIR_F0.7	Model run with weekly irrigation (irrigation factor=0.7) and time-fixed irrigation map
weekIR_season_F0.7	Model run with weekly irrigation (irrigation factor=0.7) and seasonal irrigation map
dayIR_season_F0.7	Model run with daily irrigation (irrigation factor=0.7) and seasonal irrigation map
dayIR_season_F0.6	Model run with daily irrigation (irrigation factor=0.6) and seasonal irrigation map
dayIR_season_F0.5	Model run with daily irrigation (irrigation factor=0.5) and seasonal irrigation map

5.3 Results and discussion

5.3.1 Irrigation modelling for different scenarios

From MODIS LAI time series shown in Figure 5.4, it can be concluded that if model grids are less irrigated (35%-50%), the LAI increases in the first crop season (January to March) less than for the grid cells which are more irrigated (>50%). The averaged LAI values in less irrigated grid cells for the first three months are only 55% of the values for more irrigated grid cells. The dual-seasonal change of LAI can be detected in Northern India, which coincides with two seasons of crop growth and harvest. If irrigation is not applied in the first crop season, the crop may suffer drought stress.

On the other hand, in Southern India the growing season is mainly in the monsoon period; which starts earlier and ends later than in Northern India. Therefore, the crops in Southern India rely less on irrigation. As the major crop season is within the monsoon period in Southern India, the growing of crops may not need much irrigation to sustain and the effect of irrigation on land surface fluxes is much less pronounced compared to precipitation. Since the dual-seasonal change of LAI linked with irrigation input is more prominent for the model grid cells that are more than 50 % being irrigated in Northern India, we will focus on the model validation of land surface fluxes for these model grids in later chapters.

The modelled irrigation requirement with the different model setups is shown in Figure 5.5 as well as in Table. 5.2. According to a report from FAO (FAO. 2015. AQUASTAT Country Profile – India), the water resource being used for irrigation purpose in India for the year of 2010 was estimated to be 688 km^3, which is larger than the simulated irrigation for weekly irrigation scheduling. However, the irrigation statistics were not precisely validated and vary significantly between each year. For example, the irrigation water requirement was estimated as 371 km^3 in the year of 2006 (http://www.fao.org/nr/water/aquastat/data). Figure 5.5 shows the average irrigation for each moth of 2010 and all the irrigated grid cells in Northern India where at least 50% of the area was irrigated. The simulation cases using the seasonal irrigation map (weekIR_season_F0.7) saved water in the pre-monsoon (March to May) season and resulted in the smallest irrigation amounts in one year (255 km^3). The irrigation frequency also impacts the simulated irrigation needs. If daily irrigation is assumed, simulated irrigation is much higher than if weekly irrigation is assumed, especially in the month of June, but also during most of the rest of the year. The effect is larger in June which is related to the sudden start of the irrigation after a long dry season. Simulations with a daily

irrigation for a default irrigation factor of 0.7 (dayIR_season_F0.7) results in the highest simulated irrigation requirement, while the irrigation requirement modelled by CLM decreases with the value of the irrigation factor (dayIR_season_F0.6 and dayIR_season_F0.5).

Figure 5.6 shows the accumulated runoff caused by the irrigation and precipitation in each month for the simulation scenarios. Weekly irrigation scheduling using a seasonal irrigation map as input results in the lowest simulated runoff among the simulation scenarios, except the monsoon season. On the other hand, the variation in runoff is strongly linked with irrigation frequency. The modelled runoff for daily-irrigated cases is much higher than the weekly-irrigated cases. Additionally, with the same daily irrigation frequency, the modelled runoff increases with the value of irrigation factor.

Figure 5.7 shows the modelled averaged daily soil water content (SWC) for the scenarios which use a seasonal irrigation map. Results are shown for SWC at 10 cm, 30 cm and 50 cm depth for all grid cells in Northern India which are more than 50% being irrigated. The averaged SWC corresponding to the wilting point and field capacity is also displayed. The results indicate that the SWC modelled by CLM is near the wilting point in the pre-monsoon season when there is no irrigation applied, but for all irrigation strategies the overall SWC is clearly above the wilting point. The target SWC shown in Figure 5.7 was calculated on the basis of field capacity, wilting point and irrigation factor according Equation. 5.1. Even with the default irrigation factor and intensive daily irrigation, the modelled SWC was still below the target SWC and the soil water deficit was not reduced to zero. Daily irrigation resulted also in significant surface runoff. This indicates that the default irrigation factor in CLM is too high and should be calibrated as function of the irrigation frequency and reliable water consumption data on irrigation.

Table 5.2 Summary of irrigation modelling results for different simulation scenarios for whole India, as well as the FAO statistics of irrigation amount for the year of 2010

Experiment	Irrigation (km^3)
weekIR_F0.7	453.64
weekIR_season_F0.7	255.4
dailyIR_season_F0.7	768.57
dailyIR_season_F0.6	561.41
dailyIR_season_F0.5	391.1
FAO Irrigation (2010)	688

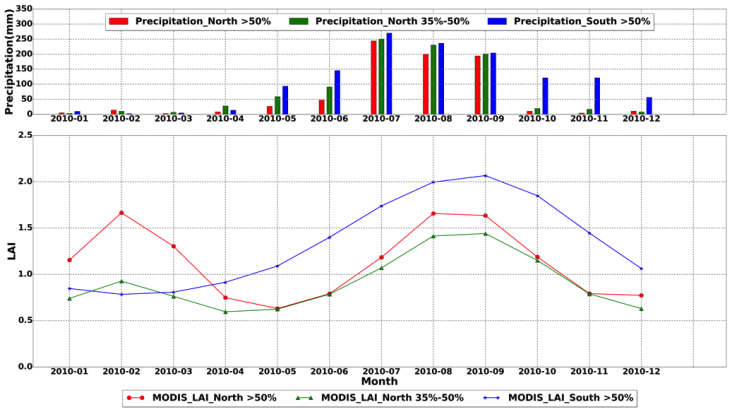

Figure 5.4 Monthly accumulated precipitation (top), and monthly averaged MODIS leaf area index (bottom) for the year of 2010; which were averaged separately for the model grids in Northern India with at least 50 % of the area being irrigated (red), 35 %-50 % of the area being irrigated (green) and the model grids in Southern India with at least 50 % of the area being irrigated (blue).

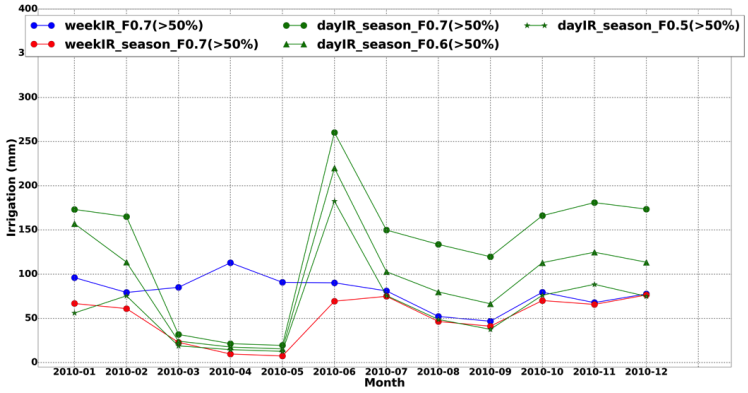

Figure 5.5 Monthly accumulated irrigation modelled by CLM with different model setups for the year of 2010. All simulation results were averaged for the model grids in Northern India with at least 50 % of the area being irrigated.

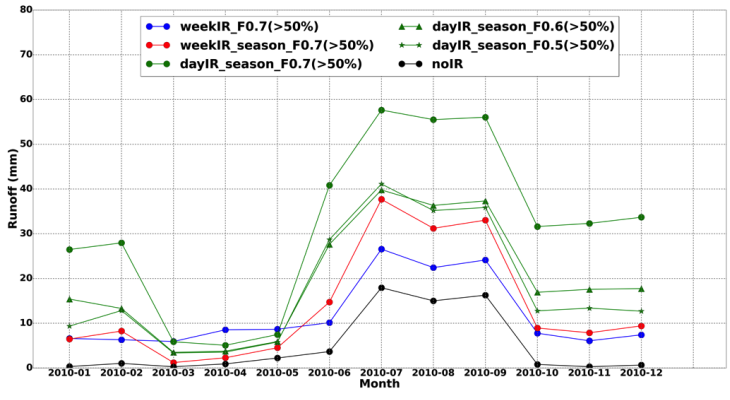

Figure 5.6 Monthly accumulated runoff modelled by CLM for different model setups for the year of 2010. All simulation results were averaged for the model grids in Northern India with at least 50 % of the area being irrigated.

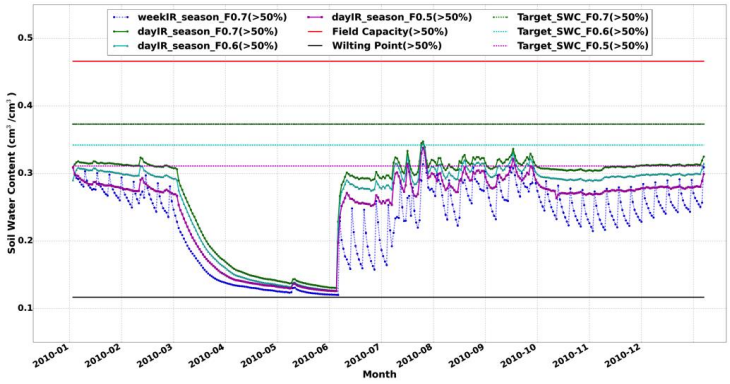

Figure 5.7 Daily modelled average soil water content at 10 cm, 30 cm and 50 cm depth with different model setups using the seasonal irrigation map for the year of 2010, along with the wilting point, field capacity and calculated target soil water content based on different irrigation factors (0.7, 0.6 and 0.5). Simulation results were all averaged for the model grid cells in Northern India with at least 50% of the area being irrigated.

5.3.2 Land surface flux modelling and validation

The spatial distributions of evapotranspiration (ET) modelled by CLM in the first three months of 2010 are shown in Figure 5.8. Compared with the MODIS and GLEAM ET in the same period, the spatial pattern of ET modelled by CLM with irrigation input is closer to the MODIS ET, especially in the northern part of India. The ET patterns modelled without irrigation input are closer to GLEAM ET. Time series of modelled ET for the 12 months in 2010 are shown in Figure 5.9 (Northern India, for grid cells which are at least 50% irrigated).

For the grid cells in Northern India, which were more than 50% being irrigated, the ET increase from January to February for the irrigated modelling scenario is possibly linked to the applied irrigation in the same period (see Figure 5.9). The temporal trends of modelled ET fluxes show the strong influence of the seasonal irrigation map. The method using the seasonal irrigation map shows the lowest ET simulation among the simulation cases with irrigation. MODIS ET shows a similar trend of increasing ET from January to February. GLEAM has low ET values in the first two months without ET increase. In the pre-monsoon season (March to May), GLEAM ET is closer to the non-irrigated CLM modelling cases than to the other irrigated cases. Except for the first three months, MODIS ET is always lower than GLEAM ET with ET-values near zero in the pre-monsoon season, which is much lower than GLEAM ET and CLM modelled ET. The reason may be the influence of cloud coverage or other uncertainties within the algorithm of the MODIS ET product. Overall, the simulation scenario using the seasonal irrigation map shows a temporal ET-pattern more similar to MODIS ET than the other simulation scenarios. The different irrigation factors did not impact modelled ET very much, indicating that also a lower irrigation factor resulted in high enough SWC to sustain crop water demand and therefore ET.

The effect of irrigation on the partitioning of ET is also plotted in Figure 5.10 (Northern India, for grid cells that are more than 50% and 35%-50% irrigated). The irrigation aims to fulfil the transpiration need of the crop, and the lower T/ET-ratio implies a lower irrigation efficiency. Both the less irrigated grid cells (35%-50%) and more irrigated grid cells (>50%) have higher T/ET-ratios for the simulation case with a seasonal irrigation map, compared to the case with a fixed irrigation map, especially in the pre-monsoon season (March to May). For the cases with daily irrigation, the modelled ET and T/ET ratio are similar for the three different irrigation factors. It implies that the irrigation being applied with a low irrigation factor of 0.5

is sufficient to sustain plant growth and transpiration, while the rest of the "over-irrigated" water is wasted through surface runoff.

As shown in Figure 5.10, for the model grid cells with lower irrigation percentage (35%-50%), but which are considered as fully irrigated pixels in the modified irrigation map, the irrigation requirement is overestimated, as the T/ET ratio is significantly lower for these grid cells than for the model grid cells with at least 50% of the area being irrigated. The T/ET-ratio for grid cells with 35%-50% irrigated area is lower than 0.4 in the first three months, compared with a value of over 0.5 for grid cells that were at least 50% irrigated in the same period. This indicates that choosing 35% irrigation as the threshold for assigning a grid cell as irrigated grid cell may overestimate the irrigation requirement for the corresponding model grid. Neglecting the irrigation requirement of model grids with less than 35% irrigated area introduces additional errors in the modelling of the irrigation requirement. In order to improve the irrigation modelling, the heterogeneity in each grid should be considered and model resolution should be increased.

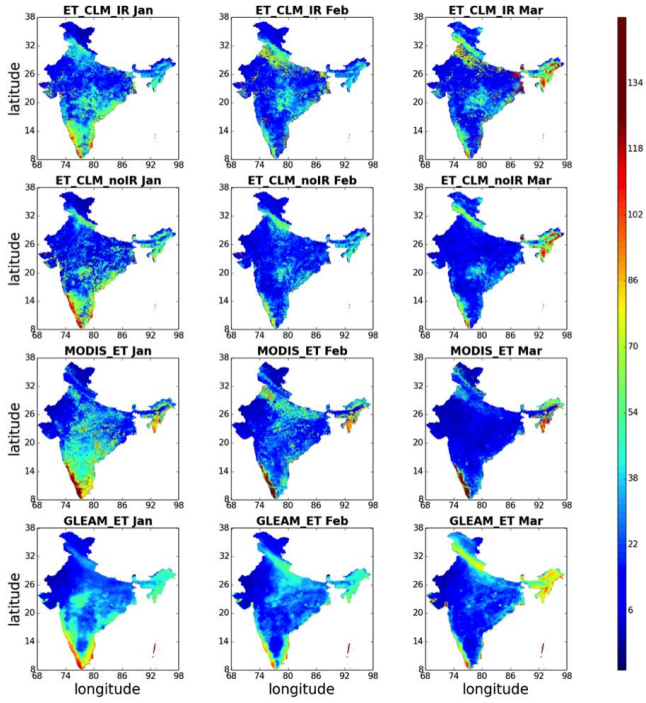

Figure 5.8 Simulated monthly accumulated evapotranspiration with seasonal irrigation (ET_CLM_IR) or without irrigation (ET_CLM_noIR); along with MODIS ET product (MODIS_ET) and GLEAM ET product (GLEAM_ET) for the first three months of the year of 2010.

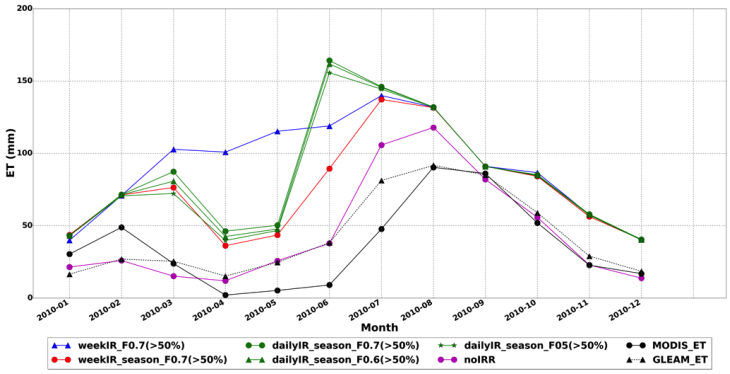

Figure 5.9 Simulated monthly accumulated evapotranspiration according different model setups along with MODIS ET and GLEAM ET for the year of 2010. Simulation results were all averaged for the model grid cells in Northern India with at least 50 % of the area being irrigated.

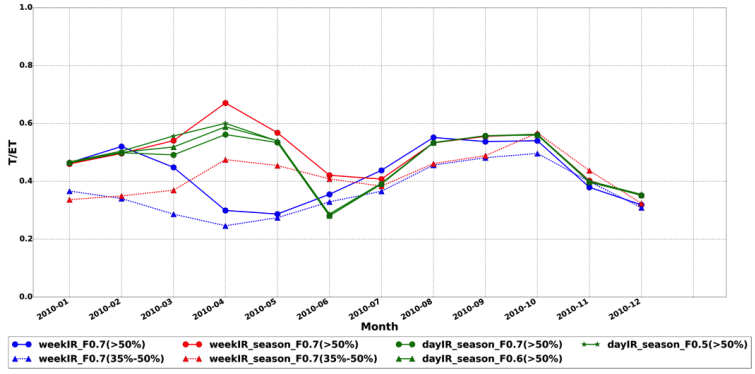

Figure 5.10 Simulated monthly ratio of transpiration to total evapotranspiration (T/ET) modelled by CLM with different model setups for the year of 2010. Simulation results were averaged for the model grid cells in Northern India with at least 50 % or 35 %-50 % of the area being irrigated.

5.4 Conclusions

Irrigation plays an important role in the water and energy cycles of the terrestrial system, especially in semi-arid regions which are susceptible to drought in the crop growing season(s). Land surface models have been used to model irrigation requirement. However, irrigation modelling is affected by uncertainties regarding the spatiotemporal distribution of irrigation. Our main research question was how the uncertainty regarding the spatiotemporal distribution of irrigation affects the simulated irrigation requirement and terrestrial hydrology

(e.g. evapotranspiration). In order to do so, the irrigation requirement and hydrological fluxes have been simulated by the Community Land Model v. 4.5 for the Indian domain for the year of 2010 using multiple simulation scenarios. The results for the simulation scenarios suggest irrigation significantly changed the land surface fluxes and water balance for the irrigated area, which implies that land surface modelling needs to consider the effect of irrigation. Moreover, setting the irrigation timing, frequency and irrigation factors are important for the large-scale irrigation modelling.

The results showed that weekly irrigation scheduling using seasonal variable irrigation maps shows higher T/ET and therefore higher irrigation efficiency than the simulation scenario with a fixed irrigation map, in the pre-monsoon season (March to May). This suggests that land surface modelling including irrigation needs to consider that cropland is only irrigated during some periods of the year. In the dry pre-monsoon period in India, large areas of cropland are not cultivated or irrigated. However, in the other two seasons (monsoon and post-monsoon) the seasonable variable irrigation map did not outperform other irrigation assigning methods, showing a similar T/ET ratio compared to the other irrigation strategies. The reason could be that the irrigation map in the monsoon and post-monsoon periods is not better than the time-fixed irrigation map.

Daily irrigation scheduling using the default irrigation factor of CLM significantly overestimates the irrigation requirement and causes substantial surface runoff. A lower irrigation factor reduces the runoff associated with intensive irrigation. In order to get a reasonable estimate of irrigation amounts, irrigation modelling has to consider the right irrigation timing as well as the right irrigation factor. The irrigation factor should be calibrated using information on the irrigation frequency and applied irrigation amount, which are unfortunately in general not available. Apart from government statistics, remote sensing data could be helpful for determining the irrigation timing and quantity to calibrate the irrigation factor.

In general, more accurate information about the timing and intensity of irrigation is expected to significantly improve the modelling of land surface fluxes and the water balance. For the Northern part of India, the double cropping season and the seasonal variation of the irrigated area should be taken into account. Without considering the temporal and spatial distribution of irrigated cropland, the land surface fluxes and water balance will not be precisely reconstructed. This suggests the need of improved information on the crop-growing pattern,

irrigation timetable and crop calendars including sowing and harvesting dates in the future, which can be assisted by remote sensing data.

As the real irrigation and ET validation data for India were not available, the global ET products based on remote sensing were used as verification. The results suggest that GLEAM ET data does not represent the temporal variation of ET related to the crop growing cycle and irrigation input, especially for the first two months of the year. The MODIS product shows an increase of ET in the first two dry months in the irrigated area of Northern India, and our simulations with CLM suggest that irrigation may be the cause of it. However, the MODIS ET product shows data gaps or very low values in the pre-monsoon season. Compared to the problematic remote sensing based ET estimation, the land model gives us another way of reconstructing land surface fluxes.

The experiments also indicated that irrigation modelling without considering sub-pixel heterogeneity might overestimate the soil water deficit and irrigation requirement especially for the partially irrigated model grid cells. A higher resolution land surface model with higher resolution irrigation input is therefore expected to provide better results. Land cover information, LAI and an irrigation map are available at 250 m-500 m resolution, so that model simulation at such a high spatial resolution could be meaningful, but the computation time will increase drastically and huge data amounts need to be handled.

Chapter 6 : Summary and outlook

Optimal irrigation management is essential to avoid unnecessary water usage and securing the food production in water-scarce regions. Irrigation activity will also affect the energy and water budgets of land surface, playing an important role in the global water cycle. The accurate determination of the soil water deficit is important for irrigation scheduling. Land surface models have been widely used to simulate the soil water content (SWC) and crop status. Data assimilation (DA) provides a method to optimally combine observations with a dynamic land surface model (CLM). A central goal of this PhD work was to test the CLM-DA method for near real-time irrigation scheduling in a real world case, and to explore the possibility of monitoring and scheduling irrigation by a CRNS probe at medium scale. Another objective was to analyse the uncertainties with respect to irrigation modelling at the large scale.

In the first study of this PhD thesis, data assimilation was used to merge real-time SWC observations from FDR sensors with the land surface model CLM to provide an improved prediction of root zone soil water deficit. The CLM model predictions including the weather forecast for the next days, and SWC measured by FDR probes were optimally combined using the Local Ensemble Transform Kalman Filter (LETKF), a sequential data assimilation method, to predict soil water deficit for the next few days and schedule irrigation accordingly. Data assimilation can improve the initial SWC conditions for the CLM model run. In addition, weather forecasts by the Global Forecast System were used as atmospheric forcing for CLM to predict short-term SWC. The difference between predicted and targeted SWC was defined as the water deficit, and the irrigation amount was calculated from the integrated water deficit over the root zone.

During the irrigation campaign for the Picassent site in 2015 and 2016, three different irrigation scheduling methods were tested on multiple citrus fields, including the CLM-DA method, the FAO water balance method and the traditional method based on farmer's experience. Compared with the traditionally irrigated fields by farmers, 24 % less irrigation water on average was needed for the CLM-DA scheduled fields, while the FAO fields were irrigated with 22% less water. Although the CLM-DA irrigated fields received less irrigation water, no significant production loss or plant water stress was detected in the CLM-DA fields. Stem water potential data and SWC recordings of the CLM-DA scheduled fields did not indicate significant plant water stress during the irrigation period. The FAO water balance

method is also an efficient irrigation scheduling approach but it is highly dependent on site-specific empirical parameters. The irrigation estimation by the CLM-DA method depends strongly on the SWC measurements at different spatial and temporal scales.

Therefore in the second study, the novel technique of Cosmic-ray Neutron Sensing (CRNS) was tested to extend the observation scale of SWC to allow irrigation scheduling at larger scales. CRNS is promising for irrigation management as the measurement footprint is representative for the root-zone at the spatial scale of tens of hectares. The potential of the CRNS technique for drip irrigation scheduling is explored in the second study (chapter 4) for the Picassent site, where the citrus fields are drip irrigated. The drip irrigated part covers 8% of the area. The overall SWC in the CRNS footprint was characterized with a field calibration method and a root mean square error of less than 0.03 cm^3/cm^3, but the experimental dataset indicated methodological limitations to detect drip irrigation. We found that the CRNS performance to sense the footprint SWC varies significantly along the study period. Meanwhile the neutron transport simulation URANOS was used to mimic the Picassent site and to simulate the effect of drip irrigation on the neutron intensity. Both the experimental data and the simulation results suggested that the large-area neutron response to drip irrigation is insignificant in our case with a single standard CRNS probe.

The second study showed that neutron transport modelling could be used to assess the suitability of the CRNS technique for certain applications. Because of the small area of irrigated patches, short irrigation time and weak irrigation intensity, SWC changes due to drip irrigation were not detectable from the recorded measured neutron intensity variation. Although the standard CRNS probe was not able to detect small-scale drip irrigation, the method might be applicable for larger irrigated areas, in drier regions, or for more intense irrigation methods. By overcoming the main limitation of statistical noise, the capability of CRNS could be improved in the future by larger and more efficient neutron detectors.

In the third study, the irrigation demand was estimated by a land surface model to reconstruct the water storage changes for the Indian subcontinent. The irrigation modelling tends to be affected by various uncertainties like irrigation frequency, irrigation factor and the spatiotemporal distribution of areas where and when irrigation is potentially applied. The analysis of those uncertainties was conducted in the third study of the PhD thesis for the India subcontinent. The irrigation requirement and hydrological fluxes over India were

reconstructed by six different simulation experiments with the Community Land Model for the year 2010.

The multiple simulation scenarios showed that the modelled irrigation requirement and the land surface fluxes differed between the six scenarios, related to the spatiotemporal uncertainty of the irrigation map, the irrigation frequency and the irrigation factor. Using a season-specific irrigation map resulted in a higher transpiration-total evapotranspiration ratio (T/ET) in the pre-monsoon season compared to other irrigation strategies, implying higher irrigation efficiency. The remote sensing based evapotranspiration products GLEAM and MODIS ET were used to compare with simulated model results, showing a similar increasing ET-trend in the pre-monsoon season as the irrigation induced land surface modelling, especially for the seasonal irrigation map. We conclude that more accurate temporal information of irrigation will result in modelled evapotranspiration closer to the spatiotemporal pattern of evapotranspiration observed by remote sensing. Another conclusion is that a higher spatial resolution in land surface modelling is needed, or an improved consideration of sub-grid heterogeneity to improve the estimation of soil water deficit and irrigation requirement. We also found that daily irrigation scheduling results in larger applied irrigation amounts, evapotranspiration and also surface runoff than weekly irrigation scheduling. If in addition the target soil water content is relatively high, intensive irrigation will result in substantial water loss through surface runoff. This indicates that the standard target soil water content (and associated irrigation factor) in a land surface model may not suit irrigation modelling at the regional scale, and should be calibrated as function of irrigation frequency and reliable statistical data on water consumption.

Overall, our results showed that the CLM-DA method is promising given its water saving potential and automated remote control, ease of incorporation of real time on-line measurements and ensemble based predictions of SWC. The advantage of CLM-DA method is the possibility to integrate many kinds of observation data into the land surface model to improve the prediction of SWC status and to efficiently design irrigation strategies. Both the observation quality and model quality can be improved further to be more sophisticated and cost-efficient, and to be used for precision agriculture.

The application of the CLM-DA irrigation scheduling approach depends on the availability of SWC measurements at different spatial and time scales, which have to provide useful information for different irrigation methods. Concerning drip irrigation, the high frequency

and short duration irrigation application requires real-time observation and high sensitivity of SWC observations. Therefore, FDR sensors are more suitable than CRNS for monitoring and scheduling drip irrigation. Possible observations to be assimilated are not only traditional SWC data, but also other indirect measurements informative about crop water stress, e.g. land surface temperature measured by drones, as well as ET measurements by eddy covariance or lysimeter. In this context, the merging of multi-source direct and indirect observations to improve the prediction of SWC and ET is of special interest.

Concerning the simulation model, a crop growth model would be a good supplement for the original CLM-DA scheme, which could provide information on the water requirement in the different growing stages of the crop, and which could directly predict the crop yield. Better estimates of crop model parameters and a better definition of the SWC threshold for irrigation, specific for different crop types, growing stages and weather conditions, would further improve the performance of the CLM-DA method. In this study, DA was proven to be an efficient way to improve root zone SWC prediction. Furthermore, it can be extended to not only update SWC but also soil and vegetation model parameters to improve further the simulation of SWC and crop status. Another extension of this PhD work in the future is to integrate a coupled model of land surface and subsurface e.g. TerrSysMP (Terrestrial System Modelling Platform) (Shrestha et al. 2014) into the data assimilation system, so that the interaction of irrigation activities and groundwater level variations can be better represented.

The application of the CLM-DA for larger areas, including more crop types and irrigation methods, is also a pending issue. This extension of the CLM-DA based irrigation scheduling to larger scales would require the integration of remote sensing based SWC observations into land surface models. However, the large scale modelling of irrigation is affected by various additional sources of uncertainty like the spatiotemporal distribution of the areas which are irrigated. Information on the timing and frequency of irrigation can be obtained for smaller studies at the field scale, but the spatiotemporal extent of irrigation is much more uncertain at the regional scale. This suggests the need of improved information on crop-growing pattern, irrigation timetable and crop calendars including sowing and harvesting dates in the future. Remote sensing data can also be helpful in this assessment. Meanwhile, the large-scale weather forecasts and in particular the precipitation forecast should also be improved further to fulfil this task.

Bibliography

Allen, R.G., Pereira, L.S., Raes, D. and Smith, M. (1998) Crop evapotranspiration-Guidelines for computing crop water requirements-FAO Irrigation and drainage paper 56. FAO, Rome 300(9), D05109.

Ambika, A.K., Wardlow, B. and Mishra, V. (2016) Remotely sensed high resolution irrigated area mapping in India for 2000 to 2015. Scientific data 3, 160118.

Andreasen, M., Jensen, K.H., Desilets, D., Franz, T.E., Zreda, M., Bogena, H.R. and Looms, M.C. (2017) Status and Perspectives on the Cosmic-Ray Neutron Method for Soil Moisture Estimation and Other Environmental Science Applications. Vadose Zone Journal 16(8).

Asoka, A., Gleeson, T., Wada, Y. and Mishra, V. (2017) Relative contribution of monsoon precipitation and pumping to changes in groundwater storage in India. Nature Geoscience 10(2), 109.

Autovino, D., Rallo, G. and Provenzano, G. (2018) Predicting soil and plant water status dynamic in olive orchards under different irrigation systems with Hydrus-2D: Model performance and scenario analysis. Agricultural Water Management 203, 225-235.

Baatz, R., Bogena, H., Franssen, H.J.H., Huisman, J., Montzka, C. and Vereecken, H. (2015) An empirical vegetation correction for soil water content quantification using cosmic ray probes. Water Resources Research 51(4), 2030-2046.

Baatz, R., Bogena, H.R., Hendricks Franssen, H.J., Huisman, J.A., Qu, W., Montzka, C. and Vereecken, H. (2014) Calibration of a catchment scale cosmic-ray probe network: A comparison of three parameterization methods. Journal of Hydrology 516, 231-244.

Ballester, C., Castel, J., Intrigliolo, D. and Castel, J. (2011) Response of Clementina de Nules citrus trees to regulated deficit irrigation. Yield components and fruit composition. Agric. Water. Manag. 98, 1027–1032.

Ballester, C., Castel, J., Jiménez-Bello, M., Intrigliolo, D. and Castel, J. (2014) Are sap flow and canopy temperature measurements useful alternatives to stem water potential for detecting plant water stress in citrus trees? Acta horticulturae (1038), 51-57.

Barker, J.B., Franz, T.E., Heeren, D.M., Neale, C.M. and Luck, J.D. (2017) Soil water content monitoring for irrigation management: A geostatistical analysis. Agricultural Water Management 188, 36-49.

Barrett, J.H. and Skogerboe, G.V. (1980) Crop production functions and the allocation and use of irrigation water. Agricultural Water Management 3(1), 53-64.

Bausch, W.C. (1995) Remote sensing of crop coefficients for improving the irrigation scheduling of corn. Agricultural Water Management 27(1), 55-68.

Blonquist, J., Jones, S.B. and Robinson, D. (2006) Precise irrigation scheduling for turfgrass using a subsurface electromagnetic soil moisture sensor. Agricultural Water Management 84(1), 153-165.

Bogena, H.R., Herbst, M., Huisman, J.A., Rosenbaum, U., Weuthen, A. and Vereecken, H. (2010) Potential of wireless sensor networks for measuring soil water content variability. Vadose Zone Journal 9(4), 1002-1013.

Bogena, H.R., Huisman, J.A., Baatz, R., Hendricks Franssen, H.J. and Vereecken, H. (2013) Accuracy of the cosmic-ray soil water content probe in humid forest ecosystems: The worst case scenario. Water Resources Research 49(9), 5778-5791.

Brown, P.D., Cochrane, T.A. and Krom, T.D. (2010) Optimal on-farm irrigation scheduling with a seasonal water limit using simulated annealing. Agricultural Water Management 97(6), 892-900.

Carruthers, I., Rosegrant, M.W. and Seckler, D. (1997) Irrigation and food security in the 21st century. Irrigation and Drainage Systems 11(2), 83-101.

Castel, J.R. (2000) Water use of developing citrus canopies in Valencia, Spain. Proceedings International Society of Citriculture, IX Congress, 223-226.

Choné, X., Van Leeuwen, C., Dubourdieu, D. and Gaudillère, J.P. (2001) Stem water potential is a sensitive indicator of grapevine water status. Annals of botany 87(4), 477-483.

Clapp, R.B. and Hornberger, G.M. (1978) Empirical equations for some soil hydraulic properties. Water Resources Research 14(4), 601-604.

Clawson, K.L. and Blad, B.L. (1982) Infrared thermometry for scheduling irrigation of corn. Agronomy Journal 74(2), 311-316.

Cosby, B., Hornberger, G., Clapp, R. and Ginn, T. (1984) A statistical exploration of the relationships of soil moisture characteristics to the physical properties of soils. Water Resources Research 20(6), 682-690.

Dabach, S., Lazarovitch, N., Šimůnek, J. and Shani, U. (2013) Numerical investigation of irrigation scheduling based on soil water status. Irrigation science 31(1), 27-36.

Davis, S. and Dukes, M. (2010) Irrigation scheduling performance by evapotranspiration-based controllers. Agricultural Water Management 98(1), 19-28.

Decker, M. and Zeng, X. (2009) Impact of modified Richards equation on global soil moisture simulation in the Community Land Model (CLM3. 5). Journal of Advances in Modeling Earth Systems 1(3).

Desilets, D., Zreda, M. and Ferre, T.P.A. (2010) Nature's neutron probe: Land surface hydrology at an elusive scale with cosmic rays. Water Resources Research 46(11), n/a-n/a.

Döll, P. and Siebert, S. (2002) Global modeling of irrigation water requirements. Water Resources Research 38(4), 8-1-8-10.

El Sharif, H., Wang, J. and Georgakakos, A.P. (2015) Modeling Regional Crop Yield and Irrigation Demand Using SMAP Type of Soil Moisture Data. Journal of Hydrometeorology 16(2), 904-916.

Entekhabi, D., Njoku, E.G., O'Neill, P.E., Kellogg, K.H., Crow, W.T., Edelstein, W.N., Entin, J.K., Goodman, S.D., Jackson, T.J. and Johnson, J. (2010) The soil moisture active passive (SMAP) mission. Proceedings of the IEEE 98(5), 704-716.

Evans, R.O., Sneed, R.E. and Cassel, D.K. (1991) Irrigation scheduling to improve water-and energy-use efficiencies, NC Cooperative Extension Service.

Evensen, G. (2003) The ensemble Kalman filter: Theoretical formulation and practical implementation. Ocean dynamics 53(4), 343-367.

Fares, A. and Alva, A.K. (2000) Evaluation of capacitance probes for optimal irrigation of citrus through soil moisture monitoring in an entisol profile. Irrigation science 19(2), 57-64.

Fernández, J. and Cuevas, M. (2010) Irrigation scheduling from stem diameter variations: a review. Agricultural and Forest Meteorology 150(2), 135-151.

Fernández, J., Palomo, M., Dıaz-Espejo, A., Clothier, B., Green, S., Girón, I. and Moreno, F. (2001) Heat-pulse measurements of sap flow in olives for automating irrigation: tests, root flow and diagnostics of water stress. Agricultural Water Management 51(2), 99-123.

Fersch, B., Jagdhuber, T., Schrön, M., Völksch, I. and Jäger, M. (2018) Synergies for Soil Moisture Retrieval Across Scales from Airborne Polarimetric SAR, Cosmic-Ray Neutron Roving, and an In Situ Sensor Network. Water Resources Research.

Fowler, M.D., Pritchard, M.S. and Kooperman, G.J. (2018) Assessing the Impact of Indian Irrigation on Precipitation in the Irrigation-Enabled Community Earth System Model. Journal of Hydrometeorology 19(2), 427-443.

Franz, T.E., Zreda, M., Rosolem, R. and Ferre, T.P.A. (2013) A universal calibration function for determination of soil moisture with cosmic-ray neutrons. Hydrology and Earth System Sciences 17(2), 453-460.

García-Tejero, I., Romero-Vicente, R., Jiménez-Bocanegra, J., Martínez-García, G., Durán-Zuazo, V. and Muriel-Fernández, J. (2010) Response of citrus trees to deficit irrigation during different phenological periods in relation to yield, fruit quality, and water productivity. Agricultural Water Management 97(5), 689-699.

Geerts, S., Raes, D. and Garcia, M. (2010) Using AquaCrop to derive deficit irrigation schedules. Agricultural Water Management 98(1), 213-216.

Gupta, H.V., Kling, H., Yilmaz, K.K. and Martinez, G.F. (2009) Decomposition of the mean squared error and NSE performance criteria: Implications for improving hydrological modelling. Journal of Hydrology 377(1-2), 80-91.

Haddeland, I., Heinke, J., Biemans, H., Eisner, S., Flörke, M., Hanasaki, N., Konzmann, M., Ludwig, F., Masaki, Y. and Schewe, J. (2014) Global water resources affected by human

interventions and climate change. Proceedings of the national academy of sciences 111(9), 3251-3256.

Han, X., Franssen, H.-J., Rosolem, R., Jin, R., Li, X. and Vereecken, H. (2015) Correction of systematic model forcing bias of CLM using assimilation of cosmic-ray Neutrons and land surface temperature: a study in the Heihe Catchment, China. Hydrol. Earth Syst. Sci. 19(1), 615-629.

Han, X., Franssen, H.-J.H., Bello, M.Á.J., Rosolem, R., Bogena, H., Alzamora, F.M., Chanzy, A. and Vereecken, H. (2016a) Simultaneous soil moisture and properties estimation for a drip irrigated field by assimilating cosmic-ray neutron intensity. J. Hydrol. 539, 611-624.

Han, X., Franssen, H.-J.H., Bello, M.Á.J., Rosolem, R., Bogena, H., Alzamora, F.M., Chanzy, A. and Vereecken, H. (2016b) Simultaneous soil moisture and properties estimation for a drip irrigated field by assimilating cosmic-ray neutron intensity. Journal of Hydrology 539, 611-624.

Han, X., Franssen, H.J.H., Montzka, C. and Vereecken, H. (2014a) Soil moisture and soil properties estimation in the Community Land Model with synthetic brightness temperature observations. Water Resour. Res. 50(7), 6081-6105.

Han, X., Jin, R., Li, X. and Wang, S. (2014b) Soil moisture estimation using cosmic-ray soil moisture sensing at heterogeneous farmland. IEEE Geoscience and Remote Sensing Letters 11(9), 1659-1663.

Hawdon, A., McJannet, D. and Wallace, J. (2014) Calibration and correction procedures for cosmic-ray neutron soil moisture probes located across Australia. Water Resources Research 50, 5029-5043.

Heidbüchel, I., Güntner, A. and Blume, T. (2016) Use of cosmic-ray neutron sensors for soil moisture monitoring in forests. Hydrology & Earth System Sciences 20(3).

Huang, X., Rhoades, A.M., Ullrich, P.A. and Zarzycki, C.M. (2016) An evaluation of the variable-resolution CESM for modeling California's climate. Journal of Advances in Modeling Earth Systems 8(1), 345-369.

Hunt, B.R., Kostelich, E.J. and Szunyogh, I. (2007) Efficient data assimilation for spatiotemporal chaos: A local ensemble transform Kalman filter. Physica D: Nonlinear Phenomena 230(1), 112-126.

Iglesias, A. and Garrote, L. (2015) Adaptation strategies for agricultural water management under climate change in Europe. Agricultural Water Management 155, 113-124.

Irmak, A. and Kamble, B. (2009) Evapotranspiration data assimilation with genetic algorithms and SWAP model for on-demand irrigation. Irrigation science 28(1), 101-112.

Iwema, J., Rosolem, R., Baatz, R., Wagener, T. and Bogena, H. (2015) Investigating temporal field sampling strategies for site-specific calibration of three soil moisture–neutron intensity parameterisation methods. Hydrology and Earth System Sciences 19(7), 3203-3216.

Jakobi, J., Huisman, J., Vereecken, H., Diekkrüger, B. and Bogena, H. (2018) Cosmic Ray Neutron Sensing for Simultaneous Soil Water Content and Biomass Quantification in Drought Conditions. Water Resources Research 54(10), 7383-7402.

Jiménez-Bello, M.Á.C., J. R. ; Testi, L. ; Intrigliolo, D. S. (2015) Assessment of a Remote Sensing Energy Balance Methodology (SEBAL) Using Different Interpolation Methods to Determine Evapotranspiration in a Citrus Orchard. IEEE Journal of Selected Topics in Applied Earth Observations and Remote Sensing 8(4), 1465-1477.

Jones, H.G. (2004) Irrigation scheduling: advantages and pitfalls of plant-based methods. Journal of experimental botany 55(407), 2427-2436.

Ke, Y., Leung, L., Huang, M., Coleman, A.M., Li, H. and Wigmosta, M.S. (2012) Development of high resolution land surface parameters for the Community Land Model. Geoscientific Model Development 5(6), 1341-1362.

Kerr, Y.H., Waldteufel, P., Wigneron, J.-P., Martinuzzi, J., Font, J. and Berger, M. (2001) Soil moisture retrieval from space: The Soil Moisture and Ocean Salinity (SMOS) mission. IEEE transactions on Geoscience and remote sensing 39(8), 1729-1735.

Köhli, M., Schrön, M. and Schmidt, U. (2018) Response functions for detectors in cosmic ray neutron sensing. Nuclear Instruments and Methods in Physics Research Section A: Accelerators, Spectrometers, Detectors and Associated Equipment 902, 184-189.

Köhli, M., Schrön, M., Zreda, M., Schmidt, U., Dietrich, P. and Zacharias, S. (2015) Footprint characteristics revised for field scale soil moisture monitoring with cosmic-ray neutrons. Water Resources Research 51(7), 5772-5790.

Kumar, K.N., Rajeevan, M., Pai, D., Srivastava, A. and Preethi, B. (2013) On the observed variability of monsoon droughts over India. Weather and Climate Extremes 1, 42-50.

Kumar, M.D. (2003) Food security and sustainable agriculture in India: the water management challenge, IWMI.

Lawrence, D.M. and Slater, A.G. (2008) Incorporating organic soil into a global climate model. Climate Dynamics 30(2-3), 145-160.

Lawrence, P.J. and Chase, T.N. (2007) Representing a new MODIS consistent land surface in the Community Land Model (CLM 3.0). Journal of Geophysical Research: Biogeosciences 112(G1).

Lawston, P.M., Santanello Jr, J.A., Franz, T.E. and Rodell, M. (2017) Assessment of irrigation physics in a land surface modeling framework using non-traditional and human-practice datasets. Hydrology and Earth System Sciences 21(6), 2953.

Leng, G., Huang, M., Tang, Q., Sacks, W.J., Lei, H. and Leung, L.R. (2013) Modeling the effects of irrigation on land surface fluxes and states over the conterminous United States: Sensitivity to input data and model parameters. Journal of Geophysical Research: Atmospheres 118(17), 9789-9803.

Li, D., Hendricks Franssen, H.-J., Han, X., Jiménez-Bello, M.A., Martínez Alzamora, F. and Vereecken, H. (2018) Evaluation of an operational real-time irrigation scheduling scheme for drip irrigated citrus fields in Picassent, Spain. Agricultural Water Management 208, 465-477.

Linker, R., Ioslovich, I., Sylaios, G., Plauborg, F. and Battilani, A. (2016) Optimal model-based deficit irrigation scheduling using AquaCrop: A simulation study with cotton, potato and tomato. Agricultural Water Management 163, 236-243.

Lorite, I., Ramírez-Cuesta, J., Cruz-Blanco, M. and Santos, C. (2015) Using weather forecast data for irrigation scheduling under semi-arid conditions. Irrigation science 33(6), 411-427.

Lu, Y., Jin, J. and Kueppers, L.M. (2015) Crop growth and irrigation interact to influence surface fluxes in a regional climate-cropland model (WRF3. 3-CLM4crop). Climate Dynamics 45(11-12), 3347-3363.

Madhusoodhanan, C., Sreeja, K. and Eldho, T. (2017) Assessment of uncertainties in global land cover products for hydro‐climate modeling in India. Water Resources Research 53(2), 1713-1734.

Mallya, G., Mishra, V., Niyogi, D., Tripathi, S. and Govindaraju, R.S. (2016) Trends and variability of droughts over the Indian monsoon region. Weather and Climate Extremes 12, 43-68.

McLaughlin, D. and Kinzelbach, W. (2015) Food security and sustainable resource management. Water Resources Research 51(7), 4966-4985.

Meijninger, W., Hartogensis, O., Kohsiek, W., Hoedjes, J., Zuurbier, R. and De Bruin, H. (2002) Determination of area-averaged sensible heat fluxes with a large aperture scintillometer over a heterogeneous surface–Flevoland field experiment. Boundary-Layer Meteorology 105(1), 37-62.

Miralles, D., Holmes, T., De Jeu, R., Gash, J., Meesters, A. and Dolman, A. (2011) Global land-surface evaporation estimated from satellite-based observations. Hydrology and Earth System Sciences 15(2), 453.

Miyoshi, T., Yamane, S. and Enomoto, T. (2007) Localizing the error covariance by physical distances within a local ensemble transform Kalman filter (LETKF). SOLA 3, 89-92.

Moran, M., Clarke, T., Inoue, Y. and Vidal, A. (1994) Estimating crop water deficit using the relation between surface-air temperature and spectral vegetation index. Remote sensing of environment 49(3), 246-263.

Moriana, A., Girón, I., Martín-Palomo, M., Conejero, W., Ortuño, M., Torrecillas, A. and Moreno, F. (2010) New approach for olive trees irrigation scheduling using trunk diameter sensors. Agricultural Water Management 97(11), 1822-1828.

Mu, Q., Zhao, M. and Running, S.W. (2011) Improvements to a MODIS global terrestrial evapotranspiration algorithm. Remote sensing of environment 115(8), 1781-1800.

Murray, S. (2013) Present and future water resources in India: insights from satellite remote sensing and a dynamic global vegetation model. Journal of earth system science 122(1), 1-13.

Oleson, K., Lawrence, D., Bonan, G., Drewniak, B., Huang, M., Charles, D., Levis, S., Li, F., Riley, W. and Zachary, M. (2013) Technical Description of version 4.5 of the Community Land Model (CLM) Coordinating. BOULDER, COLORADO, 80307-83000.

Oleson, K.W., Lawrence, D.M., Gordon, B., Flanner, M.G., Kluzek, E., Peter, J., Levis, S., Swenson, S.C., Thornton, E. and Feddema, J. (2010) Technical description of version 4.0 of the Community Land Model (CLM).

Ozdogan, M., Rodell, M., Beaudoing, H.K. and Toll, D.L. (2010) Simulating the effects of irrigation over the United States in a land surface model based on satellite-derived agricultural data. Journal of Hydrometeorology 11(1), 171-184.

Pai, D., Sridhar, L., Rajeevan, M., Sreejith, O., Satbhai, N. and Mukhopadhyay, B. (2014) Development of a new high spatial resolution (0.25× 0.25) long period (1901–2010) daily gridded rainfall data set over India and its comparison with existing data sets over the region. Mausam 65(1), 1-18.

Pardossi, A. and Incrocci, L. (2011) Traditional and new approaches to irrigation scheduling in vegetable crops. HortTechnology 21(3), 309-313.

Paul, S., Ghosh, S., Oglesby, R., Pathak, A., Chandrasekharan, A. and Ramsankaran, R. (2016) Weakening of Indian summer monsoon rainfall due to changes in land use land cover. Scientific reports 6, 32177.

Peters, R.T., Desta, K. and Nelson, L. (2013) Practical use of soil moisture sensors and their data for irrigation scheduling, Washington State University Extension.

Petr, T. (2003) Fisheries in irrigation systems of arid Asia, Food & Agriculture Org.

Playán, E. and Mateos, L. (2006) Modernization and optimization of irrigation systems to increase water productivity. Agric. Water. Manag. 80(1), 100-116.

Prabhakar, S. and Shaw, R. (2008) Climate change adaptation implications for drought risk mitigation: a perspective for India. Climatic Change 88(2), 113-130.

Provenzano, G. (2007) Using HYDRUS-2D simulation model to evaluate wetted soil volume in subsurface drip irrigation systems. Journal of Irrigation and Drainage Engineering 133(4), 342-349.

Pulido-Calvo, I. and Gutiérrez-Estrada, J.C. (2009) Improved irrigation water demand forecasting using a soft-computing hybrid model. Biosystems Engineering 102(2), 202-218.

Rallo, G., Agnese, C., Minacapilli, M. and Provenzano, G. (2011) Comparison of SWAP and FAO agro-hydrological models to schedule irrigation of wine grapes. Journal of Irrigation and Drainage Engineering 138(7), 581-591.

Rallo, G., González-Altozano, P., Manzano-Juárez, J. and Provenzano, G. (2017) Using field measurements and FAO-56 model to assess the eco-physiological response of citrus orchards under regulated deficit irrigation. Agricultural Water Management 180, 136-147.

Reichle, R.H. (2008) Data assimilation methods in the Earth sciences. Advances in Water Resources 31, 1411-1418.

Rodell, M., Houser, P., Jambor, U., Gottschalck, J., Mitchell, K., Meng, C.-J., Arsenault, K., Cosgrove, B., Radakovich, J. and Bosilovich, M. (2004) The global land data assimilation system. Bulletin of the American Meteorological Society 85(3), 381-394.

Rodell, M., Velicogna, I. and Famiglietti, J.S. (2009) Satellite-based estimates of groundwater depletion in India. Nature 460(7258), 999.

Rosolem, R., Shuttleworth, W.J., Zreda, M., Franz, T.E., Zeng, X. and Kurc, S.A. (2013) The Effect of Atmospheric Water Vapor on Neutron Count in the Cosmic-Ray Soil Moisture Observing System. Journal of Hydrometeorology 14(5), 1659-1671.

Sacks, W.J., Cook, B.I., Buenning, N., Levis, S. and Helkowski, J.H. (2009) Effects of global irrigation on the near-surface climate. Climate Dynamics 33(2-3), 159-175.

Sammis, T., Sharma, P., Shukla, M., Wang, J. and Miller, D. (2012) A water-balance drip-irrigation scheduling model. Agricultural Water Management 113, 30-37.

Scanlon, B.R., Faunt, C.C., Longuevergne, L., Reedy, R.C., Alley, W.M., McGuire, V.L. and McMahon, P.B. (2012) Groundwater depletion and sustainability of irrigation in the US High Plains and Central Valley. Proceedings of the national academy of sciences 109(24), 9320-9325.

Schattan, P., Schrön, M., Köhli, M., Baroni, G., Oswald, S. and Achleitner, S. (2018) Cosmic-ray neutron sensing of snow water equivalent in heterogeneous alpine terrain, p. 14641.

Schreiner-McGraw, A.P., Vivoni, E.R., Mascaro, G. and Franz, T.E. (2016) Closing the water balance with cosmic-ray soil moisture measurements and assessing their relation to evapotranspiration in two semiarid watersheds. Hydrology & Earth System Sciences 20(1).

Schrön, M., Köhli, M., Scheiffele, L., Iwema, J., Bogena, H.R., Lv, L., Martini, E., Baroni, G., Rosolem, R. and Weimar, J. (2017) Improving calibration and validation of cosmic-ray neutron sensors in the light of spatial sensitivity. Hydrol. Earth Syst. Sci. 21, 5009–5030.

Schrön, M., Rosolem, R., Köhli, M., Piussi, L., Schröter, I., Iwema, J., Kögler, S., Oswald, S., Wollschläger, U. and Samaniego, L. (2018a) Cosmic-Ray Neutron Rover Surveys of Field Soil Moisture and the Influence of Roads. Water Resources Research 54(9), 6441-6459.

Schrön, M., Zacharias, S., Womack, G., Köhli, M., Desilets, D., Oswald, S.E., Bumberger, J., Mollenhauer, H., Kögler, S. and Remmler, P. (2018b) Intercomparison of cosmic-ray neutron sensors and water balance monitoring in an urban environment. Geoscientific Instrumentation, Methods and Data Systems 7(1), 83-99.

Sdoodee, S. and Somjun, J. (2008) Measurement of stem water potential as a sensitive indicator of water stress in neck orange (Citrus reticulata Blanco). Sonklanakarin Journal of Science and Technology 30(5), 561.

Shah, H.L., Zhou, T., Huang, M. and Mishra, V. (2019) Strong influence of irrigation on water budget and land surface temperature in Indian sub‐continental river basins. Journal of Geophysical Research: Atmospheres.

Shah, R. and Mishra, V. (2014) Evaluation of the reanalysis products for the monsoon season droughts in India. Journal of Hydrometeorology 15(4), 1575-1591.

Shang, S. and Mao, X. (2006) Application of a simulation based optimization model for winter wheat irrigation scheduling in North China. Agricultural Water Management 85(3), 314-322.

Shrestha, P., Sulis, M., Masbou, M., Kollet, S. and Simmer, C. (2014) A scale-consistent terrestrial systems modeling platform based on COSMO, CLM, and ParFlow. Monthly weather review 142(9), 3466-3483.

Smajstrla, A. and Locascio, S. (1996) Tensiometer-controlled, drip-irrigation scheduling of tomato. Applied Engineering in Agriculture 12(3), 315-319.

Su, Z.B. (2002) A Surface Energy Balance System (SEBS) for estimation of turbulent heat fluxes from point to continental scale.

Syvertsen, J. (1982) Minimum leaf water potential and stomatal closure in citrus leaves of different ages. Annals of botany 49(6), 827-834.

Syvertsen, J., Smith Jr, M. and Allen, J. (1981) Growth rate and water relations of citrus leaf flushes. Annals of botany 47(1), 97-105.

Ticlavilca A. M., Mckee M. and Walker W. R. (2013) Real-time forecasting of short-term irrigation canal demands using a robust multivariate Bayesion learning model. Irrigaton Science 31(2), 151-167.

Turner, N.C. (1981) Techniques and experimental approaches for the measurement of plant water status. Plant and soil 58(1-3), 339-366.

Velez, J., Intrigliolo, D. and Castel, J. (2007) Scheduling deficit irrigation of citrus trees with maximum daily trunk shrinkage. Agricultural Water Management 90(3), 197-204.

Vellidis, G., Tucker, M., Perry, C., Kvien, C. and Bednarz, C. (2008) A real-time wireless smart sensor array for scheduling irrigation. Computers and electronics in agriculture 61(1), 44-50.

Vereecken, H., Burauel, P., Groeneweg, J., Klumpp E., Mittelstaedt W., Putz T., van der Kruk J., Vanderborght J. and Wendland F. (2009) Research at the Agrosphere Institute: From the Process Scale to the Catchment Scale. Vadose Zone Journal 8(3), 664-669.

Vörösmarty, C.J., Green, P., Salisbury, J. and Lammers, R.B. (2000) Global water resources: vulnerability from climate change and population growth. science 289(5477), 284-288.

Wardlaw, R. and Bhaktikul, K. (2004) Application of genetic algorithms for irrigation water scheduling. Irrigation and Drainage 53(4), 397-414.

Wei, Z., Yoshimura, K., Wang, L., Miralles, D.G., Jasechko, S. and Lee, X. (2017) Revisiting the contribution of transpiration to global terrestrial evapotranspiration. Geophysical Research Letters 44(6), 2792-2801.

Wu, C., Hu, B.X., Huang, G. and Zhang, H. (2017) Effects of climate and terrestrial storage on temporal variability of actual evapotranspiration. Journal of Hydrology 549, 388-403.

Xie, Z.-H., Zeng, Y.-J., Xia, J., Qin, P.-H., Jia, B.-H., Zou, J. and Liu, S. (2017) Coupled modeling of land hydrology–regional climate including human carbon emission and water exploitation. Advances in Climate Change Research 8(2), 68-79.

Zeng, X. (2001) Global vegetation root distribution for land modeling. Journal of Hydrometeorology 2(5), 525-530.

Zeng, Y., Xie, Z. and Liu, S. (2017) Seasonal effects of irrigation on land-atmosphere latent heat, sensible heat, and carbon fluxes in semiarid basin. Earth System Dynamics 8(1), 113.

Zeng, Y., Xie, Z., Yu, Y., Liu, S., Wang, L., Zou, J., Qin, P. and Jia, B. (2016) Effects of anthropogenic water regulation and groundwater lateral flow on land processes. Journal of Advances in Modeling Earth Systems 8(3), 1106-1131.

Zhang, K., Kimball, J.S., Mu, Q., Jones, L.A., Goetz, S.J. and Running, S.W. (2009) Satellite based analysis of northern ET trends and associated changes in the regional water balance from 1983 to 2005. Journal of Hydrology 379(1-2), 92-110.

Zhao, G. and Siebert, S. (2015) Season-wise irrigated and rainfed crop areas for India around year 2005. MyGeoHUB, doi: https://doi. org/10.13019/M2CC71.

Zhu, Z., Tan, L., Gao, S. and Jiao, Q. (2015) Observation on soil moiture of irrigation cropland by cosmic-ray probe. IEEE Geoscience and Remote Sensing Letters 12(3), 472-476.

Zreda, M., Shuttleworth W. J., Zeng X., Zweck C., Desilets D., Franz T. and Rosolem R. (2012) COSMOS: the COsmic-ray Soil Moisture Observing System. Hydrology and Earth System Sciences 16(11), 4079-4099.

Acknowledgements

First of all, I would like to thank Prof. Dr. Harrie-Jan Hendricks Franssen for his supervision for my nearly 5 years' PhD work. During my studies we had many meetings and he provided many helpful suggestions. Thanks for his detailed editing efforts for the improvements of the three papers and this PhD thesis. Moreover I am grateful to China Scholarship Council (CSC) for providing the funding for my study and life in Germany. I also gratefully acknowledge Prof. Dr. Xujun Han who taught me a lot about model, programing and data assimilation. Many thanks to Prof. Dr. Fernando Martínez Alzamora and Dr. Miguel Angel Jiménez Bello from Institute of Hydraulic and Environmental Engineering of Universitat Politècnica de Valencia for their supports and help during my visits to Valencia and conducting field experiments. I am also thankful to all the other colleagues in IVIA and Universitat Politècnica de Valencia for the installation of soil moisture sensors and conducting field measurements of stem water potential. I would also like to thank Dr. Martin Schrön and Jannis Weimar from UFZ Helmholtz Centre for Environmental Research and Dr. Markus Köhli from Heidelberg University for their help with the neutron transfer model. Moreover, I would like to thank Prof. Dr. Dhanya C. T. from Indian Institute of Technology (IIT) Delhi and Prof. Dr. Stefan Siebert from University of Göttingen for providing me the data to run the irrigation modelling of India. Then I gratefully acknowledge to Juelich Supercomputing Center for granting the required computation time on JURECA.

Besides, I would like to thank my other colleagues from the Institute of bio- and Geosciences at the Juelich Research Center:

- Prof. Dr. Harry Vereecken, the head of our institute, for his support and suggestions.
- Dr. Heye Bogena and Dr. Roland Baatz, for their help with the Cosmic-ray Neutron Sensing data.
- Guowei He and Mukund Pondkule for their help with my programing problems.
- Dr. Hongjuan Zhang and Dr. Qi Tang for their help with my PhD thesis writing.
- My officemate Dr. Parizia Ney, Sean McGovern, Yajie Sun, Phuong Ta, and Anneli Karlsson, as well as my friend Shehan Morandage, Manuela Kaufmann, Inge Wiekenkamp, Dr. Anne Klosterhalfen, for all their help during my stay in Germany.
- All the other colleagues in IBG-3 for the great time working and having fun together.

Special thanks to my parents and my sister's family, for all their love and long time support.

Band / Volume 491
Nanoscale investigation of high temperature oxidation mechanisms of high-Cr ferritic steels
A. Vayyala (2020), xix, 105 pp
ISBN: 978-3-95806-467-6

Band / Volume 492
Electrolyte development for a SOFC operating at low temperature
J. Zhang (2020), vi, 121 pp
ISBN: 978-3-95806-471-3

Band / Volume 493
Modeling and Simulation of Polymer Electrolyte Fuel Cells
S. Zhang (2020), 4, xii, 214 pp
ISBN: 978-3-95806-472-0

Band / Volume 494
Ab initio perspective on hydrogenated amorphous silicon for thin-film and heterojunction photovoltaics
P. Czaja (2020), 107 pp
ISBN: 978-3-95806-474-4

Band / Volume 495
Measurements of Atmospheric OH and HO_2 Radicals by Laser-Induced Fluorescence on the HALO Aircraft during the OMO-ASIA 2015 Campaign
C. Künstler (2020), 156 pp
ISBN: 978-3-95806-477-5

Band / Volume 496
Tomographic observations of gravity waves with the infrared limb imager GLORIA
I. Krisch (2020), vii, 187 pp
ISBN: 978-3-95806-481-2

Band / Volume 497
Aquisition of temporally and spatially highly resolved data sets of relevant trace substances for model development and model evaluation purposes using a mobile measuring laboratory
D. Klemp, R. Wegener, R. Dubus, U. Javed (2020), 110 pp
ISBN: 978-3-95806-465-2

Band / Volume 498
Charakterisierung des Werkstoffverhaltens während des Kosinterns einer neuartigen, inert gestützten Festoxidbrennstoffzelle
F. Grimm (2020), ix, 168 pp
ISBN: 978-3-95806-482-9

Schriften des Forschungszentrums Jülich
Reihe Energie & Umwelt / Energy & Environment

Band / Volume 499
WEGE FÜR DIE ENERGIEWENDE
Kosteneffiziente und klimagerechte Transformationsstrategien für das deutsche Energiesystem bis zum Jahr 2050
M. Robinius et al (2020), VIII, 141 pp
ISBN: 978-3-95806-483-6

Band / Volume 500
Mechanical Behavior of Solid Electrolyte Materials for Lithium-ion Batteries
G. Yan (2020), x, 139 pp
ISBN: 978-3-95806-484-3

Band / Volume 501
Retrieval of atmospheric quantities from remote sensing measurements of nightglow emissions in the MLT region
Q. Chen (2020), 208 pp
ISBN: 978-3-95806-485-0

Band / Volume 502
Auswirkungen der Energiewende auf das deutsche Gastransportsystem
B. Gillessen (2020), XVII, 186
ISBN: 978-3-95806-487-4

Band / Volume 503
Lagrangian Simulation of Stratospheric Water Vapour: Impact of Large-Scale Circulation and Small-Scale Transport Processes
L. Poshyvailo (2020), 124 pp
ISBN: 978-3-95806-488-1

Band / Volume 504
Water Management in Automotive Polymer-Electrolyte-Membrane Fuel Cell Stacks
S. Asanin (2020), XVIII, 172 pp
ISBN: 978-3-95806-491-1

Band / Volume 505
Towards a new real-time irrigation scheduling method: observation, modelling and their integration by data assimilation
D. Li (2020), viii, 94 pp
ISBN: 978-3-95806-492-8

Weitere ***Schriften des Verlags im Forschungszentrum Jülich*** unter
http://wwwzb1.fz-juelich.de/verlagextern1/index.asp

Energie & Umwelt / Energy & Environment
Band / Volume 505
ISBN 978-3-95806-492-8

Mitglied der Helmholtz-Gemeinschaft

JÜLICH
Forschungszentrum